UTS UNIVERSITY OF TECHNOLOGY SYDNEY

Prediction-Error Negativity in Physical Human-Robot Collaboration

by

Stefano Aldini

A thesis submitted in partial fulfilment of the
requirements for the degree of Doctor of Philosophy

Supervisor: Dist. Prof. Dikai Liu

Co-supervisor: Dr. Marc Garry Carmichael

at the
Robotics Institute
Faculty of Engineering and Information Technology
University of Technology Sydney

27th January 2021

Certificate of Original Authorship

I, Stefano Aldini, declare that this thesis is submitted in fulfilment of the requirements for the award of Doctor of Philosophy, in the School of Mechanical and Mechatronic Engineering at the University of Technology Sydney.

This thesis is wholly my own work unless otherwise referenced or acknowledged. In addition, I certify that all information sources and literature used are indicated in the thesis.

This document has not been submitted for qualifications at any other academic institution.

This research is supported by the Australian Government Research Training Program.

Signed: Production Note: Signature removed prior to publication.

Date: 27/01/2021

Prediction-Error Negativity in Physical Human-Robot Collaboration

by

Stefano Aldini

A thesis submitted in partial fulfilment of the requirements for the
degree of Doctor of Philosophy

Abstract

Robotic systems for physical Human-Robot Collaboration (pHRC) are often controlled using control systems based on the admittance or impedance of the system. The interaction forces exchanged between the robot and the human co-worker during pHRC may affect the human cognitive state. In pHRC systems, the human cognitive state is often neglected. It is hypothesised that admittance dynamics of the robot have an effect on the human co-worker's cognitive state which can be used to estimate the predictability of the robot behaviour, or simply called the robot predictability. By using an electroencephalogram (EEG) device, the brain activity of the human co-worker can be measured. A feature, called Prediction-Error Negativity (PEN), that can be found in the EEG signal and is visible in the Event-Related Potentials (ERP) has the potential to be used to objectively assess the robot predictability. This thesis addresses the following research question: can the human cognitive state be used to assess and improve the robot predictability during physical human-robot collaboration?

Firstly, the relationship between PEN and changes in the robot admittance is investigated. Changes in the robot admittance were the result of the introduction of resistive forces with first-order dynamics. An analysis of the ERP is performed in the time-domain, to determine whether different admittance dynamics result in different PEN amplitudes. It is found that admittance dynamics can modulate PEN and thus robot predictability. Secondly, six different machine learning classifiers are then compared for classification of PEN by using the data sets collected. A two-class classification problem and a three-class classification problem are formulated for the comparative study.

A Convolutional Neural Network (CNN) is found to perform best in both the formulated classification problems, when compared to the other classifiers tested. Thirdly, a singularity avoidance strategy is implemented in a practical pHRC robot and is chosen to assess whether PEN can be detected during pHRC in real applications. The relationship between PEN and human preferences is also investigated and confirmed. Finally, a PEN-based closed-loop control is implemented and it is found that this can reduce PEN by automatically tuning parameters in a singularity avoidance strategy.

Acknowledgements

This work would have been impossible without the aid and support of those around me.

Firstly, I am profoundly grateful to my supervisor Dist. Prof. Dikai Liu, who gave me the opportunity to work on this thesis. Thank you for the guidance and advice you have provided me with from the first day of my candidature, till the very end. I really appreciate this.

I would also like to thank my co-supervisor Dr. Marc Carmichael. You truly are an inspiration. Your passion for research is highly contagious and I consider myself very lucky to have had you as a mentor in my career and during the PhD. There are no words that could express my gratitude to the fullest, for the support you have given me.

I am also grateful to all the amazing people in the Robotics Institute in UTS. The culture of the institute creates one of the best work environments I have ever experienced. And it is the result of the great people that are part of it.

I would also like to thank my friends who supported me during these years. I cannot mention every single one of you, but I am sure you know who you are. Thanks to you I managed to push through challenging times. A special mention goes to my brother, friend and flatmate Massimiliano. Thanks for dealing with me even when I am close to deadlines.

Finally, I would like to thank my parents Iwona and Maurizio. I am so proud to be your son and I hope you know how much I love you.

Contents

List of Figures

List of Tables

Acronyms & Abbreviations

1D	One-Dimensional
2D	Two-Dimensional
3D	Three-Dimensional
ADL	Activity of Daily Living
ANOVA	Analysis of Variance
ASR	Artifact Subspace Reconstruction
BCI	Brain-Computer Interface
BMI	Brain-Machine Interface
BRI	Brain-Robot Interface
cHRI	Cognitive Human-Robot Interaction
CNN	Convolutional Neural Network
DDPG	Deep Deterministic Policy Gradient
DOF	Degree-of-Freedom
DLS	Damped Least Squares
EDLS	Exponentially-Damped Least Squares
EEG	Electroencephalogram
ERN	Error-Related Negativity

ERP Event-Related Potential

ErrP Error-Related Potential

FRN Feedback-Related Negativity

FIR Finite Impulse Response

GSR Galvanic Skin Response

GPR Gaussian Progress Regression

HR Heart Rate

HRI Human-Robot Interaction

IC Independent Component

ICA Independent Component Analysis

L-BFGS Limited-memory Broyden-Fletcher-Goldfarb-Shanno

L-SVM Linear Support Vector Machine

LDA Linear Discriminant Analysis

LR Logistic Regression

LSD least Significant Difference

LSL Lab Streaming Layer

ML Machine Learning

MLP Multi-Layer Perceptron

MoBI Mobile Brain/Body Imaging

MSE Mean Square Error

NN Neural Network

PEN Prediction-Error Negativity

pHRC	Physical Human-Robot Collaboration
pHRI	Physical Human-Robot Interaction
PSD	Power Spectral Density
RBF-SVM	Support Vector Machine with Radial Basis Function
RL	Reinforcement Learning
ROS	Robot Operating System
SD	Standard Deviation
SDA	Series Damper Actuators
SEA	Series Elastic Actuators
SEM	Standard Error of Means
sEMG	Surface Electromyography
SVM	Support Vector Machine
SVD	Singular Value Decomposition
VIA	Variable Impedance Actuator
vMMN	Visual Mismatch Negativity

Glossary of Terms

Admittance	Measure of how easily a force causes motion of a structure or system.
Class	Set of data having a property or attribute in common.
Cognitive	Related to mental processes.
Collaboration	The action of working with another human or robot to complete a task.
Collaborative robot	Robot designed to work in collaboration with a human operator.
Control system	System that directs and regulates the behaviour of robots.
Closed-loop system	System that is directed or regulated by a control system with an active feedback loop.
Data processing	The action of carrying out operations on data.
Data set	Collection of data.
Experiment	Scientific procedure to test a hypothesis.
Interaction	Reciprocal action or influence.
Interface	Device or program enabling the interaction between two systems.
Kinematic singularity	Robot configuration resulting in a non-invertible Jacobian matrix.
Operator	Person operating a robot system.
Negativity	Negative peak in the event-related potentials.
Participant	Person who takes part in the experiment.
Physiological signal	Signals generated by the human body.
Pipeline	Linear sequence of operations.
Predictability	The ability to be predicted.
Prediction error	Result of a mismatch between expected and real outcomes of a task.

Stimulus	Action that causes a reaction or response.
Target	Goal of the task.
Task	Work to be completed by human and/or robot.

Chapter 1

Introduction

1.1 Background

Information about the human cognitive state, and specifically the ability to predict, can be used to assess and adapt the interaction during physical human-robot collaboration. Human beings are highly adaptable and empowered by intellectual skills. On the other hand, robots feature mechanical power and follow mathematical models that lead to a controlled behaviour. When a human and a robot work together, the result is a human-robot system that embraces the strengths of both parties, but also adds complexity and safety challenges. Collaborative robots are also referred as cobots [13] and the market for cobots is expected to grow to a value of US$14.64 billion by 2027 [14].

Robots and humans can interact with each other in many ways. Physical Human-Robot Interaction (pHRI) happens when a human and a robot are in physical contact. The field of pHRI can have a wide range of scenarios. The nature of the contact and the collaborative task can help defining a more specific scope. Physical Human-Robot Collaboration (pHRC) defines a scenario in which a human operator and a robot are in contact (directly or through an object) and voluntarily exchange forces to accomplish a collaboration task. The human is fully or partially in control of the robot motions. This type of scenario includes applications with the physical contact happening by means of haptic devices or objects that are being manipulated, and with continuous exchange of forces. Examples of pHRC with industrial robots include a cobot for material handling [15], a

human-robot system for homokinetic joint assembly [16], a wearable robot tested for lifting and holding tasks [17] and a robot for abrasive blasting tasks [7]. A common application of pHRC is rehabilitation robotics and examples include a robot for hand rehabilitation [18], a lower-limb exoskeleton [19] and an exoskeleton to rehabilitate shoulder and elbow [20]. Figure 1.1 shows an example of application involving pHRC, with an operator controlling a robot in a collaborative task. In this case, the user is in physical contact with the handles mounted on the robot end-effector. The operator moves the robot through exchanged forces.

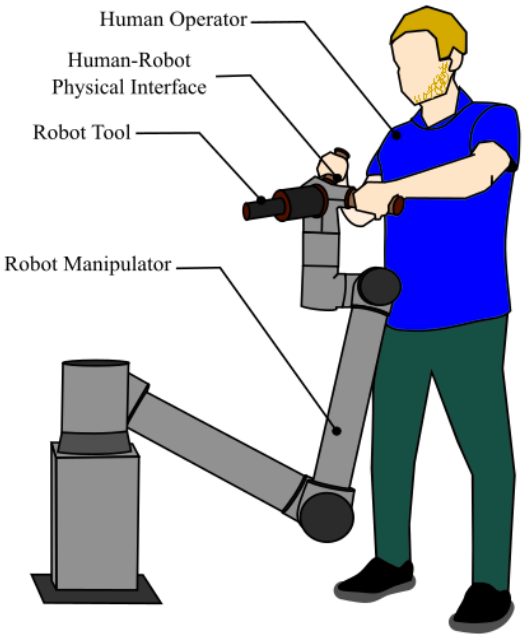

FIGURE 1.1: An example of pHRC application, with a human operator physically controlling a robot manipulator, for human-robot collaborative grit-blasting operations [1].

While traditional industrial robots prioritise accuracy, in the case of collaborative robots, safety and flexibility are often more critical. Impedance- and admittance-based controllers are usually used in pHRC applications [21, 22]. These controllers allow the use of the system impedance or admittance as a way to guide the operator through the workspace, encouraging and discouraging some directions and configurations. In the case of an admittance controller, repulsive or attractive forces can be easily introduced in the control loop. For example, if a resistive force is introduced along a specific direction of motion, the robot will present a lower admittance in that direction. This strategy can be used to guide the robot operator away from undesirable configurations such as singularities and self-collisions. A lower admittance means that the operator has to exert bigger

forces to maintain a given velocity and this usually discourages the operator from moving towards areas or configurations with lower admittance.

In many applications, other strategies are implemented in conjunction with the main control loop, such as singularity and collision avoidance and variable assistive paradigms [23–26]. Therefore, the resulting robot motions not only depend on the interaction force with the operator, but also on the combined result of the implemented strategies. As a consequence, the human operator often feels a variable admittance throughout the robot workspace. Since there is generally no feedback to the user about the varying admittance other than through the interaction force itself, this provides an avenue to study the effect of the admittance dynamics on the predictability of the robot behaviour. Dynamics of the human-robot interaction define the way the human intention is transferred to robot actions. Interaction forces represent the human intention, while robot motions represent the actions. Therefore, in this thesis, the interaction dynamics refer to the admittance dynamics of the robot [27]. For the sake of clarity, predictability is defined as the ability to be predicted. Hence, the predictability is not a property of the human operator, but a property of the collaborative robot. Being the robot admittance the relationship between human forces and robot velocities, it represents the link between human intention and robot actions. And being the predictability the result of how well human intention is translated into robot actions, the robot admittance and predictability may be related.

A recent work by Maurice et al. suggested that when manipulating complex objects, humans try to increase the predictability of the task [28]. People constantly try to predict the outcomes of tasks that they are performing [29]. This ability is the result of past experiences. In pHRC, the relationship between the admittance dynamics and the robot predictability is not clear, as no other study estimated the predictability of a pHRC robot in a quantitative way. Consequently, a rigorous mathematical approach for designing and tuning the control system is often too complicated. The robot predictability perceived by a person can however be estimated through a specific feature found in the Event-Related Potentials (ERP) [30], by using an electroencephalogram (EEG) [31]. The feature is known as Prediction-Error Negativity (PEN) [32] and is part of a family of negativities called Error-related Potentials (ErrP) or Error-Related Negativities (ERN). As PEN is caused by a mismatch between human internal models and reality, this feature is believed being directly related to predictability. PEN estimates the predictability that is perceived by a person.

Recently, there has been interest in trying to integrate robot systems with Brain-Machine Interfaces (BMI). Previous works tried to integrate the detection of ERN in human-robot interaction. Iturrate et al. [33, 34] performed an experiment in which participants were asked to judge whether a robot was performing an action correctly. They found a negativity in the ERP around 400ms following an incorrect action and implemented a reinforcement learning method to reduce the ERN. Penaloza et al. [35] used the ERN invoked by the observation of an unexpected action, to trigger safety measures in a robot during a navigation task. More recently, Ehrlich et al. [36] detected an ERN during human-robot social interaction and Salazar-Gomez et al. [37] used an ERN while a human operator supervised a robot. Salazar-Gomez et al. also used reinforcement learning to close the robot control loop on the human cognitive state and reduce the ERN.

In all the above-mentioned works, the operator was not in physical contact with the robot. There are several issues related to the use of EEG for interactions that require active motor movements. EEG is extremely impractical for real-world applications, given the current state of related hardware. This technology is however continuously improving. The work presented in this research is the first attempt at trying to use an ERN, and specifically PEN, to assess and improve the interaction during pHRC.

Understanding how pHRC control strategies affect the cognitive state of the operators can help improve the human-robot interaction. Collaborative robotics is a growing field especially in applications like rehabilitation and skill augmentation for physically demanding jobs. We are living in an aging society which has to address issues raised by human limits and disabilities, both physical and cognitive. Physically demanding tasks also introduce physical requirements to the operator that has to perform them, often leading to gender- and age-specific jobs. This results in a challenge for companies and organizations that try to ensure a workplace with fair and equal opportunities for everyone. This research aims also at building fundamental knowledge about some cognitive features, that can help in a better understanding of some neurological processes. In general, industries that benefit from collaborative robotics will also benefit from the results of this research.

1.2 Research question

The way robots and humans work together can be improved. There are several approaches to the problem, but one way of addressing this is to focus on the operator, rather than on the robot.

The human co-worker introduces many variables which are hard to predict in a human-robot system for pHRC. Currently, the human co-worker is usually seen as something external to the robot system, that has to be measured and taken into account: the user is in fact often regarded as part of the environment. In pHRC, commonly used sensors are force/torque sensors, RGB-D cameras and proximity sensors. These sensors measure quantities that are happening at a physical level, such as interaction forces and distance, as a consequence of an action. The human operator is however also able to sense and perceive. Humans plan their actions using internal models of the world. These models are continuously updated with new data coming from their sensorimotor system. Information about the human state is encoded within the human body and may be retrievable by analysing biological signals. Moreover, robot control strategies are generally not tuned for a specific human operator, but are usually targeted to generic operators.

It is still not clear what kind of information can be used to improve the human-robot interaction for a specific user, and this research aims at addressing the following question:

(Q) Can the human cognitive state be used to assess and improve the robot predictability during physical human-robot collaboration?

In particular, the expected final outcome of this research is a human-robot system that uses the human cognitive state, and more specifically PEN, as an input to dynamically adjust the behaviour of the interaction.

To the best of the author's knowledge, using PEN for assessing or improving pHRC has not been addressed before. This work will not only contribute to knowledge in the fields of neuroscience and pHRC, but will build a bridge between those two domains.

1.3 Research sub-questions and methodology

To answer the research question the following sub-questions have been identified:

Q1: What is the relationship between PEN and a change of the robot mechanical admittance that is caused by first-order resistive forces?

Q2: Can PEN be estimated with machine learning classifiers, and what classifier performs the best?

Q3: Can PEN be detected and used during real pHRC?

To address the research sub-questions the following research methodology was implemented.

1.3.1 Relationship between PEN and a change of the robot admittance caused by first-order resistive forces

Human beings are particularly complex biological systems. One specific cognitive feature, called PEN, was investigated in this thesis. The first step was to study the cognitive feature of interest through a controlled experiment with as few variables as possible. Variables such as the directions of motion allowed in the task and the nature of interaction forces were therefore limited. The experiment involved a one-dimensional (1D) task called the "swing game" (Section 3.2.2.1) and four conditions were used to analyse the effect of a first-order resistive force on the cognitive state, in case of expected and unexpected stimuli. The four conditions represented the onset of an abrupt unexpected resistive force, an abrupt expected force, a smooth unexpected force and a smooth expected force. As PEN is related to the predictability, visual and force stimuli are combined to create the four conditions. The task was then extended to a two-dimensional (2D) task to test the validity of results in a more complex task.

1.3.2 Classification of PEN through machine learning classifiers

In order to use PEN in a human-robot system that can adapt the control in a timely manner, a proper classifier had to be selected. Six classifiers with different complexity were compared and their performances were evaluated. The six classifiers compared in this thesis are the following: Linear Discriminant Analysis (LDA), Logistic Regression (LR), Support Vector Machine with a linear kernel (L-SVM), Support Vector Machine with a Radial Basis Function kernel (RBF-SVM), Multi-Layer Perceptron (MLP) and Convolutional Neural Network (CNN). A classification problem is the process of classifying instances into a number of classes. The classification problem

was initially addressed as a two-class problem in the case of an application requiring an acceptable and unacceptable PEN level. A three-class problem was also investigated in the comparative study.

1.3.3 Detection and application of PEN during real pHRC

Control strategies for practical pHRC are often subtle and present more complex dynamics than a simple first-order resistive force. An Exponentially Damped Least-Squares (EDSL) strategy for singularity avoidance was chosen to see whether PEN can be detected in practical pHRC. An experiment was used to assess PEN in pHRC during movements in the 3D robot workspace. Human preferences for control parameters used in the EDLS strategy were also investigated, to see whether there is a relationship between PEN and the participants' preference. A PEN-based closed-loop control is implemented to reduce PEN by automatically tuning parameters in a singularity avoidance strategy.

1.4 Consideration of ethics and risks

Since this research includes experiments involving human participants, risks have been addressed. Experiments presented in this research involve procedures approved by the UTS Ethical Committee with approval numbers ETH15-0038 or ETH18-2732.

1.5 Publications

1.5.1 Directly related publications

- Stefano Aldini, Ashlesha Akella, Avinash K Singh, Yu-Kai Wang, Marc Carmichael, Dikai Liu, and Chin-Teng Lin. Effect of Mechanical Resistance on Cognitive Conflict in Physical Human-Robot Collaboration. In *Proceedings of the 2019 IEEE International Conference on Robotics and Automation (ICRA)*, pages 6137–6143, Montreal, Canada, 2019. ISBN 9781538660263

- Avinash Kumar Singh, Stefano Aldini, Daniel Leong, Yu-Kai Wang, Marc Gary Carmichael, Dikai Liu, and Chin-Teng Lin. Prediction Error Negativity in Physical Human-Robot

Collaboration. In *Proceedings of the IEEE 8th International Winter Conference on Brain-Computer Interface*, Seoul, Korea, 2020

- Stefano Aldini, Avinash K Singh, Daniel Leong, Yu-Kai Wang, Marc G Carmichael, Dikai Liu, and Chin-Teng Lin. Detection and Estimation of Cognitive Conflict During Physical Human-Robot Collaboration. *IEEE Transactions on Cognitive and Developmental Systems*, Submitted

- Stefano Aldini, Avinash K Singh, Marc Carmichael, Yu-Kai Wang, Dikai Liu, and Chin-Teng Lin. Prediction-Error Negativity to Assess Singularity Avoidance Strategies in Physical Human-Robot Collaboration. In *Proceedings of the 2021 IEEE International Conference on Robotics and Automation (ICRA)*, Xi'an, China, 2021

1.5.2 Indirectly related publications

- Richardo Khonasty, Marc G Carmichael, Dikai Liu, and Stefano Aldini. Effect of External Force and Bimanual Operation on Upper Limb Pose during Human-Robot Collaboration. *The proceedings of the Australasian Conference on Robotics and Automation (ACRA)*, 2017

- Marc Garry Carmichael, Stefano Aldini, and Dikai Liu. Human user impressions of damping methods for singularity handling in human-robot collaboration. In *Australasian Conference on Robotics and Automation, ACRA*, 2017. ISBN 9781510860117

- Stefano Aldini, Marc G Carmichael, and Dikai Liu. A Risk Reduction Framework for Design of Physical Human-Robot Collaboration. In *Australasian Conference on Robotics and Automation, ACRA*, Adelaide, Australia, 2019

- Marc G. Carmichael, Stefano Aldini, Richardo Khonasty, Antony Tran, Christian Reeks, Dikai Liu, Kenneth J. Waldron, and Gamini Dissanayake. The ANBOT: An Intelligent Robotic Co-worker for Industrial Abrasive Blasting. In *Proceedings of the 2019 IEEE International Conference on Intelligent Robots and Systems (IROS)*, 2019

- Marc G. Carmichael, Richardo Khonasty, Stefano Aldini, and Dikai Liu. Human Preferences in Using Damping to Manage Singularities During Physical Human-Robot Collaboration. In *Proceedings of the 2020 IEEE International Conference on Robotics and Automation (ICRA)*, Paris, France, 2020

- Stefano Aldini, Yujun Lai, Marc G Carmichael, Gavin Paul, and Dikai Liu. Real-time Estimation of the Strength Capacity of the Upper Limb for Physical Human-Robot Collaboration. In *Proceedings of the 43rd Annual International Conference of the IEEE Engineering in Medicine and Biology Society (EMBC)*, Guadalajara, Mexico, 2021. Submitted

1.6 Thesis outline

This thesis is organised as follows:

Chapter 2

In Chapter 2, a review of related works is presented. Robot systems for pHRC, and in particular the ones that use physiological signals, are reviewed. Following, works related to ERN, especially the ones that use them in robotics, are presented.

Chapter 3

Chapter 3 evaluates whether PEN can be identified during pHRC tasks and whether it can be modulated by different robot admittance dynamics. Resistive forces used to study PEN presented first-order dynamics. The task was initially 1D, but was then extended to a 2D task to validate results in multi-dimensional tasks.

Chapter 4

Chapter 4 discusses methods to estimate online PEN. Six classifiers with different complexity were compared. The problem was first addressed as a two-class problem. In this case, the data could only present PEN or not. The problem was then extended as a three-class problem, with two levels of PEN and no PEN.

Chapter 5

In Chapter 5, an experiment is implemented to test PEN in case of a practical pHRC control strategy in the 3D workspace. A EDLS singularity avoidance strategy was chosen as the application. Two modes resulting from two sets of parameters were compared. PEN was analysed for the two modes and compared to human preferences. A a closed-loop system was implemented, which uses PEN to automatically adjust parameters of the EDLS strategy for singularity avoidance.

Chapter 6

Chapter 6 outlines the conclusion of this research, with its limitations, and the future work that could be done to progress further the knowledge in this field.

Chapter 2

Review of Related Work

Robots designed to physically interact with humans are becoming common in various application areas. Not only can collaborative robots, or cobots [13], operate in proximity to humans, their ability to work in direct physical contact leads to exciting applications. This kind of robot can be particularly helpful for hazardous tasks or if human skills are not enough to perform and complete a task. Robot capabilities such as strength and repeatability can be merged with flexibility and reactivity of humans, creating a human-robot system which combines at the same time mechanical power and intellectual skills.

Collaborative robots are robots specifically designed to interact with humans. Human-Robot Interaction (HRI) can be classified through the means of the interaction: cognitive Human-Robot Interaction (cHRI) and physical Human-Robot Interaction (pHRI) [42]. The first focuses on mental models and communication between the robot and the operator. Mutlu et al. offers an extensive review of the field and research done in cHRI [43]. If a human and a robot are physically in contact, exchanging forces in a shared workspace, their interaction is classified as pHRI. For the sake of clarity, this research investigates cognitive effects, but related to a physical interaction between human and robot.

The idea of using pHRI to augment human skills and to address challenges in industrial processes has been explored for decades [44]. Human presence in the robot workspace makes pHRI one of the most challenging research topics [45], and the use of robots that physically interact with

operators in industrial applications is gaining a lot of interest [14]. Nowadays, several robot manufacturers offer robotic platforms which can be safely used for collaborative applications [46].

As mentioned in Chapter 1, physical Human-Robot Collaboration (pHRC) is a specific type of pHRI, in which the human willingly exchanges forces with the robot to guide its motions, to accomplish a task. In this chapter, the relevant research and works are reviewed. The field of pHRC is reviewed in Section 2.1, justifying the current interest in this growing field of robotics.

In the case of physical interaction with a human operator, the robotic system has to operate with a constantly changing factor, the human. This raises the question of whether the robot should then adapt their behaviour accordingly. In order to adapt the behaviour of the robot to the human state, a state change has to be detected. Human beings are highly variable complex systems. Section 2.2 reviews the technology used in robotics to assess the human state.

Due to the complexity of EEG signals, there is a specific field that studies ways to integrate brain activity with robots. Systems in this research domain are called Brain-Robot Interfaces (BRI), and they are usually regarded as a subset of Brain-Machine Interfaces (BMI) and strongly related to Brain-Computer Interfaces (BCI). Section 2.3 reviews the current state of this technology.

Event-Related Negativity (ERN) is a family of features that can be identified in the EEG signals. The feature used in this research is part of these negativities and Section 2.4 provides the reader with a background on this specific feature.

Section 2.5 justifies the research covered by this thesis, as the current state of the knowledge presents a gap.

2.1 Physical human-robot collaboration

The main challenges in pHRC are to ensure safety and to have an intuitive interaction that can take full advantage of the operator's skills [47]. Lately, extensive work has been done to develop hardware that aims at a safer human-robot interaction [48–51]. In the last decade, several robotics manufacturers have developed industrial robots designed to operate in proximity with humans: for example, UR3, UR5 and UR10 (and their E-Series) by Universal Robots [52], Baxter and Sawyer by Rethink Robotics [53], the ABB YuMi [54], and the KUKA LBR iiwa [55]. In Figure 2.1,

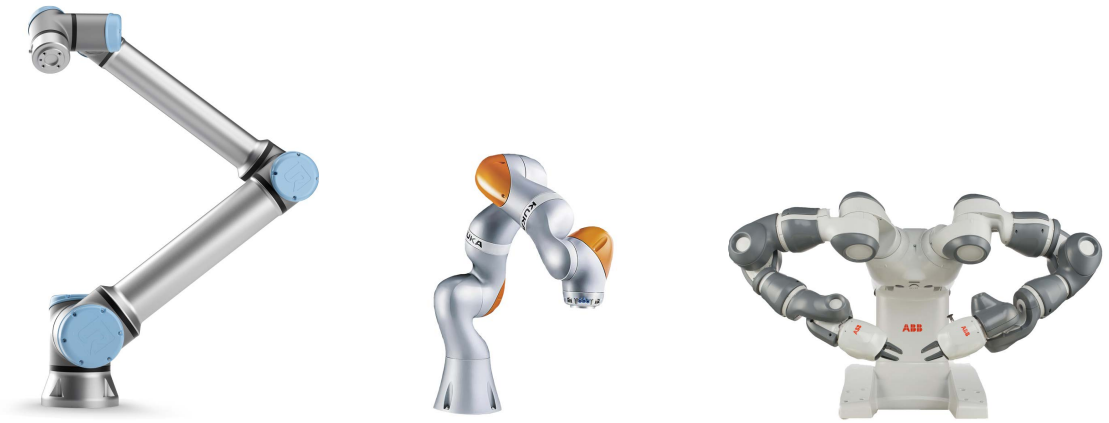

(A) UR10 (B) Kuka LBR iiwa (C) ABB YuMi

FIGURE 2.1: Examples of collaborative robots: Universal Robot UR10 [2] (A), Kuka LBR iiwa [3] (B) and ABB YuMi [4] (C).

examples of collaborative robots are shown. The release in 2016 of the Technical Specification for collaborative robots by the International Organization for Standardization [56] shows the growing interest in this kind of technology.

Collaborative robots have a different focus in terms of characteristics when compared to traditional industrial robots. Collaborative robots have joint torque sensors that allow to isolate and compensate the robot dynamics, independently from the task. This also allow to put in place safety measures based on applied torques. Traditional robots have to use high control gains to compensate the robot dynamics and at the same time control the endpoint to perform the task. By having gains that can be set specifically for the task, without affecting the compensation of the robot dynamics, collaborative robots are more flexible in terms of control gains for the task. Traditional industrial robots present high stiffness, inertia, mechanical power and, most importantly, high accuracy. For complex tasks however, especially if a physical interaction is foreseen, accuracy might be of secondary importance. Within a highly variable environment, flexibility is pivotal and robots controlled with traditional approaches are not suitable, unless the motion within the task is accurately planned. Control systems based on interaction forces are more adaptable than position- or velocity-based ones [57]. This is due to the fact that it is possible to model a desired behaviour and set a level of compliance or impedance for the robot during the interaction. For example, in the case motions in specific directions have to be discouraged, these directions will have a lower compliance or higher impedance, when compared to the directions in which motions

are encouraged. While it is possible to control traditional robots with force-based control systems, the high inertia and stiffness, typical of traditional robots, represent an issue in terms of safety.

Safety is one of the main challenges in pHRC, due to the continuous contact and the energy exchanged between robot and human operator. The International Standard ISO 10218 presents standard requirements for industrial robots [58, 59]. This standard represents the main document about safety related to industrial robotics, but it is quite generic and only partially addresses collaborative robots. A Technical Specification was only released in 2016, to extend specific requirements presented in ISO 10218 about collaborative robots [56]. Lasota et al. [60] presents a review of works about safety strategies applied in pHRC. Most of the reviewed works are for industrial collaborative tasks and they take advantage of traditional sensors, e.g. cameras, load cells and proximity sensors. A framework to reduce the risk and targeted to pHRC robots was proposed in Aldini et al. [40].

Impedance- and admittance-based control systems and their variants are the most common controllers used in pHRC [21]. They focus on modeling the interaction in terms of impedance/admittance, as a combination of stiffness and damping. Recently, many studies focused on adapting the admittance or impedance of mechatronic systems. Examples of adaptive systems include Variable Impedance Actuators (VIAs), Series Elastic Actuators (SEAs) and Series Damper Actuators (SDAs). Vanderborght et al. [48] offers a good review and classifications of these devices. Their design can be quite complex and the same review also mentions that it is possible to achieve the behaviour of a VIA by software control.

As pHRC becomes more mature, this technology is being applied to a wider spectrum of applications. Common application scenarios for pHRC still fall in the categories covered by the next two sections: industrial collaborative robots (Section 2.1.1) and robots for rehabilitation and service robots (Section 2.1.2).

2.1.1 Industrial collaborative robots

Exoskeletons are a typical example of pHRC. In a literature review about exoskeletons used in industrial applications, out of the 40 papers extracted, 18 were published in 2010 or later, showing the current interest in pHRC for industrial applications [61]. For example, the Berkeley Lower

Limb Exoskeleton (BLEEX) is designed to be worn to provide additional carrying capacity [62]. The ABLE exoskeleton is instead designed to assist in overhead operations for car manufacturing [63].

Other examples of pHRC with industrial robots include a cobot for material handling [15], a human-robot system for homokinetic joint assembly [16] and a wearable robot tested for lifting and holding tasks [17]. The ANBOT is another example of an industrial collaborative robot and was designed for abrasive blasting tasks [7].

2.1.2 Rehabilitation and service robotics

The International Organization for Standardization defines a service robot as a "robot that performs useful tasks for humans or equipment excluding industrial automation applications" [64]. This might include rehabilitation robots, but these have the specific goal of recovering deteriorated skills and delivering a restorative therapy [65]. For example, robots that help with Activities of Daily Living (ADLs) [66] do not necessarily have the goal of recovery, but might be used to help people in regaining independence from their carer, in which case they are classified as service robots. Applications of service robotics include, cooperative load carrying [67, 68], and feeding [69].

Since the main objective of pHRC is to overcome human limits, a popular application is to overcome physical limits induced by disabilities and impairments. Gassert and Dietz [70] present a recent review on rehabilitation robots for treating sensorimotors impairments. Examples of rehabilitation robots include a robot for hand rehabilitation [18], a lower-limb exoskeleton [19] and an exoskeleton to rehabilitate shoulder and elbow [20]. The MIT-Manus is another example of a pHRC robot [71]. It is a planar robot designed for the rehabilitation of elbow and shoulder.

As rehabilitation systems aim at the recovery of patients, an estimation of the human state can provide useful information that can be used for assessing the recovery or modulating the therapy. Badesa et al. [72] used physiological signals to adapt the rehabilitation therapy provided with a MIT-Manus. Schindelholz and Hunt [73] used the heart rate to control a robotics-assisted treadmill exercise for rehabilitation purposes. More works that use physiological signals in robot systems are discussed in the next section.

2.2 Physiological signals for control of robots

People in the robot workspace have priority in terms of safety, and monitoring their state could anticipate and prevent new hazards. In fact, human errors represent the most variable and unexpected hazards. The ability of human operators to predict events, given their experience and knowledge, can greatly reduce the risk associated with a collaborative system. An inherent challenge during pHRC is the high variability and complexity of the human behaviour, both psychological and physiological. With shared interests in providing “close, safe, and dependable physical interaction between human and robot" [74], many are researching strategies to estimate the state of human collaborators.

Affective control is a control strategy that takes into account the human affective state. To get information about the physical and mental state of the operator, a set of specific sensors is required. Sensors that measure biomedical parameters are not completely new in robotics, but are often used in rehabilitation robotics to measure the effects of robot-aided therapies. Human physiology has been shown to contain high variability [75, 76] due to the complex nature of the human body.

Biomedical devices that can measure physiological parameters are becoming more reliable, less expensive and more user-friendly. Several research groups are looking into integrating those devices in robot systems to provide an estimation of the human state. During the interaction, Galvanic Skin Responses (GSR) can be used to measure engagement [66] and comfort [77]. Arai et al. [78] used skin potential response signal to measure stress in the operator. Devices to measure the Heart Rate (HR) are more common and have been extensively used to measure the human state. For example, Rani et al. [79] and Villani et al. [80] used the heart rate to estimate the psychological stress. The heart rate is however affected by many factors, physical and psychological. Combinations of more than one biological signal are used by [81–83]. In particular, Kulic et al. [81] used a combination of skin conductance response, heart rate, and corrugator muscle response.

Surface electromyography (sEMG) measures muscle activity and it is a popular technology to assess the human state due to its accessibility [84]. While sEMG data may provide partial indicators for human strength capacity, the non-linearity for muscle activation and muscle contraction dynamics in human bio-mechanics is challenging for researchers [85]. Muscle activity is usually used to estimate fatigue or strength capacity. Peternel et al. [86] used sEMG for an adaptive control of an

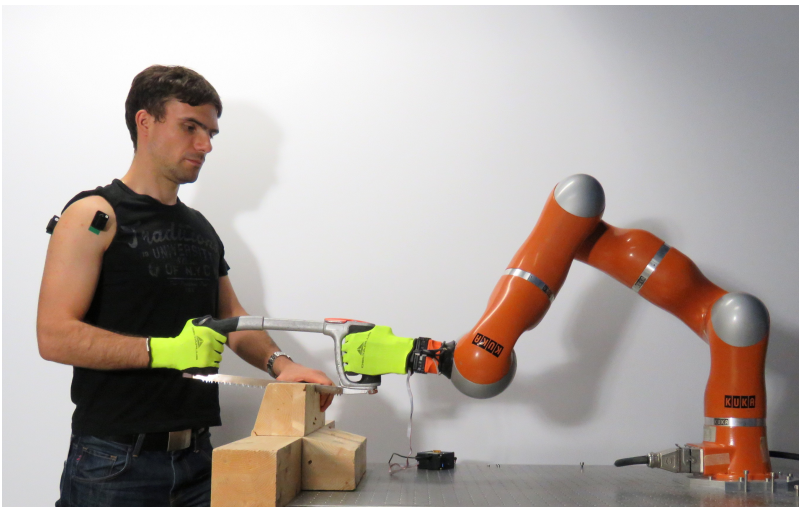

FIGURE 2.2: A robot using sEMG to collaborate with a human co-worker [5].

exoskeleton. With the aim of estimating and managing muscle fatigue in pHRC, Peternel et al. [87] used a complex bio-mechanical model offline to train a Gaussian Progress Regression (GPR) that could map joint configurations and end-point forces (on the hand) to muscle forces. In Figure 2.2, Peternel is pictured while collaborating with a robot that uses sEMG measurements. The online system would then use the obtained GPR-based model. This system still requires the human joint configuration and the interaction forces with the robot. More recently, the estimation of strength capacity has been framed as a transfer learning and deep learning problem, using sEMG to train the deep neural networks [88]. Li et al. [89] offers a recent review of HRI systems that use sEMG signals. A limitation of EMG signals, when compared to EEG signals, is the limited information that muscle activity present. While muscle activity carries information about an action that is underway, brain activity ideally presents information about the current cognitive state, together with planned actions and intentions. The current state of the hardware makes decoding brain activity a big challenge. In the long run, exploring EEG technology can however result in more benefits as opposed to EMG.

2.3 Brain-robot interfaces

Electroencephalographs (EEGs) are devices that measure the electrical activity from the brain with a high temporal resolution, compared to other existing devices for physiological measurements. EEG has been extensively used in cognitive science research [90] and for designing Brain-Robot

Interfaces (BRIs) [91]. BRIs are often used to open a new channel that helps specific operators controlling a robot. Those operators usually present disabilities or physical impairments that jeopardise their ability to control a robot. Wheelchairs are among the most common BRI systems, thanks to their very limited Degrees-Of-Freedom (DOFs) [92–95]. In this case signals coming from the EEG are converted in commands and directions of motion, such as turn left or turn right. Manipulators are also used in BRI but again with very limited DOFs [96–99]. In the case that manipulators have a high number of DOFs, the interface is then limited by the tasks. For example, Hortal et al. developed a manipulator able to reach four points in the workspace [100]. The BRI was able to successfully discriminate which of the four points the user wanted to reach in 70% of the trials. In their review, Mao et al. [91] present several BRI systems applied to humanoid robots, but admitted the great limitations due to the complexity of those systems. All these works aim at controlling the robot with EEG signals, which then limit the number of DOFs of the robot or of the task due to the complexity. None of those work use the EEG signal as a form of support to an already functioning system.

The recent interest in using BMIs in robotics, justified the release of two software packages in Robot Operating System (ROS), as middleware between technologies used in the field of BMIs and robotics [101].

2.4 Error-related negativity

As suggested by the previous section, EEG data contain valuable information about the human state and the operator's cognitive processes. Human internal models are the result of a cognitive process that simulates a task to predict its outcome [102]. A mismatch between internal models and reality causes a phenomenon called cognitive conflict or prediction error [103]. Humans have internal models of the world and use them to predict outcomes of every single task, including new ones. To have internal models proven wrong, there is no need for the human to be an expert in that task. With a new task it is likely that a person will experience more prediction errors. If a person changes the way a task is executed, they will still have an internal model that anticipates the outcome of the new task execution. Internal models can always be proven right or wrong, depending on whether expectations are met or not. For the sake of clarity, cognitive conflict is not necessarily related to the cognitive burden due to a complex task.

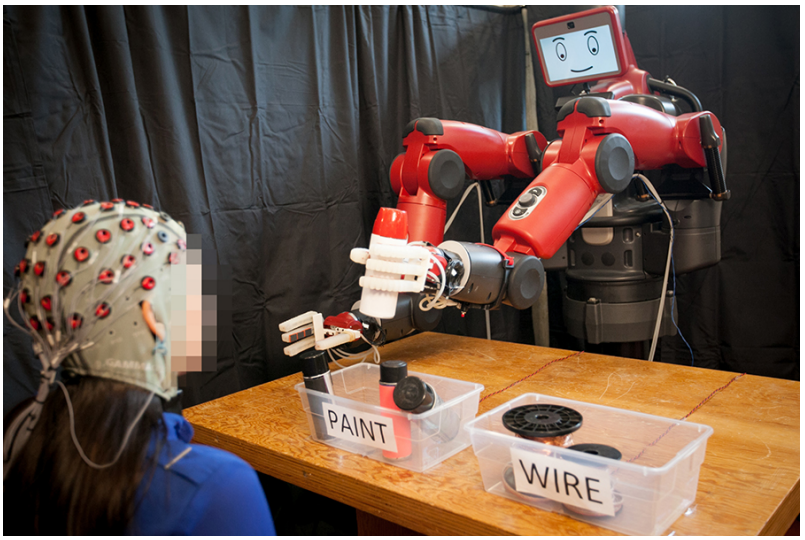

FIGURE 2.3: A Baxter robot using EEG data from a human co-worker to correct its actions during a task [6].

People are constantly trying to predict the outcome of the tasks that they are performing [29]. Using an EEG device, Falkenstein et al. [104] noticed a negative peak in the Event-Related Potential (ERP) [30] which is known as Error-related Potential (ErrP) or Error-Related Negativity (ERN). Visual Mismatch Negativity (vMMN) [105], N2 or N200 [106], Feedback-Related Negativity (FRN) [107] and Prediction-Error Negativity (PEN) [32] are all part of the same family of negativities and are caused by erroneous behaviour of tasks. Among those different types of ERN, PEN appears before terminal external error information. This suggests that PEN is indicative of predictive processes in the evaluation of errors. Moreover, PEN is evoked in tasks in which participants are actively involved in Mobile Brain/Body Imaging (MoBI) settings [108], while other negativities are evoked in tasks in which participants passively observe the erroneous behaviour. PEN is a novel form of bio-marker invoked at 50-250ms after the onset of a prediction error [32].

Past works tried to integrate the detection of ERN in human-robot systems. Penaloza et al. [35] used ERN to trigger safety measures in a robot during a navigation task. The negativity was invoked by observation of unexpected actions. In Iturrate et al. [33, 34], participants were asked to watch a robot perform a task and judge whether it was performing the action correctly. A negativity was found in the ERP around 400ms following incorrect actions. The same work also presented a reinforcement learning (RL) method to reduce the negativity. Ehrlich et al. [36] addressed ERN

during human-robot social interactions and Salazar-Gomez et al. [37] studied ERN while participants supervised a robot. Salazar-Gomez et al. also used an RL algorithm to close the robot control loop on the human cognitive state and reduce the negativity. In Figure 2.3 a participant is seen performing the experiment in [37].

In all the above-mentioned works, the operator was not in physical contact with the robot. There are several issues related to the use of EEG for interactions that require active motor movements. Limb motions introduce artifacts and confounding factors that make the processing of brain signals more difficult [109].

2.5 Summary

Robots for pHRC have to work in physical contact with a constantly changing agent, the human. The technology surrounding pHRC is quickly evolving, allowing new applications for this type of system. Safety is one of the main concerns in robots that have to work so close to humans. Control strategies that prioritise safety and flexibility over accuracy are a common choice in pHRC.

Physiological data can help in estimating the human state, but the complex nature of biological systems represents a challenge that is not easy to overcome. Artifacts and the complexity of the human body make it hard to isolate specific variables or information. This is particularly true for EEG signals. EEG signals present in fact a very poor signal-to-noise ratio, especially when associated with tasks that involve active motor movements.

PEN is a feature retrievable in EEG signals and corresponds to prediction errors. By using PEN it is possible to estimate the predictability of a collaborative robot, from the human co-worker's perspective. To the best of the author's knowledge, no one has ever used PEN in pHRC applications due to the issues related to the quality of the EEG signal during active motor movements. The three sub-questions identified in Section 1.3 aim at exploring the feasibility of using PEN as a measure of predictability in pHRC.

In this research, the effect of motor effects and confounding factors are overcome through signal processing methods and machine learning classifiers. The use of PEN is proposed to assess the

predictability of the robot behaviour, while the robot physically interacts with a human co-worker. This information can then be used to adapt the interaction during pHRC tasks.

Chapter 3

Effect of First-Order Resistive Forces on Prediction-Error Negativity During Physical Human-Robot Collaboration

3.1 Introduction

In pHRC, the human and robot mostly base their interaction on force exchange. In this research, an admittance controller is used, but the findings of this work can also be applied to impedance controllers, as the impedance is the reciprocal of the admittance. It is hypothesised that the way human forces are transformed into robot motions affects the cognitive state of the user.

As mentioned in previous chapters, when people perform a task, they constantly try to predict its outcomes [29]. In pHRC systems, admittance changes are not usually anticipated by visual cues. This makes the admittance dynamics hard to predict, and it consequently affects the predictability of the robot behaviour.

In this chapter, sub-question Q1 (Section 1.3.1) is addressed. The relationship between a change in the robot admittance and PEN is explored here. PEN is a feature that can be found in the EEG signal, as a sign of a prediction error (i.e. mismatch between the expected robot behaviour and the actual robot behaviour). PEN is an estimation, from the human co-worker's perspective, of the

predictability of the robot behaviour. As this is the seminal work investigating PEN in pHRC, the admittance change is the result of the introduction of resistive forces with first-order dynamics.

In Section 3.2, the methodology is described. Results and discussion are presented in Section 3.3. Section 3.4 discusses limitations of experiments and results and Section 3.5 draws conclusions given the results.

One of the experimental tasks detailed in this chapter was presented with preliminary results in two conference papers [1, 9]. In [1], results about the relationship between resistive forces and PEN were presented in the case of the first experiment here detailed (Experiment 1 - Exp1). At that time, only four participants undertook the experiment. In subsequent work [9], results were extended to ten participants who performed Exp1, with the research focus being on the processing pipeline, and a statistical analysis on the results was carried out. In this chapter, results for Exp1 were obtained with eleven participants and results for Exp2 were obtained with two participants. The results presented in this chapter were included in a journal paper submitted to IEEE Transactions on Cognitive and Developmental Systems [8].

3.2 Methodology

A repetitive task creates human internal models that allow people to predict the outcome of the task. If the task has a different outcome than the predicted one (the internal models are proven wrong), a prediction error should be invoked. This is the idea behind the experiments to be conducted in this research. In this section, the methodology implemented to evaluate the relationship between PEN and first-order resistive forces is presented.

3.2.1 Experimental setup

The robotic test-bed for the experiments is the ANBOT [7] and is pictured in Figure 3.1A. It is developed for collaborative grit-blasting tasks and features a UR10 manipulator by Universal Robots. The operator is in direct physical contact with the robot through the handlebars mounted on the end-effector, as shown in Figure 3.1B. On each of the handles, there is a three-position switch that was used for the experiments. A six-axis force-torque sensor is mounted between the

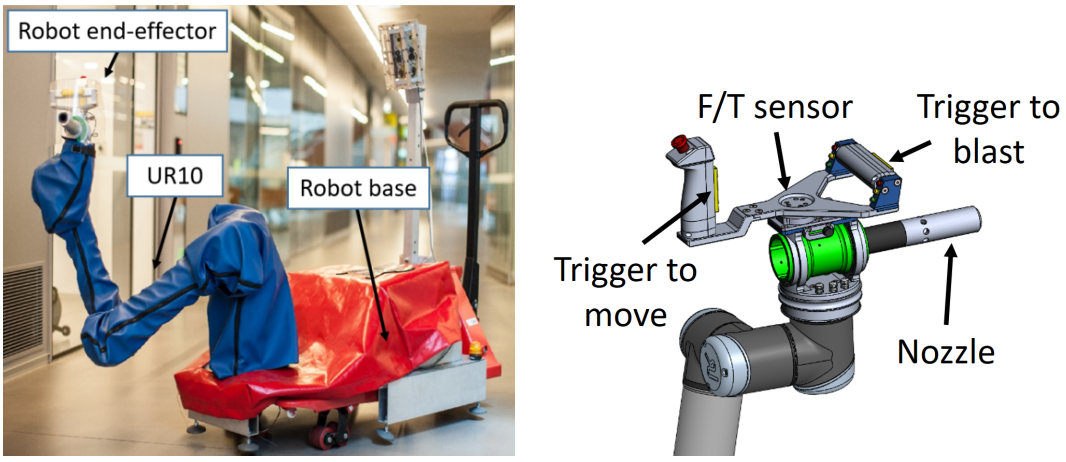

(A) ANBOT system (B) Robot end-effector

FIGURE 3.1: The ANBOT system [7] (A) and its physical interface (B).

robot end-effector and the robotic arm to measure the interaction forces. A different setup could have been used for the purpose of this research, e.g. a steering system of a car. A robotic system with multiple degrees-of-freedom (DOF) results however in more flexibility in terms of the task design.

An experimental task (Section 3.2.2) is defined that requires participants to operate the robot whilst brain activity is measured. To reduce potential artifacts and disturbances affecting the cognitive state, the task was initially designed to be as simple as possible, then extended to a more complex task. The motion was initially limited to one direction in Experiment 1 (Exp1). Exp1 was then extended to a planar task in Experiment 2 (Exp2) to see whether the findings from the one-dimensional (1D) case are also valid in a two-dimensional (2D) scenario. Robots for pHRC usually aim at giving as much flexibility as possible to the human co-worker, therefore a task with limited directions of motion might represent an unrealistic task for pHRC applications. The direction of motion has however an impact on the EEG signals [110], and this is the reason behind experiments with limited dimensions. The use of a 6-DOF robot arm is justified by the intention to move this research towards a pHRC task involving free motions in the three-dimensional (3D) space.

A 32-channel wireless EEG device named MOVE (Brain Product GmbH, Germany) is used to measure brain activity. The placement of the EEG electrodes is consistent with the 10-20 international system [111]. The contact impedance is maintained below 25kΩ with a sampling rate of 1000Hz. In Figure 3.2, a human operator is using the ANBOT while their brain activity is being recorded.

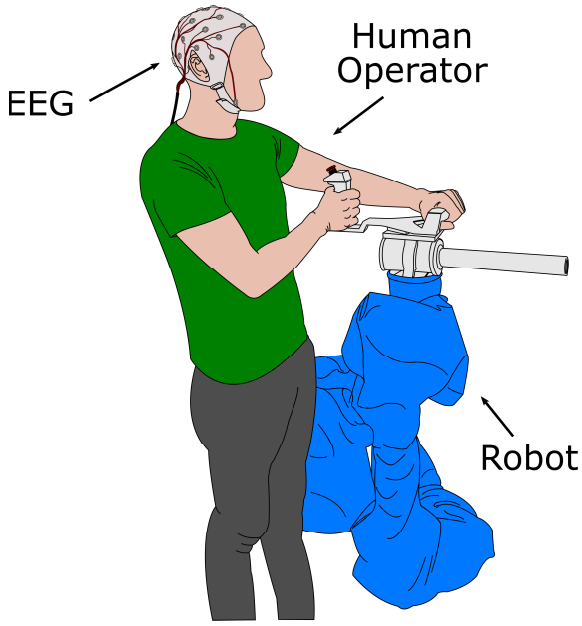

FIGURE 3.2: An operator controlling a manipulator during a pHRC application, while wearing an EEG device [8].

Data were collected from eleven healthy participants in Exp1, nine males and two females between 25 and 39 years of age. The number of participants that performed Exp1 is considered acceptable to gain evidence on whether PEN can be detected in pHRC. Only two participants (one male and one female) carried out Exp2. As mentioned above, the planar task is used to verify that the findings of Exp1 are valid for multi-dimensional tasks as well. This experiment follows the procedures approved by the UTS Human Research Ethics Committee with approval numbers ETH15-0038 and ETH18-2732.

Before starting the experiment, participants were instructed on how to control the robot and the safety measures in place. Participants were given the possibility to operate the robot to learn how to use the triggers on the robot handles, but not in the context of the experimental task. Each participant performed four sets of 125 trials, resulting in 500 trials in total per participant, as detailed in Section 3.2.2. A larger number of trials would have benefited the experiment, but the conductive gel located between the scalp and the electrodes would get too dry if the experiment lasted any longer, impacting negatively the datasets.

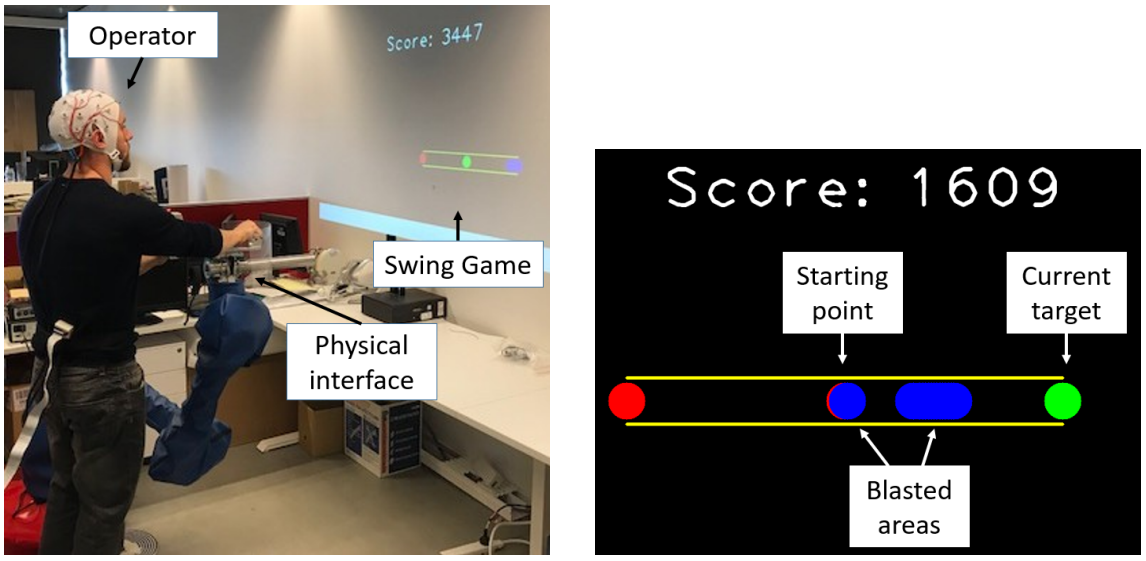

(A) Participant playing swing game

(B) The swing game

FIGURE 3.3: A participant performing the swing game in Exp1 (A) and the layout of the swing game in Exp1 (B) [1].

3.2.2 Experiment task design

In this section, the design of the experiment tasks is described for Exp1 in Section 3.2.2.1 and for Exp2 in Section 3.2.2.2.

3.2.2.1 Experiment 1 - Exp1

The "swing game" is a game implemented to create a repetitive 1D task for Exp1. The layout is shown in Figure 3.3B and is designed to be as simple as possible, to avoid giving too many cognitive stimuli to the operator. In Exp1, the operator can move the robot only horizontally, parallel to the wall where the task interface is projected. Movement in other directions is constrained by the robot in software.

The blue circle is a cursor, representing the point in the display the nozzle of the robot is aiming at; in this thesis, it will be referred as the cursor. In the game, there are three potential targets: centre, left-end and right-end. The user is instructed to move the cursor to whichever target is turned green. The other targets will be red. To keep the participant slightly engaged and to ensure that both their hands are in contact with the robot, a blasting scenario was emulated. When the trigger on the back handle of the end-effector is pressed, the robot motion is enabled, while when the

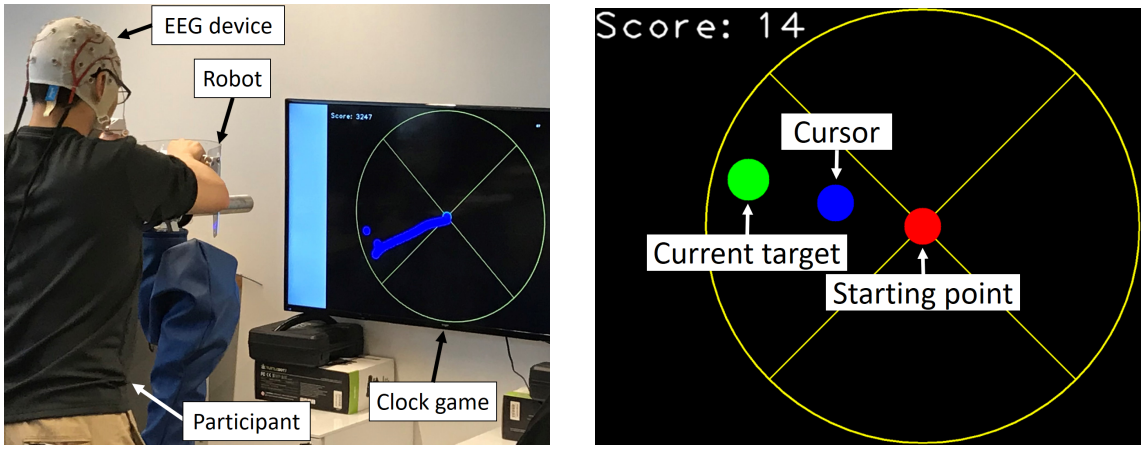

(A) Participant playing clock game (B) The clock game

FIGURE 3.4: A participant performing the clock game in Exp2 (A) and the layout of the clock game in Exp2 (B) [8].

trigger on the front handle is pressed, blue paint colours the area where the cursor is. Figure 3.1B shows the robot end-effector with its handles.

Each trial starts from the target in the centre, therefore this will be referred as the starting point. Once the cursor is placed on the starting point, one of the other targets (left-end or right-end) is randomly turned from red to green. Having the target in the centre as the starting point ensures that the participant cannot anticipate the direction of motion to get to the next target. The participant has five seconds to reach the green target otherwise the trial is reset and the current target turns red, while the starting point becomes green, to inform the participant that they have to go back. If the operator reaches the target the robot will be locked in that position till the end of the trial, preventing the robot from moving until that time has elapsed.

The score displayed on the game layout is proportional to the blasted area and inversely proportional to the distance from the current target when the time for the trial is over. Its purpose is to keep the user slightly engaged in the game.

3.2.2.2 Experiment 2 - Exp2

For the 2D task, a game called the “clock game” was designed and implemented. In this case, the operator can move the robot end-effector on a plane parallel to the task display. The clock game is a 2D extension of the swing game. As shown in Figure 3.4B, the layout presents the starting

point located at its centre, surrounded by twelve potential targets. In this game, only the current target (in green) is displayed on the screen, to reduce the number of visual inputs given to the participant. The scoring and resetting of the trials are the same as the 1D task. In Figure 3.4A, a participant is shown while performing the 2D experiment.

3.2.3 PEN stimulus

To induce PEN, an unexpected event is integrated into the games as a stimulus. In Exp1, an invisible obstacle is randomly placed halfway between the cursor and the target, with a probability of 40%. This probability is selected to prevent participants from creating an internal model in which the obstacle is likely to be encountered. When the cursor hits the obstacle the robot motions are locked and, consequently, the cursor cannot be moved to reach the target. To the participant, the obstacle is invisible and unexpected, resulting in prediction error. The robot will not move until the trial time is over, regardless of whether the operator reaches the obstacle or the target.

In Exp2, the invisible obstacle is an annular barrier placed halfway between the starting point and the target 3.6B. This is to prevent the participant from moving around the obstacle to reach the target. For the sake of clarity and consistency, this barrier is referred as an obstacle. Also in Exp2, the invisible obstacle will occur in 40% of the trials for the same reason mentioned above.

3.2.4 Control system and admittance design

The control scheme presented in [22] was adapted for the experiments presented in this chapter. An admittance-based controller is used to transform forces exerted by the operator on the handles into desired robot velocities in the Cartesian space. To avoid influencing the admittance of the robot by adding collision and singularity avoidance strategies, the task was limited to a portion of the robot workspace, in which the manipulator would always be away from potential self-collisions and singular configurations. This guarantees that the Jacobian matrix is always invertible in the task workspace, without an active singularity avoidance strategy, which would induce unintended resistive forces. A singularity avoidance strategy that generates a pseudo-inverse of the Jacobian would result on an approximation of the desired Cartesian velocities, which could itself create prediction errors. The desired Cartesian velocities are calculated as follows:

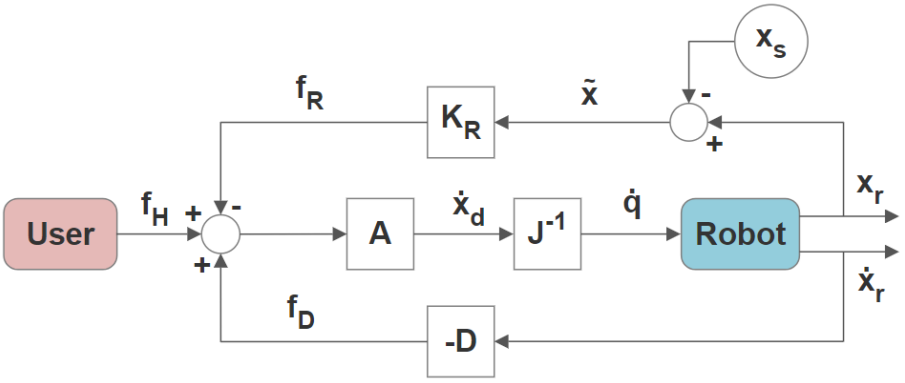

FIGURE 3.5: The implemented admittance control [1]. $\mathbf{f}_H$, $\mathbf{f}_R$ and $\mathbf{f}_D$ represent the interaction force, the resistive force and the damping force respectively. $\dot{\mathbf{x}}_d$ is the desired Cartesian velocity, $\dot{\mathbf{q}}$ are the joint velocities, $\dot{\mathbf{x}}_r$ and $\mathbf{x}_r$ are respectively the actual Cartesian velocity and position. $\tilde{x}$ is the difference between the position of the cursor and the onset position x_s of the resistive force.

$$\dot{\mathbf{x}}_d = \mathbf{A}(\mathbf{f}_H + \mathbf{f}_D - \mathbf{f}_R) \tag{3.1}$$

with $\dot{\mathbf{x}}_d$ being the vector of desired velocities of the robot end-effector in the Cartesian space, $\mathbf{A}$ is the diagonal matrix containing the admittance gains, $\mathbf{f}_H$ the vector of interaction forces exchanged with the human operator, $\mathbf{f}_D$ a force vector that smoothens the velocities in the Cartesian space and $\mathbf{f}_R$ the resistive force introduced to assess the prediction error. The resistive force is applied before both visible targets and invisible obstacles. The admittance gains are set to $0.01m/sN$ for the linear components and $0.4rad/sN$ for the angular components.

The force $\mathbf{f}_D$ is obtained by multiplying the negative actual Cartesian velocity of the robot end-effector, $\dot{\mathbf{x}}_r$, by a diagonal matrix of gains acting as a damper, $\mathbf{D}$. The linear components of $\mathbf{D}$ are set to $0.01Ns/m$, while its angular components are set to $1Ns/rad$. The block diagram of the control system is presented in Figure 5.2.

It is worth mentioning that above, in (3.1), $\mathbf{A}$ is a diagonal matrix containing the admittance gains of the robot. $\mathbf{A}$ represents the admittance of the robot when considering the sum of forces in the Cartesian space. The operator is however only responsible for $\mathbf{f}_H$ and the admittance that they experience is $\hat{\mathbf{A}}$, with elements $\hat{A}^{ii} = \dot{x}_d^i / f_H^i$, for i going from 1 to 6.

For the purpose of the experiments, the directions and orientations in which the robot end-effector cannot move are limited using a basic P controller. This regulates the position of the end-effector at

particular set points in those directions. There is no need to use a derivative term for this task, as the velocities in those directions are minimal and no chattering results even from sudden movements. With i symbolising the directions and orientations of the end-effector in Cartesian space, and $i = 1$ being the direction of motion in Exp1, the control system for the 1D task can be summarised by:

$$\begin{cases} \dot{x}_d^i = A^{ii}(f_H^i + f_D^i - f_R^i), & \text{if} \quad i = 1 \\ \dot{x}_d^i = K_P^{ii}(x_d^i - x_r^i), & \text{if} \quad 2 \leq i \leq 6 \end{cases} \tag{3.2}$$

In Exp2, the top equation in (3.2) is valid for $i = 1, 2$, the two active directions in the planar task. The proportional gains for the position control are set to $K_P^{ii} = 0.2$, expressed in N/m for the locked directions and N/rad for the locked orientations. The actual Cartesian position of the i-th direction is x_r^i, while x_d^i is the desired Cartesian position.

The resistive force f_R^i is designed to resist the motion as a compressed spring and it is used to shape the admittance in the implemented experiments. To avoid over-notation, as this force is a scalar in Exp1, it will be referred to as f_R. To study the effect of the admittance dynamics on the cognitive state of the operator, three different cases were analysed:

Case 1: Admittance rapidly decreasing before an invisible obstacle;

Case 2: Admittance slowly decreasing before an invisible obstacle;

Case 3: Constant admittance or no invisible obstacle.

If considering a constant interaction force, a rapidly decreasing admittance translates into Cartesian velocities rapidly decreasing.

The decrease in admittance can be represented by its gradient. In the case of no invisible obstacle, the operator will expect a reduction of the admittance before the visible target, consequently, that case does not produce any prediction error. In this case, the user has a visual cue that the change in admittance will result. That condition is treated as if there was no change in the admittance, therefore a zero-gradient curve. It is worth reminding the reader that the change in admittance is the result of the introduction of a resistive force. This force is related to the distance to the target, as explained later in this section.

To analyse whether it is the change in admittance that introduces a negativity rather than the presence of the invisible obstacle, the same decrease of admittance is applied before the visible

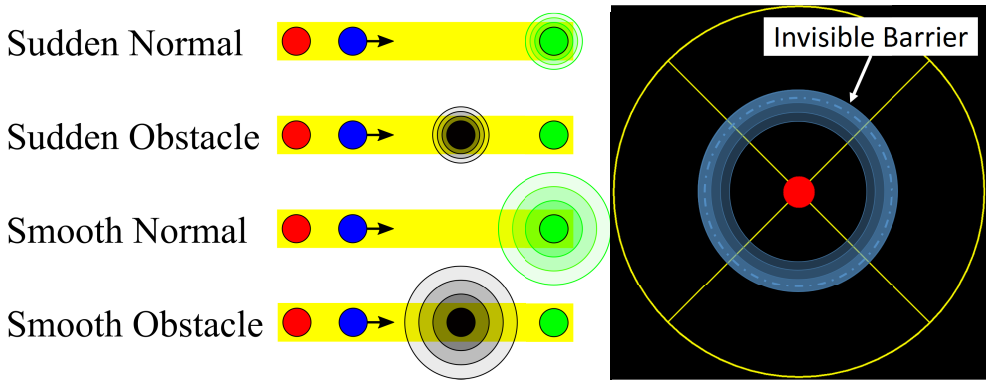

(A) Conditions in Exp1 (B) Obstacle in Exp2

FIGURE 3.6: The four conditions in Exp1 (A) [1]. In this picture, the red circle is the starting point, the blue one is the cursor and the green one is the target. The black circle is the invisible obstacle. The circles around the target and obstacle represent the resistive force. And visual representation of the invisible annular barrier, in Exp2 for the Obstacle condition (B) [8].

targets and invisible obstacles. As there are two different gradients for the admittance in the case of obstacles and the same two admittance gradients in the case of no obstacle, the experiment has a total of four conditions:

Condition 1: *Sudden-Normal* (Su-Nor): abrupt force, without obstacle;

Condition 2: *Sudden-Obstacle* (Su-Ob): abrupt force, with obstacle;

Condition 3: *Smooth-Normal* (Sm-Nor): smooth force, without obstacle;

Condition 4: *Smooth-Obstacle* (Sm-Ob): smooth force, with obstacle.

The *Normal* condition refers to trials without an obstacle, while the *Obstacle* condition presents the invisible obstacle. To describe the nature of the decrease of the admittance, *Sudden* and *Smooth* are used. For example, a Sudden-Obstacle (Su-Ob) condition refers to trials with a sudden decrease of the admittance and an invisible obstacle. For the swing game, this translates in the four conditions shown in Figure 3.6A.

The conditions represented in Figure 3.6A can be mapped to the admittance gradients mentioned above. A Sudden-Obstacle corresponds to an admittance curve with a high gradient, while the Smooth-Obstacle corresponds to a curve with a low gradient. The zero-gradient curve corresponds to having no unexpected stimulus, so to Sudden-Normal and Smooth-Normal conditions.

The reader is reminded that to generate an unexpected scenario in the clock game, the obstacle has the form of an annular barrier (Figure 3.6B), to avoid the participant moving around the obstacle

to reach the target, in the 2D case.

To modulate the admittance and its gradient, the resistive force f_R is used. This force has first-order dynamics as a higher order would have naturally led to question what parameters are affecting PEN the most. As this is the first attempt to detect PEN in pHRC applications, tasks and forces are designed to be as simple as possible. The resistive force is designed to resist the motion as a compressed spring and is calculated using Hooke's Law:

$$f_R = K_R \tilde{x} \tag{3.3}$$

The stiffness gain is K_R and is multiplied by $\tilde{x}$, the difference between the position of the cursor and the onset position x_s of the resistive force. The position of the cursor in the game is x_p (the point in the display aimed by the nozzle of the ANBOT). The position x_t corresponds to the location of the target in the case of Normal conditions and to the location of the invisible obstacle in the case of Obstacle conditions. With the cursor coming from the starting point, x_f is located before the target or the obstacle, so that the onset of the force would be located at $x_s = x_t - x_f$. Therefore, (3.3) becomes:

$$\begin{cases} f_R = 0, & \text{if} \quad x_p \leq x_s \\ f_R = K_R(x_p - (x_t - x_f)), & \text{if} \quad x_s \leq x_p \leq x_t \end{cases} \tag{3.4}$$

As mentioned above, when x_p reaches x_t, the robot motions are stopped. As the force is calculated with respect to the position of the cursor in the game, x_p and x_f are expressed in pixels (px). The conversion factor between pixels and the robot movements is $1px = 1.15mm$. The stiffness is set to $K_R = 0.5N/px$, which corresponds to $434.78N/m$.

In Exp1 the targets are located $265px$ from the starting point, while the obstacles are 132 pixels from it. To experience an abrupt resistance, in the Sudden condition, x_f is located $20px$, or $2.3cm$, before the centre of the target or the obstacle. In the case of a Smooth condition, x_f is positioned $80px$, or $9.2cm$, from the target or the obstacle. K_R and x_f are chosen with the specific purpose of having a clear difference in admittance between the different conditions. K_R is the same in all conditions, due to the fact that the cursor stops moving when the obstacle or target are reached

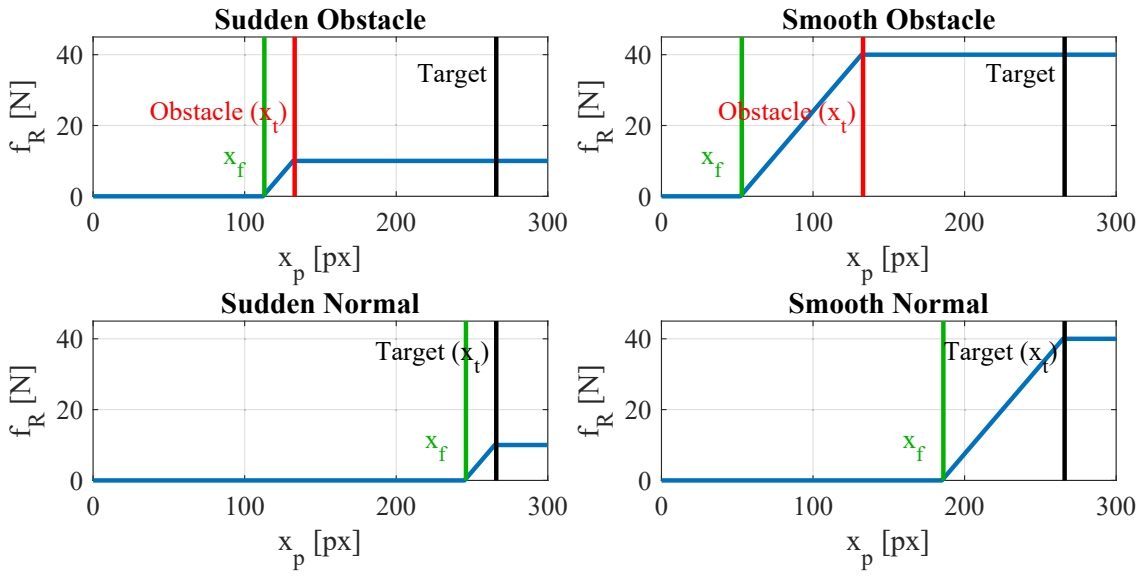

FIGURE 3.7: The resistive force f_R for each condition, with respect to the cursor position x_p, in the 1D scenario [8].

and, together with the clear difference of x_f, the admittance results decreasing much quicker in the case of the Sudden conditions.

Figure 3.7 shows f_R with respect to x_p, for the four conditions, in the case of Exp1. With a black vertical line, the position of the target is reported. The target is visible for all the conditions. In the case of Obstacle conditions, the location of the obstacle is reported with a red vertical line. The resistive force in the case of Smooth condition builds up to a higher value, but it takes longer in terms of time. It can be noticed that the force starts increasing earlier in that case.

In the case of Exp2, the resistive force is also calculated with (3.4) and with the same parameters specified above in this same section, but with the difference that $\mathbf{f}_R$ and $\tilde{\mathbf{x}}$ have two components and $\mathbf{K}_R$ is a 2×2 diagonal matrix.

3.2.5 EEG signals pre-processing

PEN is a negative deflection in the ERP happening around $50 - 250ms$ after the stimulus in the frontal area of the brain [32]. Therefore, for measuring PEN, the most critical channel is Fz, which is a mid-line frontal EEG channel and its location on the device is shown in Figure 3.8.

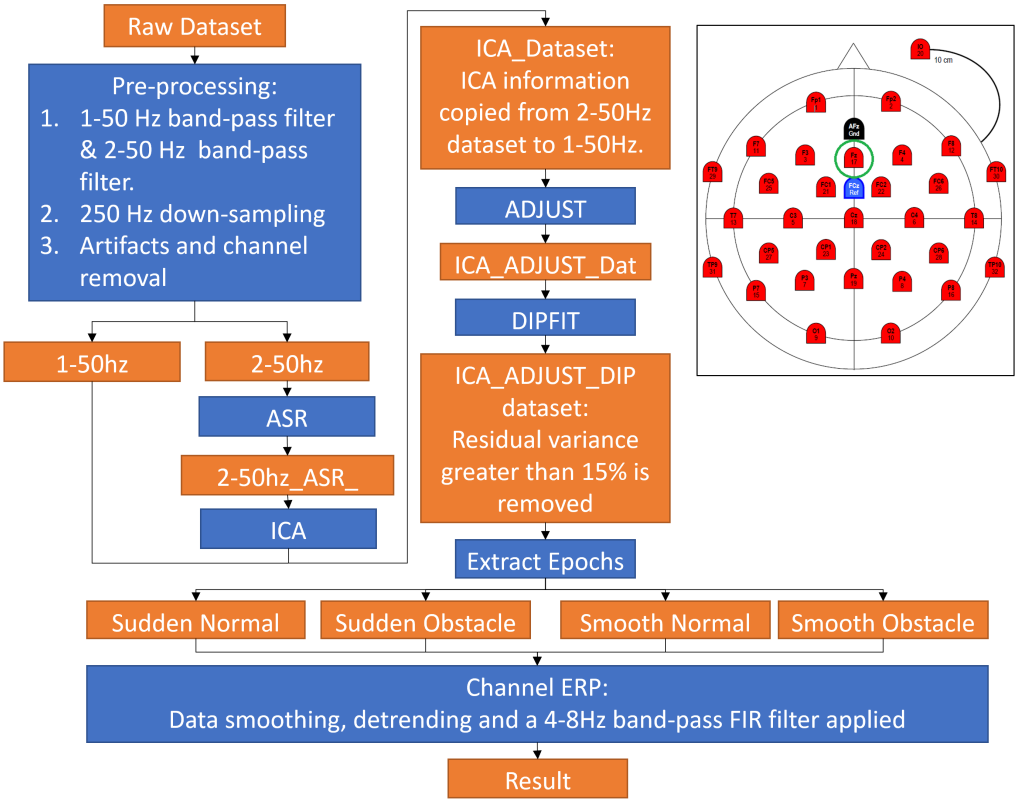

FIGURE 3.8: The pipeline used to process the EEG signals offline for the ERP analysis [9] and, on the right, the EEG cap with the channel highlighted which is used to extract PEN, i.e. Fz [1].

Figure 3.8 is a visual representation of how the EEG signals are processed for the ERP analysis. EEGLAB [112] on MATLAB R2018a (Mathworks Inc, USA) was used to process the data. The raw signals are filtered using a 1Hz high-pass and a 50Hz low-pass Finite Impulse Response (FIR) filter. The same raw signals are also filtered in the range 2-50Hz, to remove noise for the Independent Component Analysis (ICA) [113] common around 1Hz. To reduce the time required for processing the signals, the data is down-sampled to 250Hz. EEG channels with a too high noise-to-signal ratio and artifacts related to eye movement, muscle activity and other noise are rejected using Artifact Subspace Reconstruction (ASR) [114].

ICA is then applied to the 2-50Hz data set. The obtained Independent Components (ICs) are copied to the 1-50Hz data set. Because this experiment was conducted in a MoBi environment with a robot, the signals are highly contaminated by noise, and even if ASR was applied before ICA, the resultant ICs were further filtered using an automatic EEG artifact detection algorithm with the help of ADJUST [115]. The dipoles of the ICs are then evaluated and the ICs with a residual variance greater than 15% are removed. Epochs are extracted from 500ms before the force

stimulus is applied to the user to 1000ms after the stimulus. The force stimulus is represented by the onset of the resistive force and the extracted epochs are then divided by the four task conditions described in Section 3.2.4. From the resulting data sets, only the frontal channel Fz is then used to plot the ERP.

A total of 5500 trials were conducted with Exp1 from all the participants together and 1000 trials were collected with Exp2, with 60% representing a Normal condition and 40% an Obstacle condition. Half of the trials presented a Sudden resistive force and the other half a Smooth resistive force. Therefore, the trials can all be divided into four data sets, given the different conditions: Sudden Normal, Sudden Obstacle, Smooth Normal and Smooth Obstacle (Figure 3.6A).

3.3 Results and discussion

In this section results are presented and discussed for Exp1 in Section 3.3.1 and for Exp2 in Section 3.3.2.

3.3.1 Experiment 1 - Exp1

Epochs were extracted according to trial conditions and the ERP amplitudes were obtained. The ERP amplitudes shown in Figure 3.9 are the results of the average between all the trials carried out by all participants. The bands around the curve represent the variance between different participants. The curves are sorted by condition and the zero of the x-axis (time [ms]) represents the time of the onset of the resistive force. The area of the plot highlighted in green corresponds to the time range in which PEN may be found, i.e. between 50ms and 250ms. In the case of the Sudden-Obstacle condition (blue curve), around 200ms it can be noticed a negative deflection, which corresponds to PEN. Following the negativity, a positive peak appears around 350ms. That feature is associated with memory processing and is known as P300. When an unexpected stimulus is received, a P300 is invoked while the participant updates their internal model [116]. In this work, the baseline is the ERP amplitude in between -100ms and 0ms, which represent the cognitive state of the participant before the stimulus. For the other conditions, the ERP curves are comparable to that baseline.

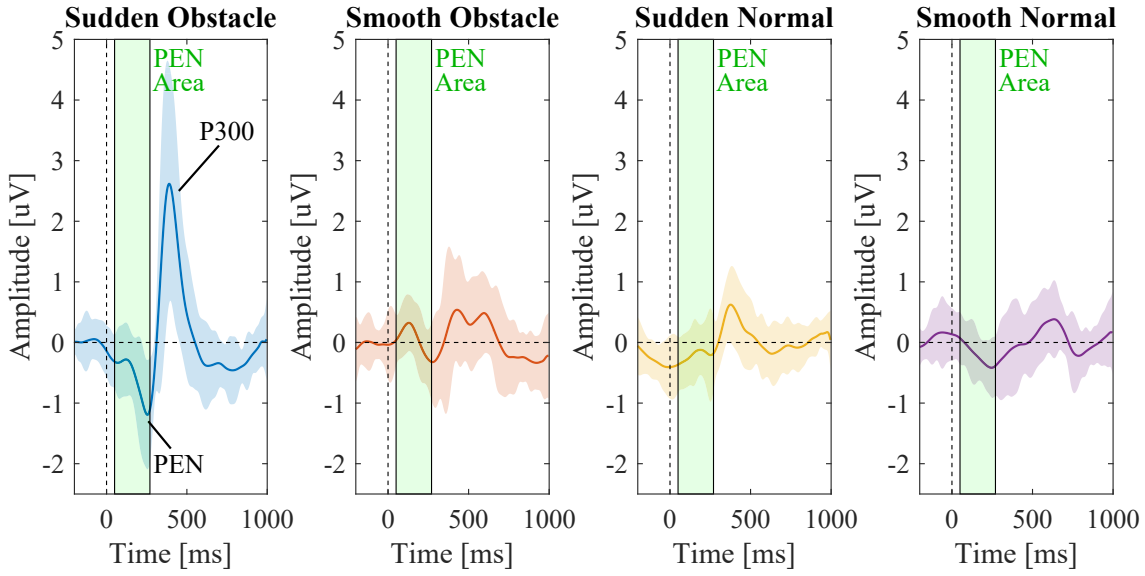

FIGURE 3.9: Average ERP amplitude for each condition, in Exp1. The zero-time corresponds to the onset of the resistive force and the area highlighted in green corresponds to the time period in which PEN may be found [8].

Figure 3.10 shows the ERP amplitudes of a single participant divided by conditions. In this case, the bands represent the variance between the trials. It can be noticed that the curves are similar to the average results, shown in Figure 3.9, with a clear PEN in the case of an invisible obstacle with a sudden resistive force. The condition Smooth-Obstacle is comparable to the conditions with no invisible obstacle in both Figure 3.9 and Figure 3.10. Since the same force as Sudden-Obstacle is applied before the target in the Sudden-Normal condition, it can be assumed that the only presence of an abrupt force is not enough to invoke PEN. In fact, in the case of a visible target, the user can predict the presence of the force. Even if the two Normal conditions represent the case in which no PEN should be invoked, the plots of all four conditions are presented separately to highlight that the investigated EEG feature is not a result of the resistive force. In the ERP plots, PEN was only observed in the case of an unexpected sudden resistive force, and not in the other conditions.

To investigate PEN at an individual level, the ERP amplitude was analysed for each participant in all the conditions. Table 3.1 presents the minimum of the ERP amplitudes in the time range going from 150ms to 250ms for each participant. When compared to the other conditions, Sudden-Obstacle presents an ERP amplitude that is higher (more negative) in 81.8% of the participants. These results suggest that the way the admittance is designed affects the cognitive state of the operator. Results also demonstrate that PEN can be detected and used to estimate the predictability

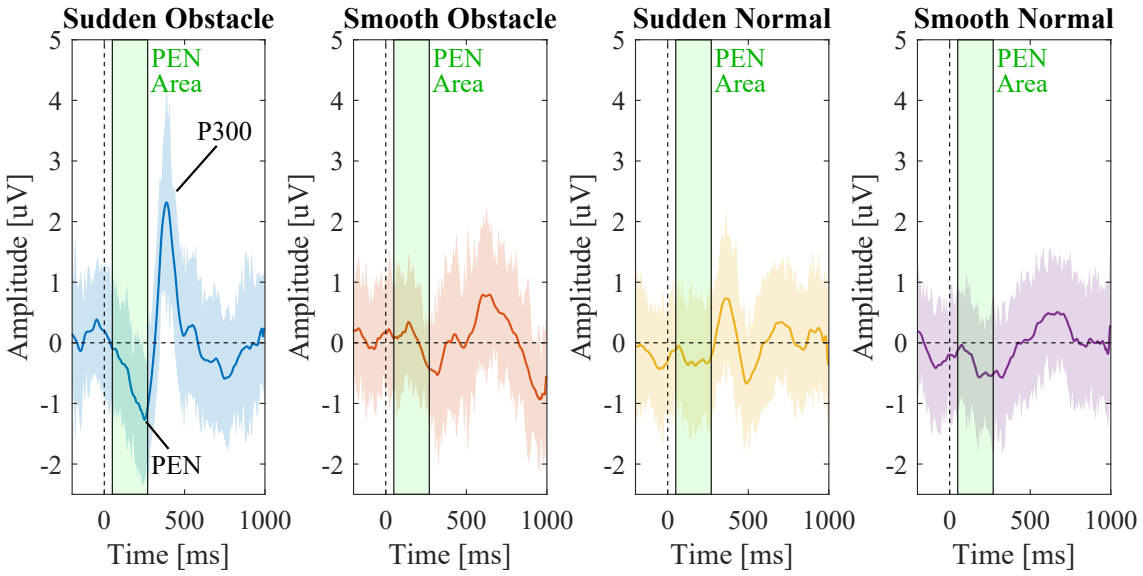

FIGURE 3.10: ERP amplitude for each condition for a single participant, in Exp1. The zero-time corresponds to the onset of the resistive force and the area highlighted in green corresponds to the time period in which PEN may be found [8].

TABLE 3.1: Minimum average ERP amplitude in the time interval from 50ms to 250ms from the onset of the force in Exp1, for each participant organised by condition [8].

Participant	**ERP Amplitude (μV)**			
	Su-Ob	Sm-Ob	Su-Nor	Sm-Nor
P1	-1.0786	-0.0066	-0.2839	-0.6513
P2	-0.4405	0.0200	-0.5954	-0.4802
P3	-0.2999	-0.2190	-0.2994	-0.2097
P4	-1.4791	-0.3895	-0.4473	-0.6795
P5	-1.7164	-1.0034	-1.1080	-0.4853
P6	-1.7172	-0.0759	0.3640	-1.4271
P7	-3.0991	-1.1285	-1.2540	-0.7947
P8	-1.1466	-0.2015	-0.2420	-0.4035
P9	-1.6187	-0.4788	-0.2107	0.3536
P10	-0.3459	0.3043	-0.0308	-0.9644
P11	-1.8357	-0.6131	-0.2148	-0.0763

of the collaborative robot, from the human co-worker's perspective. In Table 3.1, the condition Smooth-Obstacle does not present a negative deflection higher in magnitude when compared to the conditions with no invisible obstacle.

To analyse whether the variation of the negativity is statistically significant among all conditions,

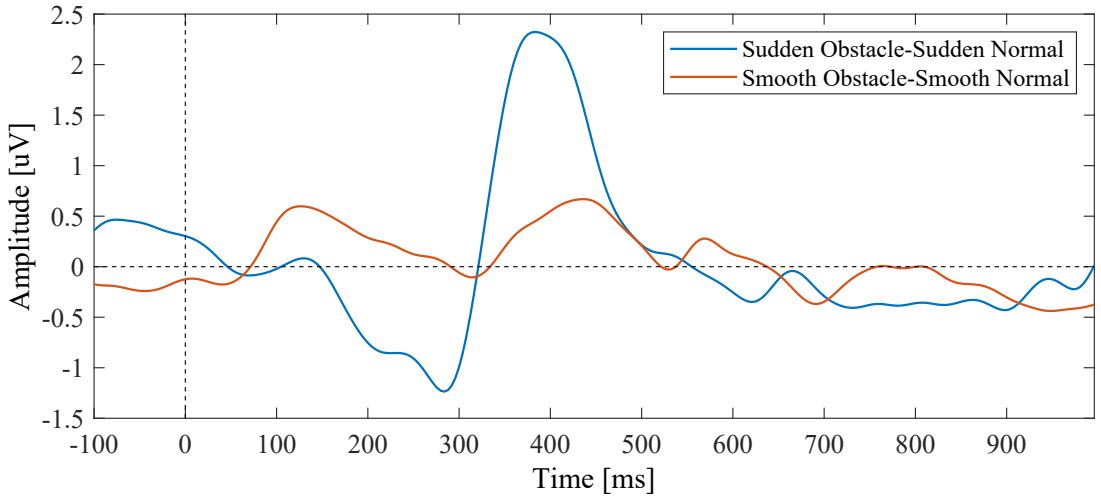

FIGURE 3.11: Difference of the average ERP amplitude (shown in Figure 3.9) between the conditions featuring an obstacle and the ones without, in Exp1. The zero-time corresponds to the onset of the resistive force.

an ANOVA test on 2×2 experiment design conditions was performed, considering the two force types (Smooth and Sudden) and two task conditions (Normal and Obstacle). Results show that the force conditions have a significant effect, with $F(1, 10) = 12.067$ and $p = .006$. The task conditions resulted in being significantly different as well, with $F(1, 10) = 7.816$ and $p = .019$. The interaction between force and task conditions was also analysed and they resulted in being significantly different, with $F(1, 10) = 16.117$ and $p = .002$. A paired t-test was then used as a post-hoc comparison, to further investigate whether the conditions have a significant effect on PEN. The results suggest that there is a significant statistical difference between Sudden-Normal and Sudden-Obstacle, with $p = .001$, and between Sudden-Obstacle and Smooth-Obstacle, with $p < .001$. There was however no statistical difference between Smooth-Obstacle and Smooth-Normal, with $p = .517$. Sudden-Obstacle and Smooth-Normal were also compared and it was found that $p = .009$, suggesting that those conditions are statistically different. Similarly, the post-hoc test between Smooth-Obstacle, Sudden-Normal, and Smooth-Normal was found to be not statistically significant, with $p > .05$. This ERP analysis suggests that the four conditions cannot be divided into three PEN levels as anticipated, but only two: PEN is shown in the case of the condition Sudden-Obstacle and PEN is not detectable for all the other conditions.

To further emphasise the difference between Normal conditions from the ones with the invisible unexpected obstacle, in Fig. 3.11 the difference between their ERP amplitude is presented. In this

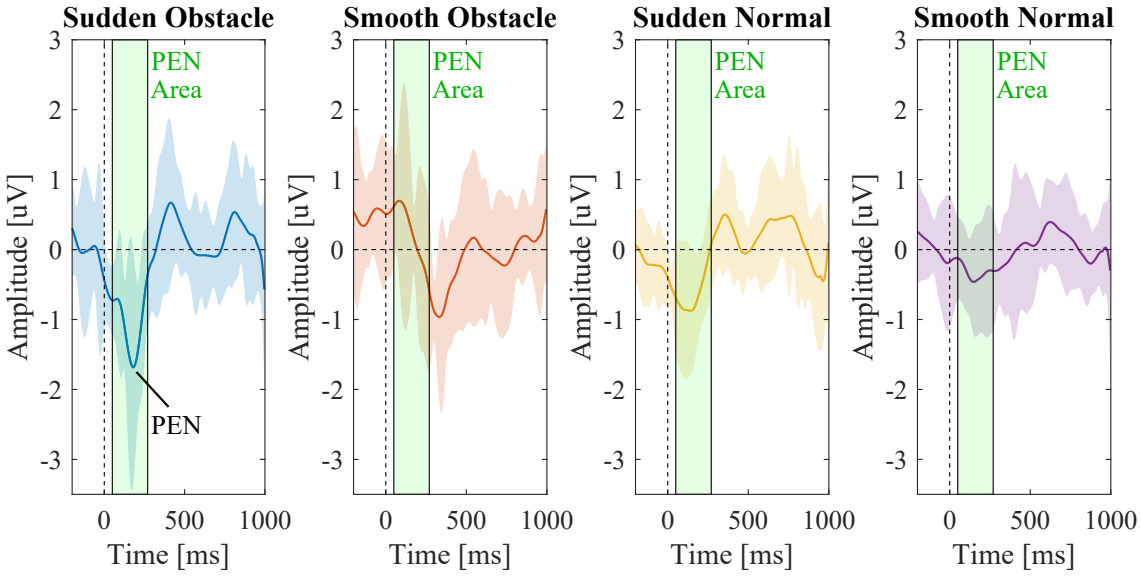

FIGURE 3.12: Average of the ERP amplitude for each condition, in Exp2. The zero-time corresponds to the onset of the resistive force and the area highlighted in green corresponds to the time period in which PEN may be found [8].

plot, the negativity around 250ms becomes even more prominent, in the case of a sudden resistive force. With smooth forces, that start further away from the obstacle, the PEN is negligible.

The ERP curves presented in Figure 3.9 suggest that the resistive force modulates the PEN. With a wider, smoother resistance around the obstacle, in Smooth-Obstacle conditions, the participant presented a smaller PEN amplitude (less negative). On the other hand, when an abrupt resistive force is applied, participants present more negative PEN, translating in a greater prediction error. This means that abruptly interrupting the robot motion during a collaborative task without any feedbacks, e.g. visual cues, will likely lead to a prediction error. On the other hand, applying wider and smoother resistive forces to avoid undesired areas of the workspace would decrease the PEN level. It is hypothesised that this is a consequence of the operator being able to better anticipate the workspace dynamics when the robot starts resisting the motion sooner and more gently.

3.3.2 Experiment 2 - Exp2

Results of the 2D scenario support the findings of the 1D scenario, suggesting that the design of the interaction dynamics affects the cognitive state of the robot operator. The following results are

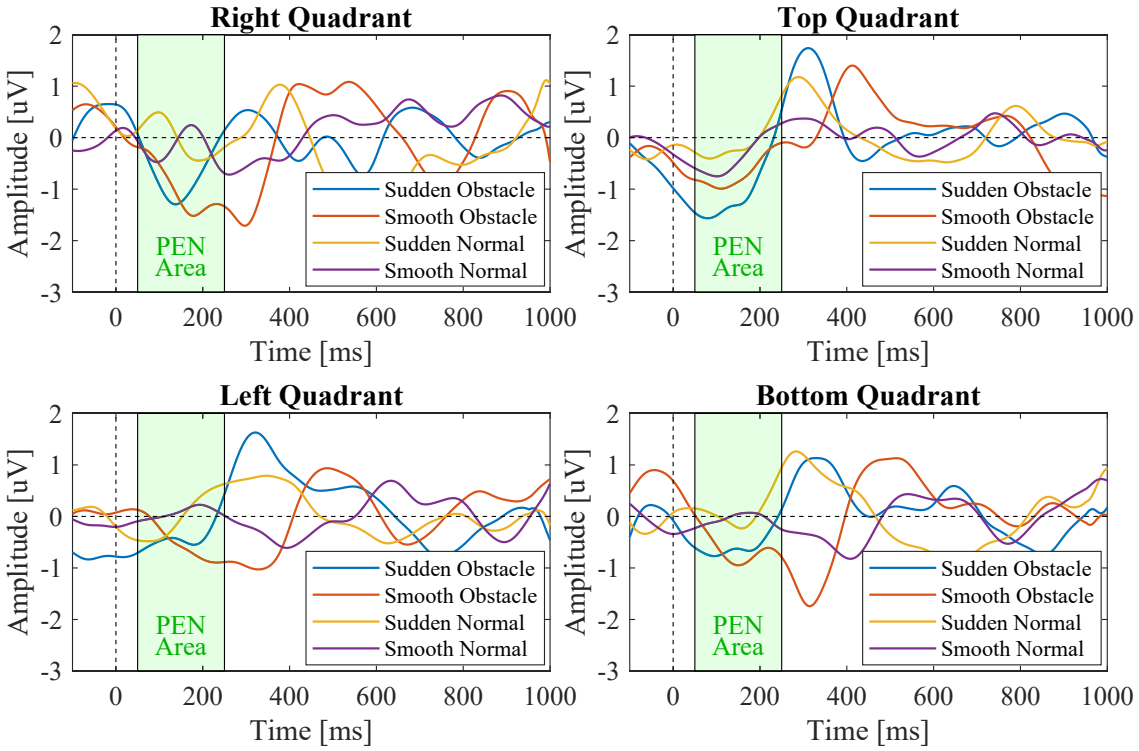

FIGURE 3.13: ERP plots for each quadrant of the clock game in Exp2, with the time range in which PEN is retrievable highlighted in green.

obtained processing and analysing the data collected from two participants while using the clock game. A study size of two participants does not represent a robust sample, especially for statistical analysis. In this work, the extension to the 2D scenario has the purpose of verifying that the results from the mono-dimensional task can be extended to multi-dimensional scenarios without losing validity.

In Figure 3.12, the ERP amplitude for each condition is presented as an average between the two participants. It can be noticed a higher PEN (more negative) in the case of the condition Sudden-Obstacle. The condition Smooth-Obstacle also presents a negative peak but is out of the time range in which PEN is normally found, i.e. between 50ms and 250ms from the onset of the stimulus.

In the case of the 2D scenario, the targets were grouped in quadrants to see if the direction of motion has an influence on PEN (Figure 3.13). The direction seems to not have an influence on PEN, which remains higher in the case of the condition Sudden-Obstacle.

In the case of the bottom quadrant, the PEN peak is less obvious but still present. That might be due to the participant being cautious when moving the ANBOT in that direction to prevent the

elbow joint of the UR10 from colliding with the floor. This hypothesis was made after the trials, and hence it was not possible to ask participants if this was the case.

3.4 Limitations

These experiments have limitations that should be addressed in the future. The impact that previous experience with collaborative robots has on prediction errors is not taken into account. Moreover, only two participants performed the 2D task and, ideally, it would be good to have a larger sample of participants to perform statistical analysis.

The experiments in their current form are long, repetitive and tiring, and could lead to mental fatigue. Participants might also get physically fatigued, given that the experiment is performed in a standing pose. There might be potential artifacts that could not be removed with current methods. Since the stimulus is a force exchange that introduces many variables, both in the physical and mental domain. Confounding factors like stress, workload and fatigue could influence the results. Information from other physiological signals could help isolate those factors. For example, using sEMG could isolate muscular activity that usually introduces noise in the EEG signals.

The experiment tasks in 1D (Exp1) and 2D (Exp2) made it easier to control events and conditions. This is however a simplified representation of the real world. The collected data might still be used as training sets for machine learning classifiers aimed at detecting the presence of PEN. While specific events might be harder to identify in the absence of a clear task in the free space, the features identified in the EEG signals should be the same in the case of a prediction error.

Another limitation of this work is the nature of the resistive force. As this is the first time PEN is assessed in pHRC scenarios, tasks and forces are as simple as possible. Nowadays, in pHRC applications, those forces are usually more complex and do not present first-order dynamics.

3.5 Conclusions

Two experiments were performed to understand the effect of changes in the robot admittance, through first-order resistive forces, on predictability of the collaborative robot, from the operator's

point of view. The robot admittance was designed to result in four conditions that could be grouped into three PEN levels. These three levels would correspond to three cases of admittance dynamics. Results show that an admittance that smoothly decreases, helps the operator predict upcoming changes in the dynamics when compared to an abrupt admittance decrease. This is particularly relevant when considering the interaction dynamics with multiple control strategies implemented, e.g. singularity and collision avoidance. Only in the case of a sudden and unexpected reduction of admittance, the operator presented PEN in the ERP plots. The three anticipated PEN levels cannot be identified in the ERP plots. Exp2 demonstrated that results obtained with Exp1 are valid also in the case of two-dimensional tasks. Results from Exp2 also suggest that the direction of motion does not have an impact on PEN.

Results presented in this chapter demonstrate that PEN and interaction dynamics are related, at least in the case of first-order resistive forces. In 81.8% of the participants, the condition Sudden-Obstacle presents a more negative ERP amplitude. It was found that the computational cost in the data processing is very high (especially because of ICA), therefore, the need becomes apparent for methods for online detection and classification of PEN. Also, machine learning classifiers might be able to differentiate three levels of PEN, even if they are not visible in the ERP plots. Therefore, the next chapter will investigate methods for online estimation of PEN, and will address the classification problem as both a two- and three-class problem.

Chapter 4

Methods for Estimation of Prediction-Error Negativity in Physical Human-Robot Collaboration

4.1 Introduction

In the previous chapter, results showed that interaction forces could affect the predictability of the robot behaviour, from the human co-worker's point of view. In particular, in Section 3.3.1, it is demonstrated that PEN can be found in the ERP in the case of unexpected abrupt resistive forces. By using the cognitive state of the operator, the robot can take it into account and adapt its behaviour. In the case of prediction errors (i.e. mismatch between the expected robot behaviour and the actual robot behaviour), the robot can implement a strategy which aims to reduce PEN, enhancing the predictability of the robot behaviour.

For pHRC applications, if the human-robot interaction depends on the cognitive state of the user, a timely estimation of the cognitve state is pivotal. The time it takes for a machine learning classifier to provide feedback is one of their defining characteristics, and real-time processing is highly desirable [117]. If forces exchanged between humans and robots rely on signals coming from the EEG, the time it takes to process those signals has a significant impact on the control system.

Decreasing the time for processing EEG signals may reduce the accuracy. An incorrect estimate of the human cognitive state, i.e. PEN, might result in an uncomfortable or unsafe interaction. A limitation in EEG-based interfaces is the often low signal-to-noise ratio, which is further decreased where a user's motor movements are involved. This usually results in a challenging compromise between prepossessing, computation time, and acceptable accuracy of the estimation method.

As suggested by results in the previous chapter, the admittance dynamics affects the PEN level. This leads to the need of a method to continuously assess the cognitive state during the interaction. No previous work investigated the challenge of continuously looking for PEN during a pHRC application. In this chapter, sub-question Q2 (Section 1.3.2) is addressed. Six different machine learning classifiers are compared on the EEG data sets collected from eleven participants during a human-robot collaborative task. The task is the one described in Chapter 3 as the swing game, used in Experiment 1 (Exp1). In the next section (Section 4.2), the implemented pipeline and the classifiers are described, along with the analysis carried out. In Section 4.3, the performance of the classifiers are presented and discussed. Finally, Section 4.5 summarises findings. Part of the results presented in this chapter were included in a paper submitted to IEEE Transactions on Cognitive and Developmental Systems [8].

4.2 Methods

EEG data were recorded from participants performing a collaborative task with a robot with four experiment conditions or scenarios as stated in Section 3.2.4. They are:

Condition 1: *Sudden-Normal*: abrupt force, without obstacle;
Condition 2: *Sudden-Obstacle*: abrupt force, with obstacle;
Condition 3: *Smooth-Normal*: smooth force, without obstacle;
Condition 4: *Smooth-Obstacle*: smooth force, with obstacle.

Participants and experimental setup are the same as Exp1 presented in Section 3.2.1. The collaborative task is the swing game, detailed in Section 3.2.2.

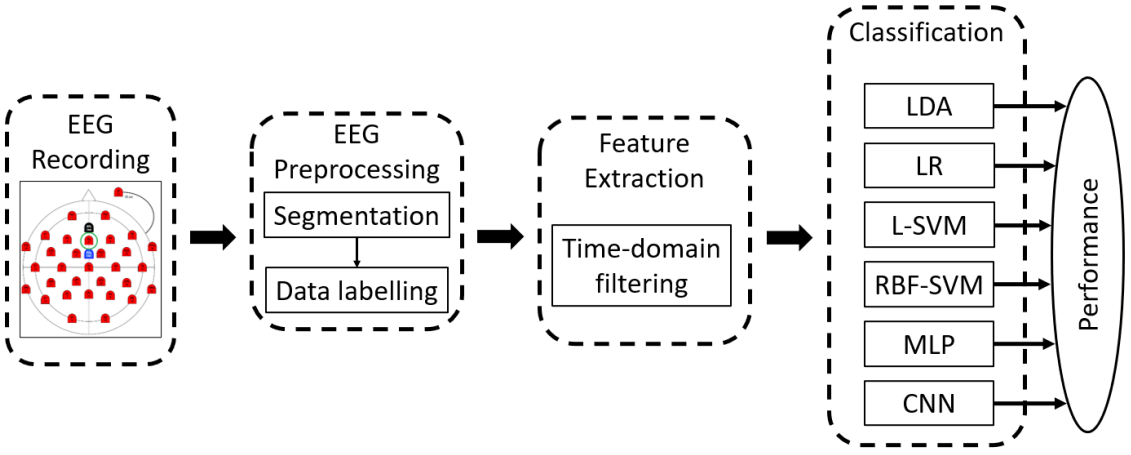

FIGURE 4.1: The implemented pipeline to compare performances of the classifiers [8]. The recorded brain activity was first segmented, labelled and filtered with a FIR. The data was then passed through the classifiers and performances were compared.

4.2.1 Detection and classification of PEN

In order to detect a prediction error, a classifier which can promptly and accurately estimate PEN has to be integrated into the human-robot system.

While stimulating the participant with the collaborative task, EEG data were recorded. To remind the reader what pattern the classifiers need to detect, Section 3.3.1 presented ERP plots resulting from the four conditions. In the Sudden-Obstacle condition, PEN can be seen, followed by the positive peak P300.

EEG data have a poor signal-to-noise ratio. For online detection of specific features, the data cannot go through complex and time-consuming processing. Therefore, the pipeline presented in Section 3.2.5 cannot be used for online detection. In Figure 4.1, a new strategy is presented from a high-level perspective. With this new strategy, during an online application, the raw signal has only to be filtered with a simple finite impulse response (FIR) filter before going through the classifier. The machine used to train and test the performance of the classifiers has an NVIDIA Quadro P5000 GPU, with CUDA 9 and cuDNN v7, in Tensorflow, using the Keras and Scikit Learn API.

The number of trials on average for each participant was 107 ± 13 for Smooth-Obstacle condition, 98 ± 18 for Sudden-Obstacle condition and 305 ± 19 for combined Sudden-Normal and Smooth-Normal conditions. For each participant, 60% of the trials were used to train the classifier, 20%

for validating and 20% for testing. The stratified sampling [118] has been used to divide data into training, validation, and testing. For the training set, the data was segmented by selecting the features, based on when the robot started applying a resistive force, before reaching the target or the obstacle. The selected interval is from -0.2s to 1s, where zero is the instant the robot starts resisting the human motion. As a consequence, each trial consists of dimension 32×1200, where 32 is the number of EEG channels and 1200 is the number of sample points in each channel. The data was subsequently labelled, depending on the experiment condition and according to the number of classes to identify with the classifiers. The raw signals were band-pass filtered in the range of 1-15 Hz and the resultant signals were used for classification. In Figure 4.1, this corresponds to the time-domain filtering block. The band-pass filtered range corresponds to the δ, θ and α bands [119], since PEN is commonly associated with brain activity in the α and θ bands (4-13Hz) [120, 121].

The fact that classifiers are detecting PEN is an assumption. These classifiers are looking for common patterns, between the training and testing data sets. Other underlying cognitive processes might be discerning factors between the identified classes. As the conditions in Exp1 were however specifically designed to study PEN, it is speculated that prediction errors are the source of differences between the classes.

4.2.2 Classifiers

To detect PEN, popular classification methods for ERP were chosen, with increasing level of space and computational complexity in order from linear, logarithmic, non-linear to artificial neural-network and deep learning. Lotte et al. presented a detailed review of classification algorithms used for EEG-based BCIs [122]. The classifiers evaluated in this chapter are the following:

- Linear Discriminant Analysis (LDA);
- Logistic Regression (LR);
- Support Vector Machine with a linear kernel (L-SVM);
- Support Vector Machine with a Radial Basis Function kernel (RBF-SVM);
- Multi-Layer Perceptron (MLP);

- Convolutional Neural Network (CNN).

The six classifiers used in this work are described in the following: *Linear Discriminant Analysis* (LDA) is a classifier widely used in BCI applications. LDA has very low computational requirements, which makes this classifier a popular choice for online BCIs. LDA does not, however, perform well with complex non-linear EEG data without preprocessing, usually resulting in poor accuracy. *Logistic Regression* (LR) is a discriminative learning classifier. Results are usually more accurate than the ones obtained with LDA, but, when data is sparse or high-dimensional, LR can lead to overfitting issues. A Limited-memory Broyden-Fletcher-Goldfarb-Shanno (L-BFGS) solver is used for the LR. *Support Vector Machine* (SVM) classifiers can have different complexities depending on their decision boundaries. If the decision boundaries are linear, the corresponding SVM is defined as linear SVM (L-SVM). It is possible to have non-linear boundaries by using a kernel function. SVMs that use Radial Basis Function kernels (RBF-SVM) are commonly used in BCI research. They have good generalisation properties, perform well with high-dimensional problems and are not sensitive to over-training. All those advantages come at the cost of execution speed. *Neural Networks* (NNs) consist of artificial neurons that can result in non-linear decision boundaries. NNs are very flexible and can approximate any continuous function, given they are provided with enough layers and nodes. A MultiLayer Perceptron (MLP) is used. *Convolutional Neural Networks* (CNNs) [123] are deep NNs that use matrix convolution in at least one of their layers. They have the advantage of automatically optimising weight parameters to reduce classification mistakes. This characteristic leads to a short pre-processing time.

For the RBF-SVM classifier, γ = 'scale', with γ defining the influence of a single training trial. The MultiLayer Perceptron (MLP) used in this research has 100 hidden layers, learning rate α = 1 and the maximum iterations are set to 1000, using Adam [124] optimiser with auto batch size selection. The other parameters were set as default, as mentioned in SciKit MLP [125]. The number of hidden layers (100) has also been chosen as its default value in SciKit MLP. As the development of the MLP classifier is not part of this thesis, the reader is directed to [125] for further details on the MLP used.

The CNN model used in this research is known as DeepConvNet [126]. It consists of four convolutional blocks and a classification block. The first convolutional block is specially designed to handle EEG inputs, and the other three are standard convolution ones followed by a softmax [127]

classification with Adam [124] used as optimiser, with batch size in a range of 10 to 16, early stopping based on validation loss with patience of 20 epochs and a dropout rate for best performance chosen between 25% and 50%. In multi-layer neural networks, such as CNNs, an epoch is defined as the process of passing the entire data set once both forward and backward through the network [128]. The number of filters used in the CNN is 25, 50, 100, and 200 for each consecutive convolution layer, with the number of kernels equal to five. The parameters for all the compared classifiers have been set up before training and testing for all participants.

During Normal conditions (Sudden-Normal and Smooth-Normal), the operator can see the target and therefore there will not be a prediction error regardless of the dynamics of the resistive force applied. For that reason, the conditions Sudden-Normal and Smooth-Normal are considered as one class. Firstly, the problem was addressed as a two-class classification, with the class Sudden-Obstacle versus all the other conditions combined. The Sudden-Obstacle and Smooth-Obstacle conditions can, however, produce different magnitudes of PEN, with Sudden-Obstacle being higher (producing a more negative peak). Therefore, performances of the same classifiers were also tested in the case of three classes: Sudden-Obstacle, Smooth-Obstacle and Normal. These would represent three different levels of PEN, that could be potentially used in applications that require a more precise estimation of the PEN level.

To compare the results of different classifiers, performances were evaluated in terms of overall accuracy and mean-squared error (MSE). The best performing classifier was then considered to question whether the classifier is feasible for a real-time robot application and its computation time to predict (PT) was taken into account. The number of classes is imbalanced, for different levels of PEN. Therefore, to better understand the performance of the classification algorithms, the precision (Pre), recall (Rec), and F1-score (F_1) were also evaluated for a targeted level of PEN (i.e. Sudden-Obstacle condition).

The accuracy and loss with respect to the number of epochs used in the CNN was also used to evaluate the performance of the classification algorithm. To train and validate the CNN, early stopping was used in the case of no changes in validation loss up to 20 epochs. The loss represents the difference between the values predicted by the network and the true values, giving a measure of how well the deep learning algorithm is able to reduce the error.

4.3 Results and discussion

The performances of the six classifiers in the case of two classes (i.e. Sudden-Obstacle versus Smooth-Obstacle, Sudden-Normal and Smooth-Normal combined) are summarised in Table 4.1. The accuracy is reported for all participants (with P01, being Participant 1, for example). The mean and the standard deviation (SD) of the accuracy are also reported at the bottom of the table. These results are the outcome of the testing phase of the classifiers. The accuracy of CNN is considerably higher than any one of the other classification algorithms. In the best case, with participant P11, the accuracy reached a level of 93.1%, with the CNN. The mean accuracy for CNN is 82.1% $\pm$ 5.2%, which is high considering that the data is only filtered in terms of frequency before being fed into the classifier. In terms of the applicability of the CNN to a real pHRC task, results seem promising, but the possibility of a misclassification has to be taken into account. To alleviate this, a possible solution could be to adapt the nature of the resistive forces only after the detection of several PEN.

In Table 4.2, the mean squared error (MSE) is reported for the six classifiers and for each participant, for the two-class problem. These results confirm that the CNN performed best, when compared to the other five classifiers.

In Figure 4.2 the precision, recall and F_1-score are reported for the six classifiers. The values reported are the mean values across all participants. The CNN presents better results than the other classifiers. The computational time required by CNN during the testing phase to classify a trial is on average 0.34s $\pm$ 0.07s, for the two-class problem, which is comparable to the human reaction time.

In Figure 4.3, the accuracy and loss with respect to the number of epochs used in the CNN are shown for both the training and validating phase, for participant P11. It can be noticed that, after about 60 epochs, the accuracy and loss of the network become nearly constant. This means that approximately 60 epochs are enough for the CNN to obtain results with about the same precision.

Some applications might require a more precise estimation of PEN. This leads to the necessity of the classifier to detect multiple PEN levels. In the experiment, the condition Smooth-Obstacle is expected to have a reduced level of PEN. In the case when the classifier is required to detect three classes, the accuracy is still acceptable for the CNN. The three classes are here representing

TABLE 4.1: Resulting performances of the classifiers, in terms of accuracy (expressed in %), for each participant, in the case of two classes: Sudden-Obstacle versus all the other conditions combined. In the last two rows, mean and standard deviation (SD) are reported [8].

		LDA	LR	L SVM	RBF SVM	MLP	CNN
		Accuracy [%]					
Participant	P01	62.75	71.3	73.3	75.3	72.1	79.2
	P02	50.0	75.3	78.2	74.7	79.8	80.61
	P03	61.1	75.1	77.9	79.4	76.9	77.5
	P04	56.6	74.6	75.1	77.3	74.8	83.3
	P05	66.2	76.2	75.1	76.5	67.6	83.6
	P06	39.1	69.0	76.3	75.4	75.4	89.9
	P07	52.3	69.7	72.5	72.5	66.6	78.0
	P08	51.2	69.9	72.8	72.8	67.9	80.4
	P09	48.7	65.0	66.3	67.9	66.7	76.4
	P10	62.1	64.1	68.8	69.1	65.8	81.5
	P11	39.9	69.5	70.3	72.5	69.9	93.1
Mean		53.6	70.9	73.3	74.0	71.2	82.1
SD		9.1	4.1	3.7	3.4	4.8	5.2

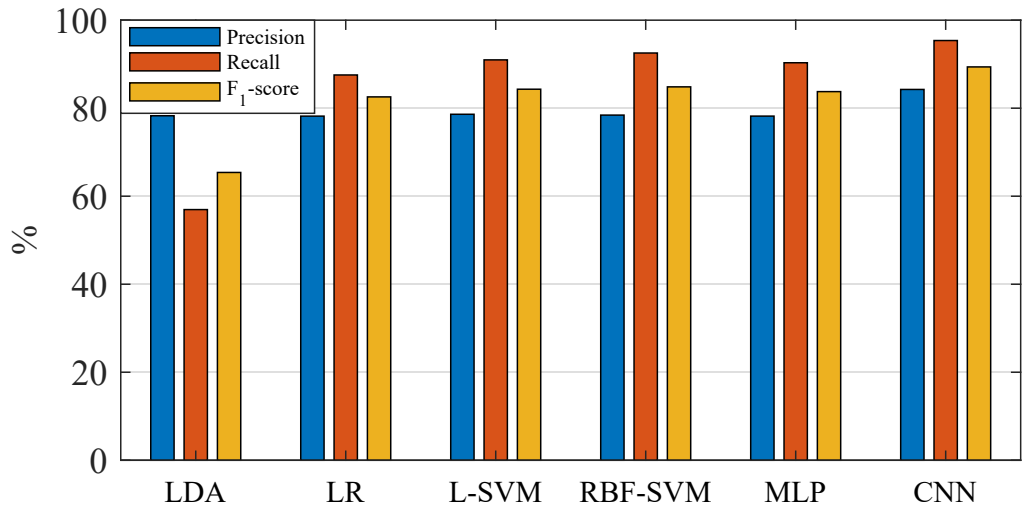

FIGURE 4.2: Mean precision, recall and F_1-score with respect to the classifiers [8].

the following conditions: Sudden-Obstacle, Smooth-Obstacle and Normal (Sudden-Normal and Smooth-Normal combined). In Table 4.3, accuracy, MSE and prediction time are reported only for the CNN classifier, as it performed better than the other classifiers. In the case of three classes, the mean accuracy for LDA is 37.9%, for LR is 53.7%, for L-SVM is 54.1%, for RBF-SVM is

TABLE 4.2: Resulting mean squared error (MSE) of the classifiers for each participant, in the case of two classes: Sudden-Obstacle versus all the other conditions combined. In the last two rows, mean and standard deviation (SD) are reported.

		LDA	**LR**	**L SVM**	**RBF SVM**	**MLP**	**CNN**
		Mean Squared Error (MSE)					
Participant	**P01**	0.34	0.30	0.34	0.39	0.27	0.18
	P02	0.15	0.15	0.17	0.20	0.17	0.06
	P03	0.25	0.24	0.27	0.18	0.22	0.23
	P04	0.27	0.27	0.27	0.22	0.27	0.20
	P05	0.38	0.32	0.33	0.27	0.31	0.22
	P06	0.49	0.35	0.29	0.28	0.32	0.26
	P07	0.50	0.26	0.26	0.27	0.27	0.25
	P08	0.20	0.17	0.17	0.17	0.17	0.17
	P09	0.23	0.18	0.16	0.18	0.16	0.04
	P10	0.32	0.30	0.30	0.37	0.37	0.16
	P11	0.28	0.32	0.31	0.23	0.29	0.12
Mean		0.31	0.26	0.26	0.25	0.26	0.17
SD		0.11	0.07	0.07	0.07	0.07	0.07

53.6% and for MLP is 46.9%. The mean accuracy for the CNN is 66.7% $\pm$ 10.2%, with a value of 91.1% for participant P11 as the best performance. This participant seems however to be an outlier, as most of the other participants present a much lower accuracy. The performance of the CNN for three classes is lower than the performance resulting from classifying two classes. This is probably due to the fact that CNN is sensitive to the size of the data provided. With three classes, the number of available training data for each class is smaller than in the case of classifying only two classes. It is speculated that with more data the performance of the CNN would improve significantly. The results still suggest that there is a difference between the condition Smooth-Obstacle and the Normal conditions, even if it is not noticeable on the ERP plots. The average computational time to classify a feature is 0.26s $\pm$ 0.05s.

The class corresponding to high PEN levels is the condition Sudden-Obstacle. Thus, the precision, recall and F_1-score (F_1) of this class are also reported in Table 4.3 for each participant, for the three-class problem.

If the CNN is used to detect the PEN level and then this information is fed into a closed-loop

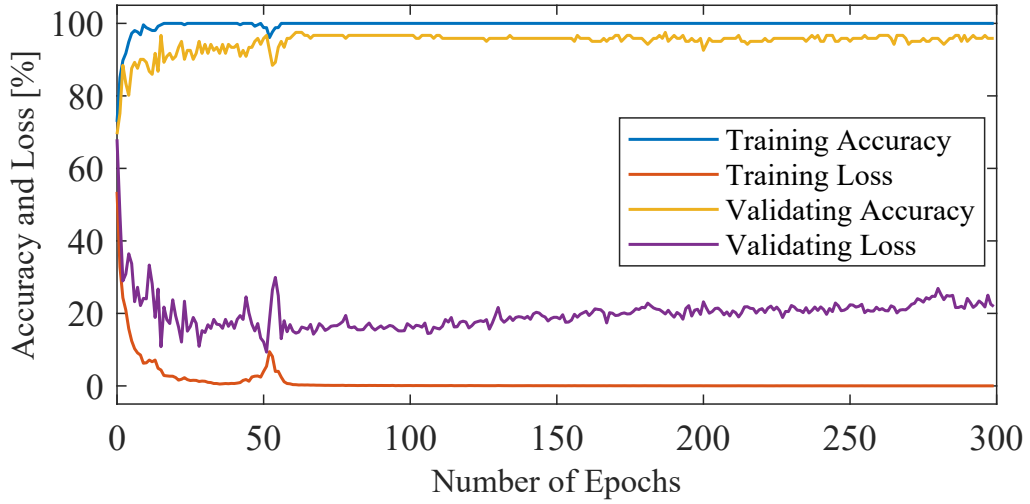

FIGURE 4.3: Accuracy and loss during the training and validating phase of the CNN, with respect to the number of epochs.

system, the precision of the network has to be taken into account, allowing the robot to react safely, also in the case of a false positive. Considering the mean values, the classifier might still be acceptable for three classes.

The computational time depends on the specifications of the machine used to process the data. On a machine with a less powerful Graphics Processing Unit (GPU) the time required to detect a prediction error might be longer.

These results can lead to human-robot systems that compromise between reducing PEN and having robust pHRC strategies. For example, if repulsive forces are too gentle in control strategies for singularity or collision avoidance, this might affect the robustness of the human-robot system. Multiple PEN levels could lead to thresholds that maximise robot predictability while maintaining acceptable robustness.

4.4 Limitations

Most of the limitations outlined in Section 3.4 are also valid for the results presented in this chapter, as the data sets and task are the same.

It was assumed that what distinguishes different classes is the presence and amplitude of PEN. This is however an assumption and the classifiers are not looking for a specific feature, but for similar

TABLE 4.3: Accuracy (Acc) in %, Mean Square Error (MSE) and prediction time (PT), in seconds, in the case a Convolutional Neural Network (CNN) is used to classify three classes: Sudden-Obstacle, Smooth-Obstacle and Normal. precision (Pre), recall (Rec) and F_1-score (F_1) are also reported for the Sudden-Obstacle class [8].

		Acc [%]	**MSE**	**PT [s]**	**Sudden-Obstacle**		
					Pre	**Rec**	**F_1**
Participant	**P01**	58.4	1.01	0.17	0.48	0.58	0.52
	P02	61.2	1.06	0.15	0.63	0.61	0.62
	P03	59.8	1.08	0.20	0.68	0.60	0.57
	P04	71.6	0.58	0.15	0.73	0.72	0.71
	P05	66.4	0.64	0.16	0.55	0.66	0.56
	P06	78.0	0.36	0.24	0.78	0.78	0.78
	P07	64.2	1.72	0.16	0.50	0.35	0.37
	P08	56.9	1.17	0.18	0.36	0.57	0.44
	P09	60.0	1.03	0.16	0.56	0.60	0.56
	P10	66.7	0.70	0.20	0.66	0.67	0.60
	P11	91.1	0.23	0.16	0.90	0.89	0.89
Mean		66.7	0.87	0.18	0.62	0.64	0.60
SD		10.2	0.42	0.03	0.15	0.14	0.15

patterns to the ones provided during the training phase. There might be some other underlying cognitive process happening, that can help discern the different classes.

The collaborative task used to collect the EEG data is one-dimensional and repetitive. Results presented in this chapter might not be valid for a task in the 3D space, especially in the case of a non-repetitive task. Even if the nature of PEN in the ERP is independent from the task, it might add variability and confounding factors to the signal. For example, if the task involves a bigger range of motions there will be more muscular activity that will add noise to the EEG signal.

Only the EEG data was used as an input for the classifiers in this research. By adding data from the robot, such as interaction force, end-effector velocity and position, it might be possible to increase the accuracy.

Performances were the result of an intra-subject analysis (classifiers were trained and tested on the same participant). It would be interesting to evaluate the classifiers based on an inter-subject analysis, in which the classifiers are trained with the data set belonging to one participant and tested on the others.

As in Chapter 3, the simple nature of the stimulus (i.e. force with first-order dynamics) represents a big limitation. Whether the classifiers would be able to detect PEN caused by a force with more complex dynamics remains an open question.

4.5 Conclusions

This chapter investigated methods to estimate PEN, and consequently estimate the robot predictability, during pHRC applications. Six classifiers were compared in two-class and three-class classification problems. Results show that the CNN classifier performed the best, with an average accuracy of 82.1% $\pm$ 5.2%, in the two-class problem. The same classifier resulted in an average accuracy of 66.7% $\pm$ 10.2% when classifying three classes. The lower accuracy can be justified by the lower number of trials per class, reducing the size of the training data sets. Results of the three-class classification problem suggest that, despite the results obtained in the ERP in Chapter 3, there is a difference between the three classes.

In both the two-class and three-class classification problems, with the machine used in this research, the prediction time is comparable to the human reaction time, suggesting that the CNN performs quickly enough to be used for real-time detection of PEN and to adapt the robot behaviour to reduce the PEN level.

The CNN accuracy is believed to be promising and adequate to implement a closed-loop system, if the accuracy itself is taken into account. For example, to mitigate a lower accuracy, it is possible to implement a control system that updates its behaviour only after several cognitive conflicts.

This chapter addressed the problem of an online estimation of PEN. This is critical to develop a pHRC system that can use this information in real-time to adapt its behaviour.

Chapter 5

Detection and Application of Prediction-Error Negativity in a Real Control Strategy for Physical Human-Robot Collaboration

5.1 Introduction

In Chapter 3, it was found that a change in the robot system admittance can generate detectable PEN. The change in admittance was the result of the introduction of an unexpected resistive force with first-order dynamics. Moreover, among the six classifiers compared in Chapter 4, a CNN was found as the best performing classifier for estimating PEN.

Whether PEN can be detected in real practical pHRC control strategies is still unclear. Normally, the admittance that the human operator perceives is modulated to encourage or discourage directions of motion or specific configurations. This results in human-robot interactions with complex dynamics. Typical strategies that affect the robot admittance in pHRC are assistive strategies or control strategies for singularity and collision avoidance. In this chapter, a singularity avoidance strategy was chosen to test whether PEN can be measured and used to adapt the human-robot interaction. However, a similar approach can be used for other strategies, such as collision avoidance.

Kinematic singularities are a classical problem of robot manipulators. They occur when the robot Jacobian matrix loses rank and its inverse degenerates. The inverse of the Jacobian is often needed to calculate the joint velocities required to achieve desired Cartesian velocities. A typical strategy for alleviating this problem is to approximate the inverse of the Jacobian with another matrix, maintaining numerical stability but sacrificing exactness. A common strategy is to use a modified version of the Jacobian matrix close to a singularity, such as the transpose of the Jacobian [129] or a matrix created with the Damped Least-Squares (DLS) strategy [130]. In the case of robots for pHRC, this means that, when the robot is close to a singularity, the user intention is not translated into the desired robot motions, and this may affect the predictability of the robot behaviour.

In [12], Carmichael et al. compared six different sets of parameters for the Exponentially Damped Least-Squares (EDLS) strategy for singularity avoidance. Carmichael et al. used a questionnaire to evaluate human preferences for those parameters. As those parameters ultimately affect the perceived robot admittance, it is questioned whether there is a relationship between what human co-workers prefer and the robot predictability. Maurice et al. [28] demonstrated how humans prioritise predictability, when physically interacting with objects with complex dynamics.

If different PEN levels can be found when comparing control parameters that result in different admittance dynamics, it might also be possible to automatically adapt those parameters based on PEN estimated using the CNN described in Chapter 4. In this chapter, sub-question Q3 (Section 1.3.3) is explored. Three more questions need to be addressed in order to answer Q3:

- Q3.1: Can PEN be detected when implementing a practical singularity avoidance strategy in pHRC?
- Q3.2: Are PEN and human preferences related when comparing different control settings in a singularity avoidance strategy?
- Q3.3: Can PEN be used to adapt the singularity avoidance strategy by closing the loop on the cognitive state of the human co-worker?

Results aiming at answering the Q3.1 and Q3.2 were submitted to the 2021 IEEE International Conference on Robotics and Automation (ICRA) [10].

5.2 Methodology

Two experiments with a similar setup were performed. Experiment 3 (Exp3) addresses question Q3.1 and Q3.2. Exp3 investigates whether a pHRC singularity avoidance strategy that subtly affects the robot admittance can induce detectable PEN. The same experiment is used to assess the relationship between human preferences and PEN. Experiment 4 (Exp4) addresses question Q3.3. This experiment is performed to evaluate whether it is possible to close the loop on the human operator to adapt the singularity avoidance strategy.

5.2.1 Experimental setup and task

The following setup is used for Exp3 and Exp4. A pHRC system named ANBOT was used for the experiments. The robot system is presented in [7] and uses a UR10 robot arm. The motions are achieved through an admittance-based control system that uses a force/torque sensor mounted on the end-effector. The brain activity was recorded from participants using a 32-channel EEG system named MOVE, produced by Brain Product GmbH, Germany. The electrodes were placed in line with the 10-20 international system [111] and the contact impedance was maintained below 50kΩ. The sampling rate of the EEG device is 1000Hz. It is worth mentioning that setting up the EEG device with the proper impedance for each electrode takes twenty to forty minutes. This affected the decision of limiting the time required for participants to perform the experiments, to ensure subjects were not fatigued. The time required to set up the EEG device represents a big limitation for the application of this technology in real-world scenarios. Technology is however getting better every year, and in the future it might be possible to reduce considerably this time.

For Exp3, EEG data were collected from fourteen healthy participants, eleven males and three females, between 22 and 42 years of age. Five of those participants (four males and one female, between 28 and 42 years old) also performed Exp4. The experiments follow the procedures approved by the UTS Human Research Ethics Committee with approval number ETH18-2732.

After setting up the equipment for the experiments, for each participant, baseline data were collected while they were seated. As baseline data, one minute of brain activity was recorded with eyes closed and one minute with eyes open. The participants were then asked to explore the robot workspace, by freely interacting with the robot in the 3D space. They were specifically given the

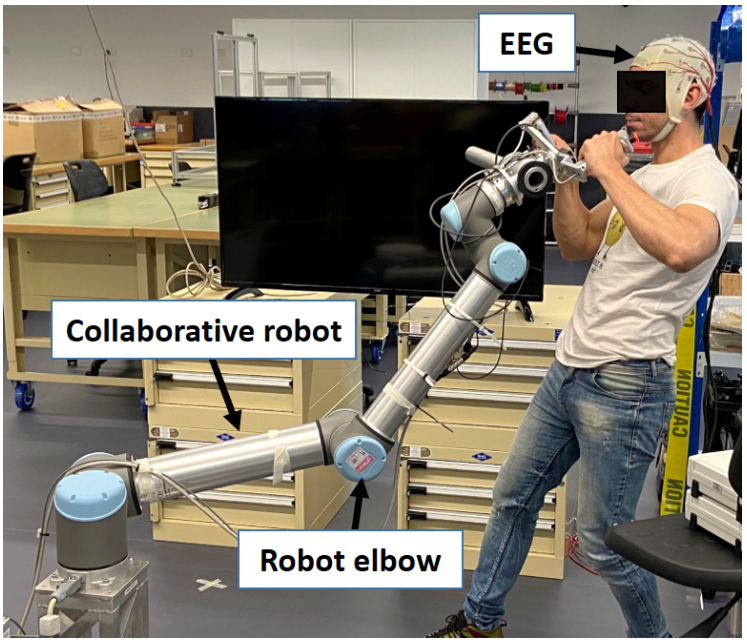

FIGURE 5.1: A participant performing one of the experiments, with the collaborative robot close to a kinematic singularity [10].

task to move the robot throughout the workspace and assess the robot behaviour. As most of the participants were new to pHRC systems or unaware of what a singular configuration is, they were explicitly asked to move the robot close to specific configurations, such as the one in which the angle of the robot elbow (joint 3) of the UR10 is 180 degrees (robot elbow is straight). In Figure 5.1, a participant is shown while collaborating with the robot close to a singular configuration.

For Exp3, participants are provided with an A/B toggle switch on the end-effector, to freely select one of two sets of parameters (modes) for the singularity avoidance strategy. The two modes are later explained in Section 5.2.2.1. Participants could test both modes as many times as they wanted, allowing them to fully experience and explore differences between the two modes. To obtain sufficient trials for both modes, each participant was recorded for ten to twenty minutes.

Exp4 is designed to assess the feasibility of a closed-loop system that uses PEN to adapt a pHRC singularity avoidance strategy. For Exp4, participants are asked to freely move the robot arm throughout the workspace, but especially to move close to singular configurations. The toggle switch was disabled and the participants were made aware of it. Each participant was recorded for about fifteen minutes. Exp4 was always performed after Exp3 and there was always a break of at least five minutes between the two experiments.

To see whether PEN correlates with human preferences, each participant was asked to fill in a questionnaire, immediately after performing Exp3. The questionnaire is based on [12] and is designed to assess human preferences when comparing two sets of parameters for the singularity avoidance strategy. The questionnaire consists of the following six questions:

1. Which mode was the smoothest to use?
2. Which mode was the most responsive?
3. Which mode felt like you were most in control?
4. Which mode was the least frustrating to use?
5. Which mode felt the safest to use?
6. Overall, which mode do you prefer and why?

For the last question participants were provided with space to elaborate on why they preferred one mode over the other. Participants were also asked whether they have used a robot arm before, whether they know how robot arms work and whether they know what a robot kinematic singularity is.

5.2.2 Interaction dynamics

The admittance-based controller presented in [22] has been adapted for these experiments. The block diagram of the implemented control system can be seen in Figure 5.2. This is an admittance-based controller, in which forces are transformed into Cartesian robot velocities $\dot{\mathbf{x}}_d$. $\mathbf{K}_A$ is a diagonal matrix with the admittance gains, with $0.01m/sN$ for the linear components and $0.4rad/sN$ for the angular components. $\mathbf{F}_H$ is the vector of forces resulting from the interaction with the human operator and $\mathbf{F}_D$ is a damping force to smoothen the motion. $\mathbf{K}_D$ is a diagonal matrix, with linear components set to $0.01Ns/m$ and angular components set to $1Ns/rad$. $\mathbf{F}_C$ is a force vector repelling the operator from configurations that would result in a collision between parts of the robot system. Collisions between the robot and the floor have also been addressed with this block. The collision avoidance strategy was kept active during the experiments, to replicate a real scenario with multiple control strategies that could affect the perceived robot admittance. Moreover, most

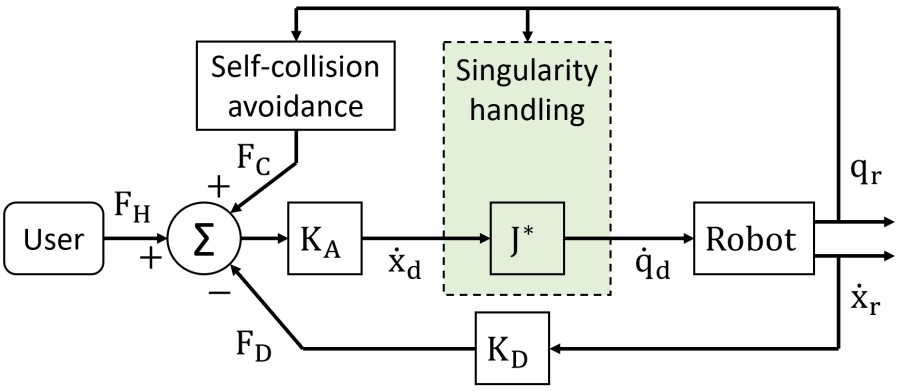

FIGURE 5.2: Block diagram of the implemented control system [10]. $\mathbf{F}_H$, $\mathbf{F}_C$ and $\mathbf{F}_D$ are the interaction forces, the forces generated by self-collision avoidance and the damping forces. $\mathbf{J}^\star$ is the Jacobian matrix modified by the EDLS strategy. $\dot{\mathbf{x}}_d$ and $\dot{\mathbf{x}}_r$ are the desired and real Cartesian velocity. $\dot{\mathbf{q}}_d$ are the desired joint velocities and $\mathbf{q}_r$ are the real joint positions. $\mathbf{K}_D$ is the damping matrix to smooth the Cartesian velocity and $\mathbf{K}_A$ contains the admittance gains.

of the forces resulting from the collision avoidance block can be visually anticipated, and therefore unlikely to cause significant PEN. It is worth mentioning that the robot admittance perceived by the user is also affected by the manipulability (and dexterity) of the robot arm. Robot manipulability is generally defined through ellipsoids. Manipulability ellipsoids vary throughout the workspace, affecting the perceived admittance of the robot. The perceived robot admittance decreases when approaching singular configurations as a consequence of a change in the manipulability ellipsoid. While the manipulability of the robot could potentially affect the robot predictability, in proximity of singularities, the effect of the manipulability is negligible when compared to the effect of the selected singularity avoidance strategy.

The singularity handling strategy that was chosen is the exponentially damped least-squared (EDLS) strategy presented in [131]. This strategy was chosen as it is designed specifically for pHRC, and has parameters allowing the "feel" of the singularity avoidance strategy to be tuned. The robot Jacobian matrix $\mathbf{J}$ is decomposed using the Singular Value Decomposition (SVD) method resulting in $\mathbf{J} = \mathbf{U}\mathbf{\Sigma}\mathbf{V}^T$. $\mathbf{U}$ and $\mathbf{V}$ are both orthonormal matrices, while $\mathbf{\Sigma}$ is a diagonal matrix with the same dimensions as $\mathbf{J}$ and containing the singular values σ_i, with $i = 1, \cdots, 6$ in the case of a six degrees-of-freedom (DOF) robot able to move in a 6-DOF space. As the robot gets closer to a singular configuration the singular values approach zero, resulting in a Jacobian matrix that degenerates when inverted. Therefore, singular values can be a good measure of how close a robot is to a singular configuration. In the case of small σ_i, the inverse of the Jacobian matrix is modified

into $\mathbf{J}^{\star} = \mathbf{V}\mathbf{\Sigma}^{\star}\mathbf{U}^{T}$, with $\mathbf{\Sigma}^{\star}_{ii} = s_i/\sigma_i$, and s_i is equal to:

$$s_i = \begin{cases} 1-\beta^{\left\lceil \frac{\sigma_i - \bar{\sigma}_0}{\bar{\sigma}_1 - \bar{\sigma}_0} \right\rceil}, & \text{if } \sigma_i > \bar{\sigma}_0 \\ 0, & \text{otherwise} \end{cases} \tag{5.1}$$

In (5.1), $\bar{\sigma}_0$ and $\bar{\sigma}_1$ define the resulting damping rate and β is a small value, set to 0.02 in this case. The values $\bar{\sigma}_0$ and $\bar{\sigma}_1$ can be different depending on whether the robot is approaching a singularity or moving away from it. This results in two sets of values, $\bar{\sigma}_{0a}$ and $\bar{\sigma}_{1a}$ if the robot is moving away from a singularity, and $\bar{\sigma}_{0b}$ and $\bar{\sigma}_{1b}$ if the robot is moving towards it. In that case, an asymmetric behaviour is obtained. This permits more damping to be applied in one direction and less in the other. The operator has to be discouraged from approaching the singularity, not from moving away from it, and an asymmetric approach allow targetting that behaviour. The reader is directed to [131] for a comprehensive overview of the implemented strategy.

Carmichael et al. [12] used their questionnaire to evaluate human preferences in terms of damping and asymmetry of the EDLS strategy to handle singularities in pHRC. Results indicate that fast asymmetric damping rate was preferred over slow symmetric damping. The damping rate (fast or slow) is set by the difference $\bar{\sigma}_1 - \bar{\sigma}_0$. The smaller the difference, the faster is the damping rate, as it results in a sudden onset of this.

5.2.2.1 Experiment 3 - Exp3

In Exp3, two of the settings utilised in [12] were used here for comparison. The most (mode A) and least (mode B) preferred sets of parameters, as reported in [12], were used. They are reported in Table 5.1. Even though 69 participants took part in the experiment presented in [12], only seven of them directly compared those two specific sets of parameters. To have a larger cohort, after completing the task, the fourteen participants taking part in Exp3 were asked to fill in the same questionnaire outlined in [12]. As also the data collected in [12] was used in this thesis, a total of 21 people filled in the questionnaire.

TABLE 5.1: Parameters for the two compared modes [10].

Mode	Description	Parameter			
		$\bar{\sigma}_{0a}$	$\bar{\sigma}_{1a}$	$\bar{\sigma}_{0b}$	$\bar{\sigma}_{1b}$
A	Fast Asymmetric	0.15	0.25	0.25	0.35
B	Slow Symmetric	0.25	0.45	0.25	0.45

The set of parameters in mode A translates to a motion with negligible damping while moving away from a singularity. For $\sigma_i < \bar{\sigma}_{0b}$, the joint velocity is equal to zero when the joint is approaching singularity, which means that for mode A the minimum σ_i is 0.25. With the same mode, when moving away from singularity, the user experiences damping for $0.15 < \sigma_i < 0.25$. Therefore, when moving away from a singular configuration, mode A results in no damping being applied. With mode B, the operator experiences damping when approaching singularity, but also when moving away from a singular configuration. In Figure 5.3 and Figure 5.4 the singular value reciprocal is shown with respect to the singular value, for mode A and mode B respectively. The singular value reciprocal is equal to $\mathbf{\Sigma}_{ii}^{-1} = 1/\sigma_i$ in the case of no EDLS strategy implemented (i.e. undamped) and $\mathbf{\Sigma}_{ii}^{\star} = s_i/\sigma_i$, in the case of the EDLS strategy. In the case of mode A, when the operator is moving towards a singular configuration $\bar{\sigma}_{1b}$ is smaller. Therefore, the workspace in which the operator's intention is transformed in expected robot motions is bigger. In fact, the undamped and damped curves in Figure 5.3 and Figure 5.4 start diverging in $\bar{\sigma}_1$ when moving towards a singularity.

5.2.2.2 Experiment 4 - Exp4

In Exp4, the aim is to see whether it is possible to adapt online the parameters of the EDLS strategy, based on the detection of PEN. In this experiment there is no mode to select. A visual representation of the closed-loop system is shown in Figure 5.5.

In this case, $\bar{\sigma}_{0a}$ and $\bar{\sigma}_{0b}$ are set equal to 0.25. This value was chosen for safety reasons, to ensure the user is discouraged from reaching singular configurations, as a minimum of damping is guaranteed at all times. Parameters $\bar{\sigma}_{1a}$ and $\bar{\sigma}_{1b}$ are automatically set by a reinforcement learning (RL) algorithm. The RL algorithm used in Exp4 is a Deep Deterministic Policy Gradient (DDPG) algorithm. The robot arm is seen as the agent, while the environment state is a continuous space

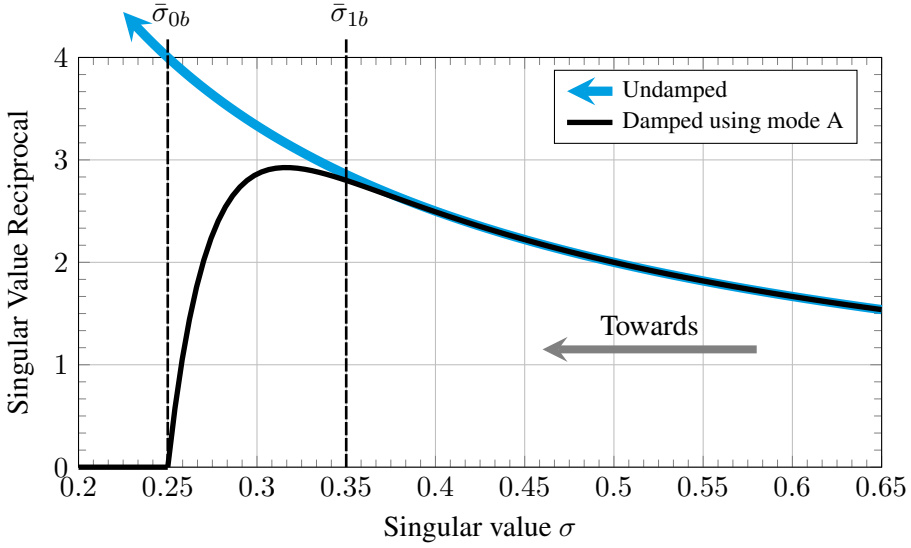

FIGURE 5.3: Singular value reciprocal with respect to the singular value, in the case of mode A in Exp3, when the operator is moving towards a singular configuration.

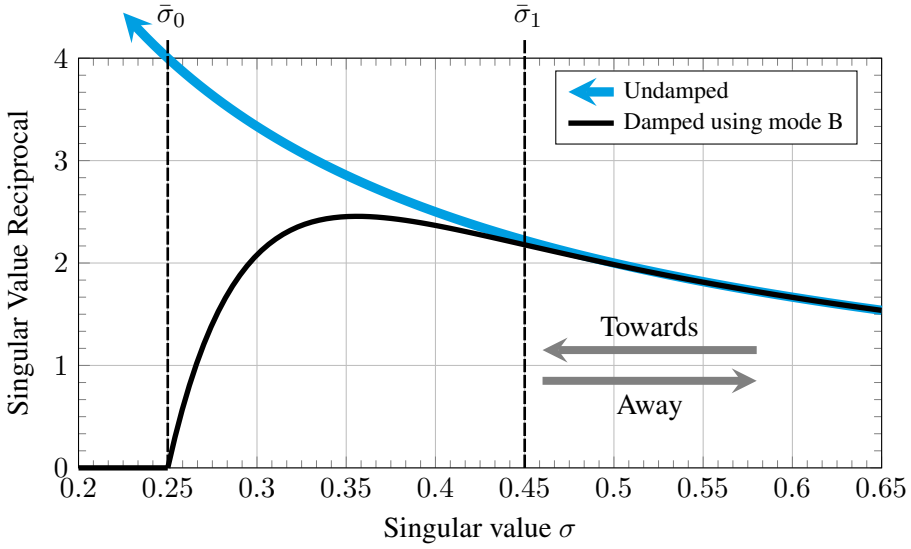

FIGURE 5.4: Singular value reciprocal with respect to the singular value, in the case of mode B in Exp3, when the operator is moving towards and away from a singular configuration.

with Cartesian positions, velocities and interaction forces. The action of the RL algorithm is to set $\bar{\sigma}_{1a}$ and $\bar{\sigma}_{1b}$. The reward is a function of PEN amplitude and spectral power: the higher the PEN amplitude and the power spectral density (PSD) are, the lower is the reward and vice versa. The environment of the algorithm is the 3D robot workspace and the goal is to reduce PEN and PSD. Exp4 lasts fifteen minutes for each participant.

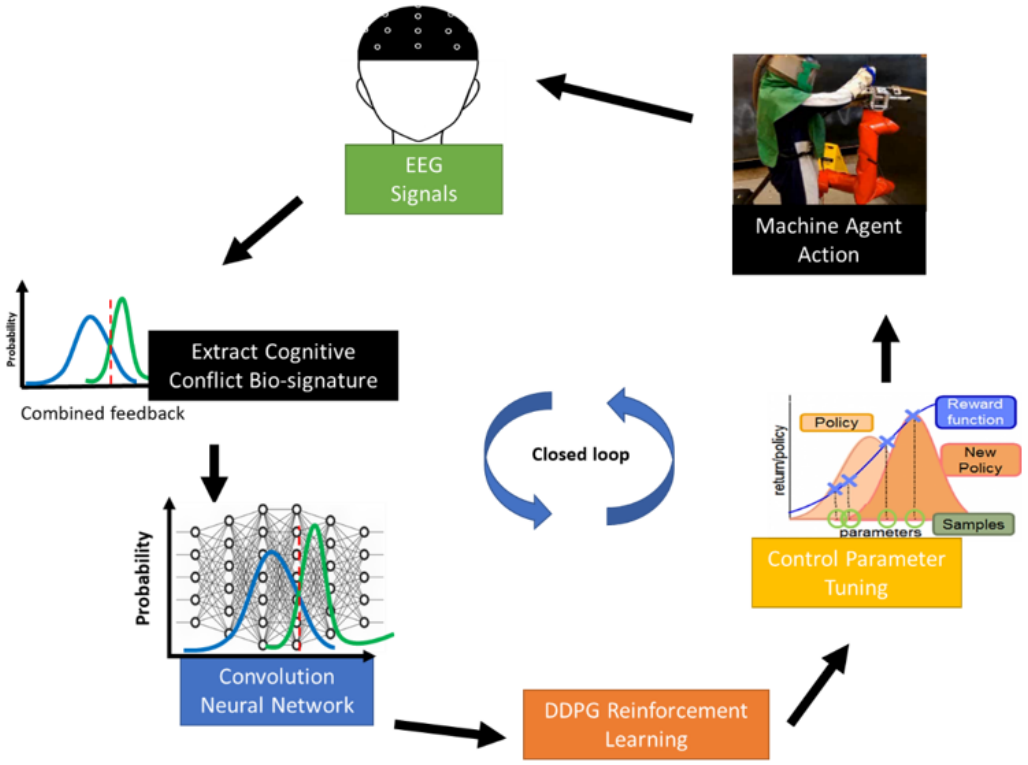

FIGURE 5.5: Closed-loop system to adapt the pHRC control strategy by PEN detection. While the user physically interact with the robot, EEG signals are being recorded. PEN is being detected by CNN and a reinforcement learning algorithm is responsible of tuning control parameters.

Actor and critic networks of the DDPG algorithms are shallow neural networks that use the mean-squared error (MSE). Three possible rewards are given: good, medium and bad. The reward is provided every 1.2 seconds and is based on the estimation of PEN through a CNN with a time-encoding kernel (EnK) presented in [132]. The full data sets from Exp1 in Chapter 3 were used to train the CNN as a three-class classification problem. If the CNN detects a signal comparable to the condition Sudden-Obstacle the reward is bad, as it presents a high level of prediction errors. If the signal is comparable to Smooth-Obstacle the reward is medium and if it is comparable to Sudden- or Smooth-Normal then the reward is good. For Exp4, a trial is defined as a full loop of the DDPG algorithm to get an action.

As mentioned above, the outputs of the DDPG algorithm are $\bar{\sigma}_{1a}$ and $\bar{\sigma}_{1b}$. Parameters $\bar{\sigma}_{0a}$ and $\bar{\sigma}_{0b}$ are set to 0.25, to limit the number of variables that the algorithm has to set. For safety reasons, boundaries were set for $\bar{\sigma}_{1a}$ and $\bar{\sigma}_{1b}$ to values in the range of 0.35 and 0.45. This ensures that the admittance does not vary too much. At the beginning of the experiment, the RL algorithm is

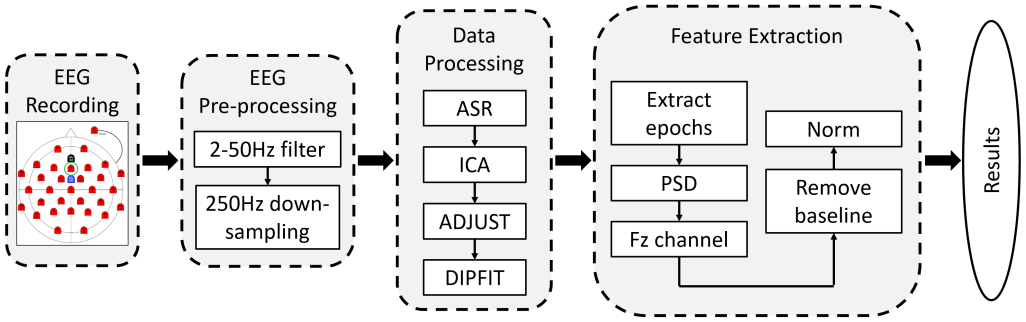

FIGURE 5.6: The pipeline used to process the EEG signals offline for the ERP analysis [10]. After recording the brain activity, the data sets are first filtered and down-sampled. The resulting data sets are then cleaned from artifacts and noise. Epochs are then extracted and the PSD calculated for Fz channel. The baseline is then removed and results are normalised.

expected to set those parameters in a randomised way. With $\bar{\sigma}_1$ close to the lower limit, the operator would experience fast damping, while close to the upper limit, they would experience slow damping. Since the algorithm is setting $\bar{\sigma}_1$ for both directions (approaching and leaving singular configurations), the RL algorithm is responsible for the symmetry of the singularity avoidance strategy.

5.2.3 Data processing

For both the experiments, MATLAB R2018a (Mathworks Inc, USA) was used to process the data and Figure 5.6 shows the pipeline implemented for the ERP analysis. A band-pass filter was used to reject common noise, followed by down-sampling the data to 250Hz. With EEGLAB [112], Artefact Subspace Reconstruction (ASR) [114] was used to reject channels affected by muscle activity, eye movement or other noise. Independent Component Analysis (ICA) [113] was then applied to the data sets, followed by ADJUST [115], an automatic EEG artifact detection algorithm which further filtered the Independent Components (ICs). The dipoles of the ICs were then evaluated with DIPFIT and the ICs with a residual variance greater than 10% were removed.

In the experiments, there is no discrete clear stimulus, but continuous more subtle stimuli. To compare the modes in Exp3, events related to the dynamics of the mode are required. From here on, σ is used to indicate the critical singular value, i.e. the smallest singular value. As shown in Figure 5.7, the deviation of $\mathbf{J}^{\star}$ from $\mathbf{J}^{-1}$ becomes more evident when $\sigma < \bar{\sigma}_1$. Therefore, that condition is considered as an event. The effect of the EDLS strategy becomes even more

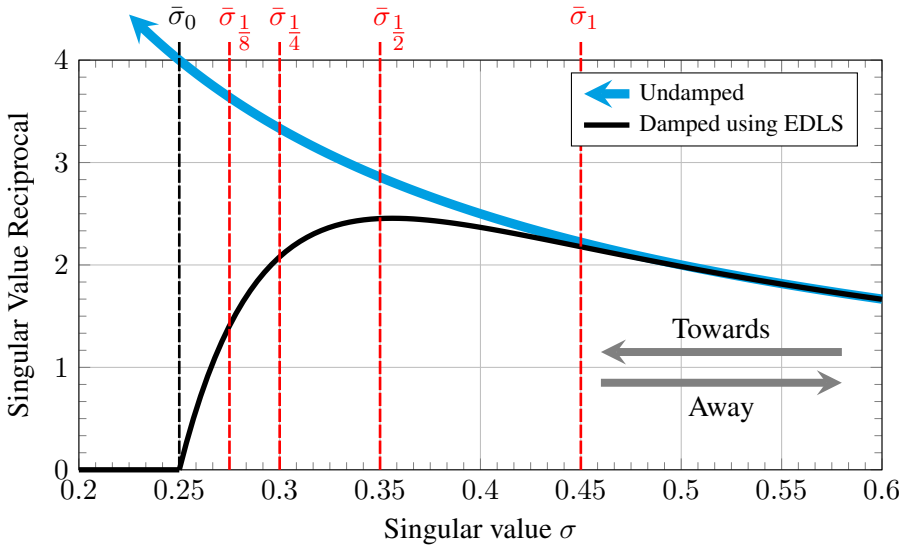

FIGURE 5.7: In red, triggers for events in mode B in Exp3 [10].

evident as the singular value σ decreases further. As people have different sensitivity, the following conditions are also considered as events: $\sigma < \bar{\sigma}_{1/2}$, $\sigma < \bar{\sigma}_{1/4}$ and $\sigma < \bar{\sigma}_{1/8}$, with $\bar{\sigma}_{1/2} = (\bar{\sigma}_1 + \bar{\sigma}_0)/2$, $\bar{\sigma}_{1/4} = (\bar{\sigma}_{1/2} + \bar{\sigma}_0)/2$ and $\bar{\sigma}_{1/8} = (\bar{\sigma}_{1/4} + \bar{\sigma}_0)/2$. Each event is associated with a marker. Lab Streaming Layer (LSL) and the application LabRecorder were used to synchronise the EEG signals with the event markers. Since in this chapter the symmetry of the approach is also considered and its impact on the robot predictability, different event markers are used to highlight conditions while the user is moving away from a singular configuration. Table 5.2 summarises the markers used, and which condition they correspond to. Since mode A presents no damping when the user moves away from a singularity, only one marker is used to indicate the event. This is triggered by the user moving away from a singularity after any of the markers related to the user moving towards a singularity in mode A. The presence of markers to extract epochs also allows to isolate the effect of the singularity avoidance strategy from the self-collision avoidance strategy and the intrinsic change of the robot manipulability throughout the workspace.

The event markers are used to extract the epochs in Exp3. In the ERP, PEN is a negative deflection happening around 50-250ms after the stimulus, in the θ (4-8Hz) or α (8-13Hz) bands. Therefore, for each event, epochs are extracted from the marker to 400ms after it. As a continuous stimulus is being used, a simple time-domain analysis would not be appropriate. The user is free to move how they please, so the events are not equally spaced in time or consecutive. A time-frequency analysis is instead performed and the power spectral density (PSD) is then computed in $\mu V^2/Hz$, for the θ

TABLE 5.2: Event markers used to extract epochs from the collected data sets. The markers are presented with their corresponding condition, direction and mode [10].

Marker (Abbrev.)	**Condition**	**Direction**	**Mode**
ApproachingA1 (AppA1)	$\sigma < \bar{\sigma}_1$	Towards	A
ApproachingA2 (AppA2)	$\sigma < \bar{\sigma}_{1/2}$	Towards	A
ApproachingA3 (AppA3)	$\sigma < \bar{\sigma}_{1/4}$	Towards	A
ApproachingA4 (AppA4)	$\sigma < \bar{\sigma}_{1/8}$	Towards	A
LeavingA (LeaA)	After appr.	Away	A
ApproachingB1 (AppB1)	$\sigma < \bar{\sigma}_1$	Towards	B
ApproachingB2 (AppB2)	$\sigma < \bar{\sigma}_{1/2}$	Towards	B
ApproachingB3 (AppB3)	$\sigma < \bar{\sigma}_{1/4}$	Towards	B
ApproachingB4 (AppB4)	$\sigma < \bar{\sigma}_{1/8}$	Towards	B
LeavingB1 (LeaB1)	$\sigma < \bar{\sigma}_1$	Away	B
LeavingB2 (LeaB2)	$\sigma < \bar{\sigma}_{1/2}$	Away	B
LeavingB3 (LeaB3)	$\sigma < \bar{\sigma}_{1/4}$	Away	B
LeavingB4 (LeaB4)	$\sigma < \bar{\sigma}_{1/8}$	Away	B

and α bands, for each of the extracted epochs. Welch's overlapped segment averaging estimator is used to compute the PSD with an overlapping window of 50%. A greater negativity will produce a higher PSD. For each participant, the mean of the PSD was calculated for all the epochs with the same event. The focus is on the mid-line frontal EEG channel Fz, as PEN is typically found in the frontal area of the brain. Before starting Exp3, baseline data were recorded for one to two minutes, with the participant sitting with their eyes open. The baseline data set is also processed with the first three blocks in Figure 5.6. The PSD of the processed baseline was then computed and subtracted from each event PSD. As the PSD can differ greatly between different participants, the results were normalised for each participant.

The PSD data from θ and α bands have been further statistically analysed using SPSS (IBM SPSS Inc Version 24). A repeated measure analysis of variance (ANOVA) was performed followed by post-hoc analysis using least significant difference (LSD).

In Exp4, an event-based comparison is not needed. As the RL algorithm aims at decreasing PEN and spectral power, the data sets were divided in three subsets. Only the first and last subset of each data set were compared to see whether the RL algorithm is reducing PEN. The first subset was named T_1 and the last one was named T_2. The average PSD for each frequency band was

computed for T_1 and T_2, only for the frontal and central mid-line channels (i.e. Fz and Cz). The topography of the scalp was also evaluated for all channels for the two subsets.

5.3 Results and discussion

Section 5.3.1 presents results of Exp3, with the relevant discussion. As previously mentioned, Exp3 answers questions Q3.1 and Q3.3. Exp3 addresses whether a real pHRC control strategy can generate a detectable PEN and whether human preferences are related to robot predictability. Section 5.3.2 outlines and discusses results obtained from Exp4. Exp4 aims at understanding whether a robot system that closes the control loop on the cognitive state of the human operator to maximise the robot predictability is feasible.

5.3.1 Experiment 3 - Exp3

To answer the question of whether a pHRC singularity avoidance strategy with complex dynamics generates PEN, and whether it can be detected, results from the ERP analysis are presented for Exp3, specifically in terms of PSD.

Two participants had to be excluded from the EEG data analysis, due to their EEG data being corrupted. In the case of one participant, the contact impedance between electrodes and scalp was wrong, because of the reference electrode not being properly positioned. The experiment went ahead, but the resulting EEG data presented a too low signal-to-noise ratio. The second participant was excluded because the relative data set was too short. The EEG device ran out of battery in the middle of the experiment. This resulted in not having enough data corresponding to all the events. As a consequence, results about the brain activity in Exp3 are for a cohort of twelve participants. The technical difficulties were specific to the device used and not to the EEG technology in general, so it does not impact the practicability of EEG-based applications in pHRC.

The normalised PSD, calculated in $\mu V^2/Hz$, is shown in Figure 5.8A for the θ-frequency band and in Figure 5.8B for the α-frequency band. The reader is reminded that the PSD is normalised in the [0 1] range for each participant, due to the fact that PSD has a big variation between people. A high PSD suggests that a negativity is happening after the event marker used to extract that

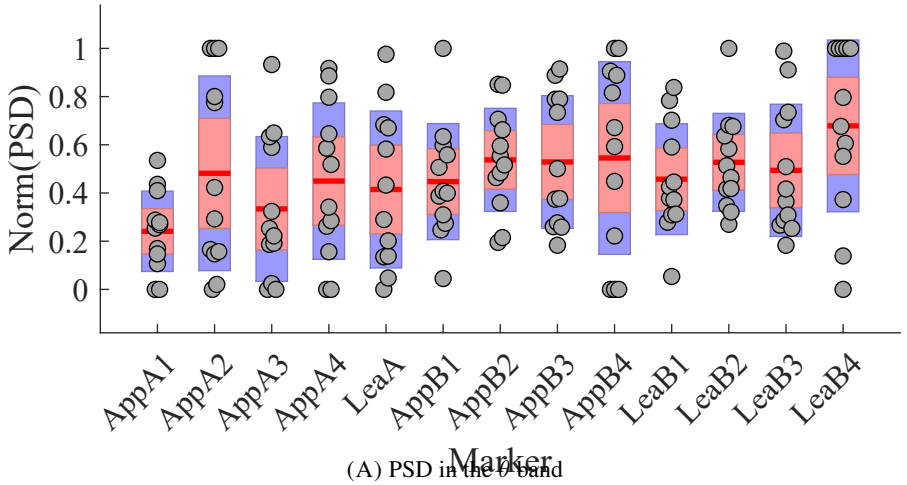

(A) PSD in the θ band

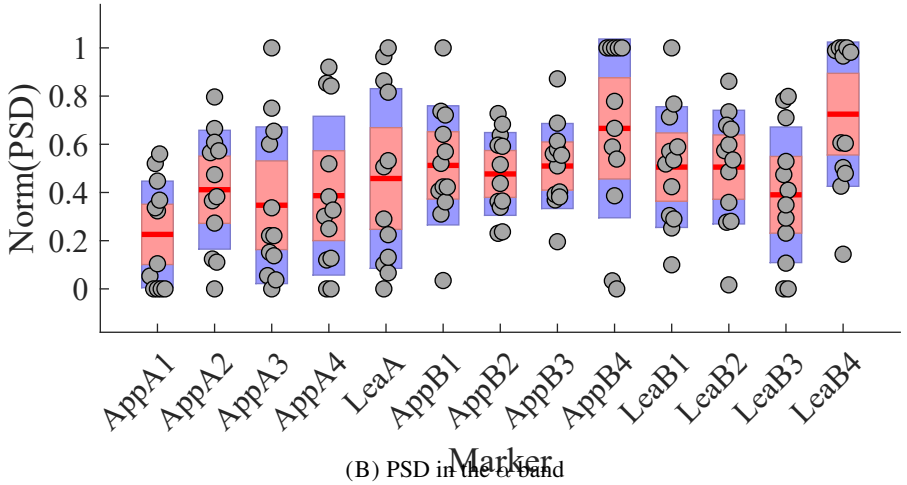

(B) PSD in the α band

FIGURE 5.8: Normalised power spectral density in the θ (A) and α (B) bands for channel Fz, with respect to each event [10]. Plots generated with the notBoxPlot function [11]. Grey circles represent the data points and the thick red line is the mean value. The standard error of means (SEM) with a 95% confidence interval is reported as a pale red bar and the standard deviation is the pale blue bar.

epoch. In the plots, the data points are represented as grey circles, the mean is a thick red line, the standard error of means (SEM) with a 95% confidence interval is reported as a pale red bar and the standard deviation is the pale blue bar. Figure 5.8A shows a higher mean of PSD for most of the events related to mode B. When an operator is moving towards a singularity, in the presence of a slow damping rate, the operator seems to experience a slight increase of PSD in the θ band. This means that, with mode B, the more the Jacobian $\mathbf{J}^{\star}$ diverges from the actual Jacobian $\mathbf{J}$, the more the robot predictability decreases.

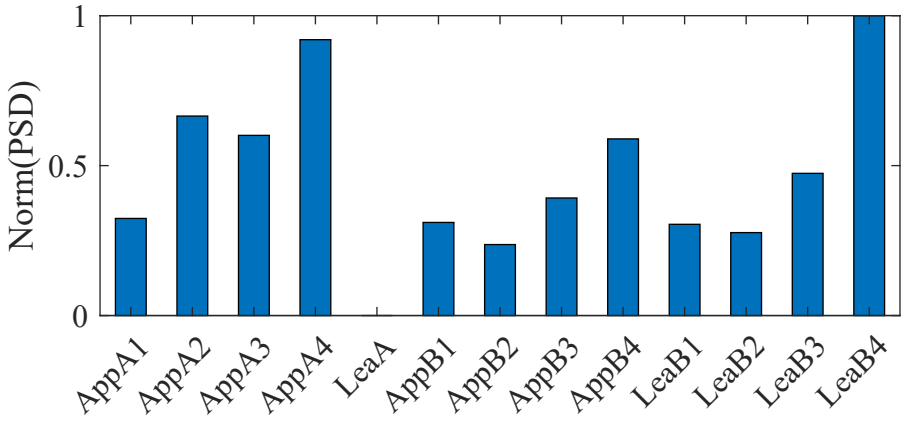

FIGURE 5.9: Normalised power spectral density in the α band for the outlying participant, with respect to each event [10].

In the case of moving away from a singular configuration, the two modes translate into very different dynamics, as one is undamped and the other presents a slow damping rate (Section 5.2.2.1). Results indicate that the two modes are perceived differently while leaving a singularity. Participants present higher PSD with mode B, especially for $\sigma < \bar{\sigma}_{1/8}$ (LeaB4). In that case, the participant experiences large damping while trying to move away from a singularity, which can be counter-intuitive.

Figure 5.8B shows PSD in the α band. In this frequency range, differences between the two modes are even more obvious. All the events corresponding to the user approaching a singularity with mode B (symmetric slow damping rate) present a higher mean than the same events in the case of mode A (asymmetric fast damping rate). In the case of participants moving away from a singularity, results are similar to the ones in the θ band, suggesting that participants find more predictable undamped dynamics.

It is worth noticing the presence of outliers in both frequency bands. In particular, one of the participants presented high PSD in the case of most of the events with mode A. In Figure 5.9, the normalised PSD of the outlying participant is shown in the form of a bar graph, for the α band. This participant seems to experience prediction errors in the case of fast damping, when approaching singularity.

One of the participants has previous experience with robots for pHRC and is familiar with singularity avoidance strategies. Even considering their previous experience, this participant experiences a higher PSD while approaching a singular configuration in the case of mode B. Unfortunately, only

this participant had previous experience with pHRC systems within the cohort. It would have been interesting to see whether previous experience plays a role in predicting interaction dynamics with collaborative robots.

ANOVA was conducted on 12 factors, as only 12 participants present valid EEG data. Therefore, one of the events had to be excluded from this analysis. The event corresponding to the marker LeaA was the one excluded, as it presents no damping. There was a statistically significant difference between PSD from θ band for all twelve events, with F-value $F(1, 11) = 7.886$ and p-value $p = .017$. The post-hoc analysis using LSD showed that there was a significant difference between AppA1 to AppB3 ($p = .010$), LeaB1 ($p = .013$), LeaB2 ($p = .009$), AppA3 to AppB3 ($p = .040$) and LeaB4 ($p = .029$), and AppB1 to LeaB2 ($p = .045$). Other events do not present a significant difference.

Similarly, there was a statistically significant difference for PSD from the α band for all twelve events, $F(1, 11) = 8.647$, $p = .013$. The post-hoc analysis using LSD showed that there was significant difference between between AppA1 to AppB3 ($p = .001$), AppB4 ($p = .008$), LeaB2 ($p = .015$), LeaB3 ($p = .022$), AppA3 to LeaB4 ($p = .036$), AppA4 to LeaB4 ($p = .014$), AppB3 to AppA1 ($p = .001$), AppB4 ($p = .049$), AppB4 to AppA1 ($p = .008$), LeaB3 ($p = .046$), LeaB2 to AppA1 ($p = .015$), and LeaB3 to AppA1 ($p = .022$), AppB4 ($p = .046$). Other events do not have a difference that is statistically significant.

Results suggest that there is a difference in terms of PEN in the ERP induced by modes A and B. This indicates that PEN generated by a change of the parameters in the singularity avoidance strategy can be detected.

The two modes result in different robot admittance dynamics, in proximity of a singular configuration. To answer the question whether PEN, and consequently the robot predictability, affects human preferences when comparing two admittance dynamics in pHRC (Q3.2), the results obtained from the ERP analysis were compared to the answers collected from the questionnaire. Results presented in [12] show the strategy resulting from mode A, as the overall favourite between six different settings. On the contrary, mode B was ranked as the least favourite. Directly comparing those two singularity avoidance strategies in [12] were seven participants. One out of those seven was excluded because of not conforming to the protocol. Of the remaining six participants, five chose mode A as the overall favourite mode and one chose “Neither”, but adding as a comment

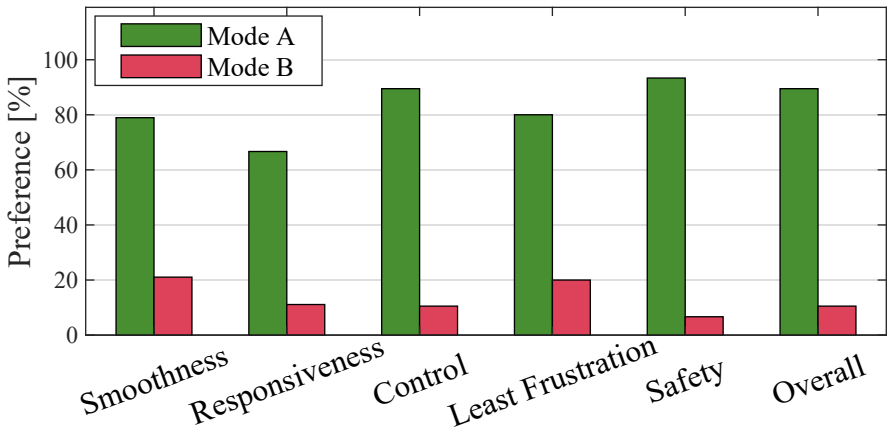

FIGURE 5.10: Normalised preferences between modes A and B [10], using the questionnaire presented in [12].

that "Maybe mode A is better, as the other mode requires more force". Out of the fourteen participants to partake in Exp3, two answered that they prefer mode B. As the reason they chose B, one stated that "the robot felt smoother" with that mode, while the other participant answered that "the robot felt lighter". All the other subjects preferred mode A. Overall, twenty participants answered the questions in the questionnaire, directly comparing modes A and B. For completeness, in Figure 5.10 the answers to all the six questions in the questionnaire are reported in percentages. Most participants strongly preferred mode A.

In the questionnaire, also the outlying participant mentioned above strongly preferred mode A, even if their ERP suggested PEN happening when that mode was used. They justified their choice with the comment "There was less resistance and I felt like I was more in control of the robot arm". For this specific participant, it looks like their preference does not match the ERP results.

The two participants that preferred mode B present greater PSD when using that mode. Also in this case their answers to the questionnaire do not match the ERP results.

Overall, results indicate that the singularity avoidance mode that most participants preferred (i.e. mode A) are also the ones that cause fewer prediction errors (i.e lower PSD) when approaching singularity. This suggests that the robot predictability affects the user preference when it comes to control strategies in pHRC and that PEN may be a useful measure for tuning these strategies to the user's preferences.

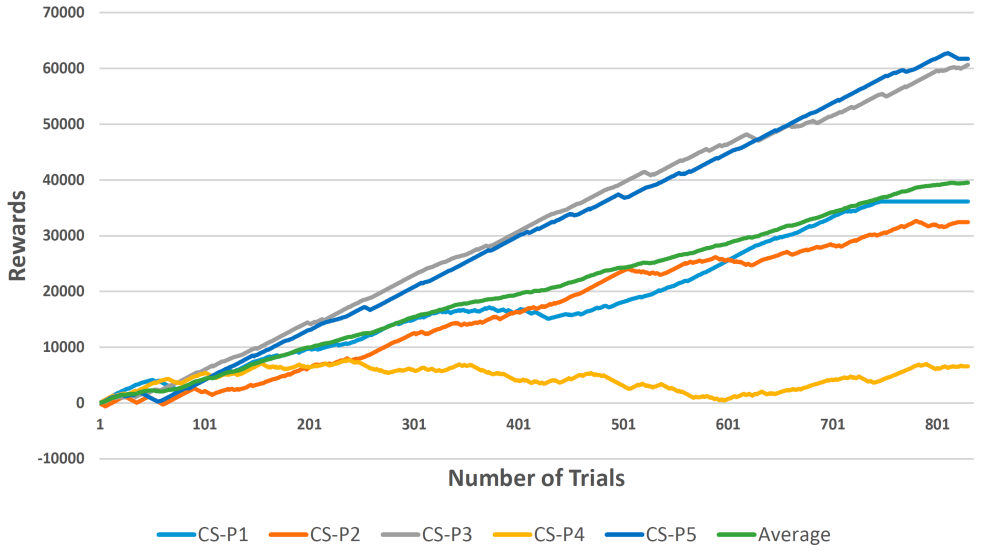

FIGURE 5.11: Rewards with respect to the number of trials for the five participants. The Average is also reported.

5.3.2 Experiment 4 - Exp4

Five subjects performed Exp4. This experiment aims at assessing the feasibility of a human-robot system that closes the robot control loop on the human cognitive state to improve the robot predictability. Since only five participants conducted Exp4, results are only preliminary.

As mentioned in Section 5.2.2.2, a DDPG algorithm was used to select $\bar{\sigma}_{1a}$ and $\bar{\sigma}_{1b}$. In Figure 5.11 the cumulative rewards of the RL algorithm are shown for each participant, with respect to the number of trials, with participant 1 named CS-P1, participant 2 named CS-P2, and so on. The green curve represents the average. It is interesting to note that while for most participants it looks like the cumulative reward is increasing over time, for participant 4 (yellow curve), the cumulative reward is not increasing as expected. Since the reward is a function of PEN, this suggests that the algorithm is failing at reducing PEN for this specific participant. In Figure 5.12, the changes in cost of the actor and critic are reported for one selected participant.

The parameters $\bar{\sigma}_{1a}$ and $\bar{\sigma}_{1b}$ do not settle to a value, but they keep changing depending on the environment state, which is defined by end-effector position and velocity, and interaction forces. In Figure 5.13, $\bar{\sigma}_{1a}$ is shown for one participant with respect to the number of trials. As the goal of the RL algorithm is to reduce PEN and the PSD, this was expected.

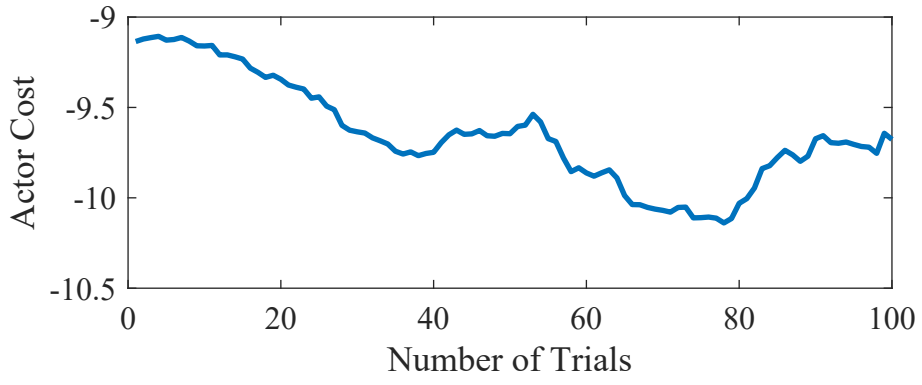

(A) Actor cost

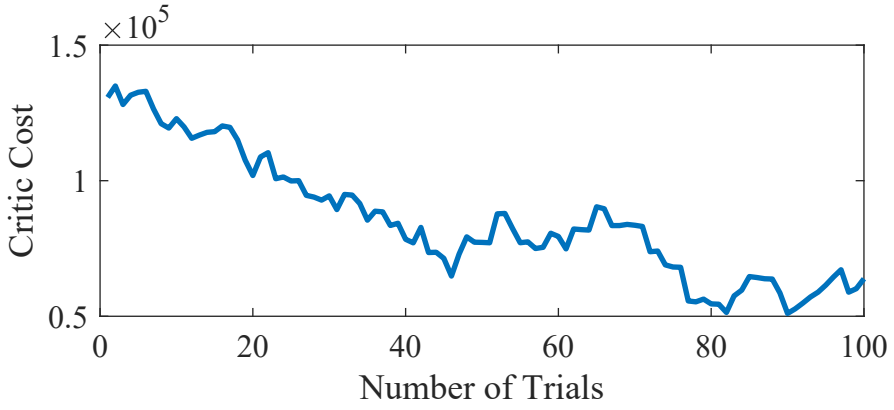

(B) Critic cost

FIGURE 5.12: Changes in cost of actor (A) and critic (B) for one selected participant.

To analyse the results of this approach on the cognitive state of the human operator, the EEG data were processed with the pipeline presented in Section 5.2.3 and summarised in Figure 5.6. The following results are focused on the frontal lobe of the brain, as shown by the topographic map (Figure 5.14A) and dipole (Figure 5.14B).

In order to investigate whether the RL algorithm is reducing PEN and PSD, the processed data were divided into three subsets, as mentioned in Section 5.2.2.2, corresponding to a time of about five minutes for each subset. $T1$ corresponds to the data collected during the first five minutes of Exp4, while T_2 corresponds to the data collected during the last five minutes of Exp4. In Figure 5.15A, a bar graph shows the PSD in $\mu V^2/Hz$ of each participant for the α-frequency band and the two mid-line channels, Fz and Cz, for subset $T1$ and $T2$. Excluding participant CS-P1 (blue bar), all the other participants present a lower PSD in the last part of the experiment, suggesting that the RL algorithm is reducing PEN. The PSD of CS-P1 is also high compared to the other participants.

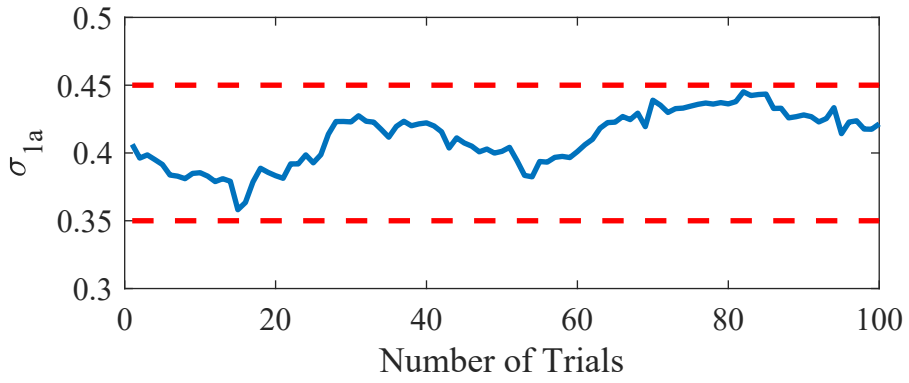

FIGURE 5.13: The parameter $\bar{\sigma}_{1a}$ for one participant, with respect to the number of trials.

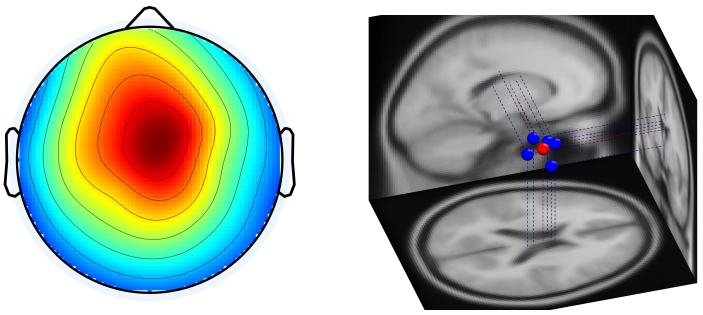

(A) Topographic map of the signal

(B) Dipole

FIGURE 5.14: Topography map (A) and dipole (B) of the EEG data after applying the processing pipeline summarised in Figure 5.6.

This might result from a signal with poor signal-to-noise ratio. In Figure 5.15B, the PSD for the same data subsets is shown in the θ-frequency band. In this frequency range, there seems to be no consistent effect of the implemented approach.

Since the classification is based on all the available channels, in Figure 5.16, the topographic maps of one participant are shown with all the available channels. The maps are divided by frequency band and the columns indicate respectively subset $T1$ (beginning of Exp4), subset $T2$ (end of Exp4) and the difference $T2 - T1$. When all channels are used the frequency bands with more activity are δ and θ. In this case, the maps relative to $T2 - T1$ present negative power, suggesting that PEN decreases with respect to the number of trials.

Results for Exp4 are only preliminary results as more participants are required to perform an adequate statistical analysis. The presented results suggest however that not only a closed-loop

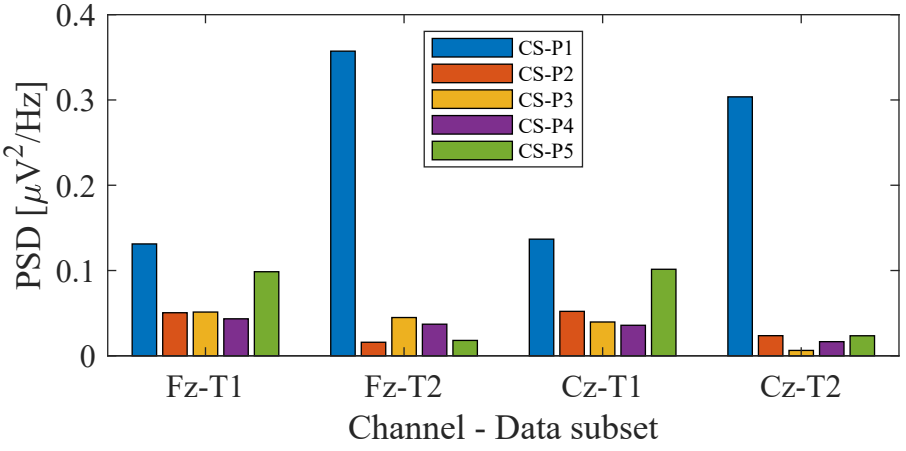

(A) PSD in the α-band

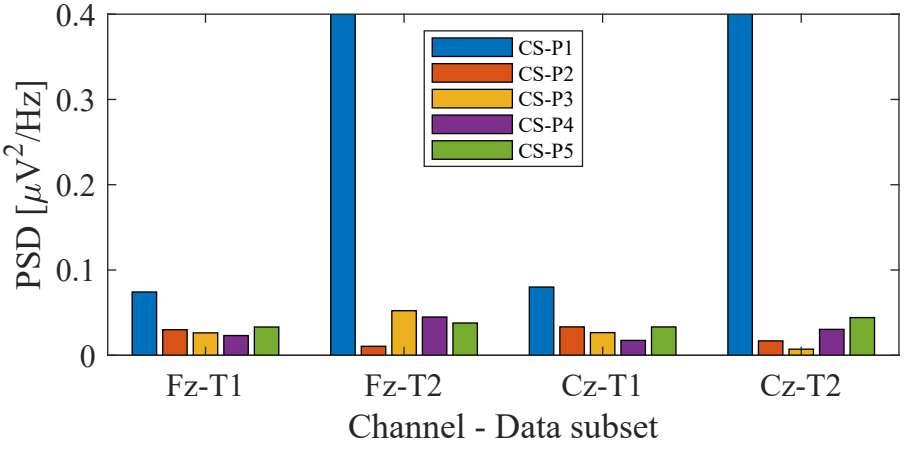

(B) PSD in the θ-band

FIGURE 5.15: PSD ($\mu V^2/Hz$) of each participant with respect to the channel and data subset, for the α-frequency band (A) and θ-frequency band (B).

system is feasible, but it also reduces PEN over time, consequently increasing the robot predictability.

5.4 Limitations

Results of Exp3 have some limitations. Some events have a much smaller number of epochs because they are less likely to be triggered (e.g. $\sigma < \bar{\sigma}_{1/8}$). To have a larger sample, the duration of the experiment should be increased for each participant. The current duration of the experiment is however already about one hour long, including the setup and the questionnaire.

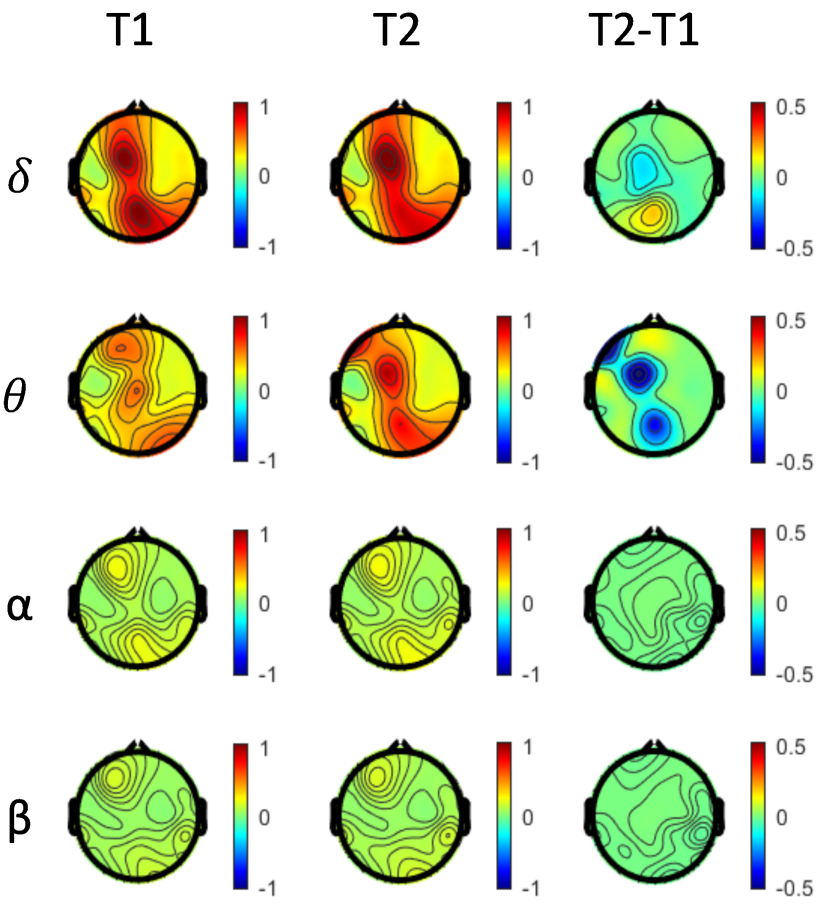

FIGURE 5.16: Topographic map of the PSD [dB] by frequency bands, at the beginning of Exp4 (T1), at its end (T2), and difference T2-T1.

Only five participants performed Exp4. A larger cohort would allow a relevant statistical analysis. In this case, a longer experiment would result in better accuracy.

A comparison between data sets from Exp3 and data sets from Exp4 would also be interesting. Having an adaptive control might not increase the robot predictability, when compared to a control with static parameters.

Performance of the CNN presented in Chapter 4 were the result of an intra-subject analysis (the classifier was trained and tested on the same participant). The CNN used in Exp4 was trained with all the data sets collected during Exp1. This means that it has been trained with data from several participants and then used to classify PEN in different participants. The actual accuracy of the CNN is therefore unknown.

In this work, the learning process of the participants has not been considered. Experience might affect robot predictability and the results presented. With a larger cohort, it would have been interesting to analyse whether experience in pHRC and familiarity with singularity avoidance strategies have an effect on the way PEN is modulated. Possibly, a person that has a deeper understanding of the underlying control algorithm could better anticipate the resulting interaction dynamics.

5.5 Conclusions

In this chapter, three questions were addressed (i.e. Q3.1, Q3.2 and Q3.3). Question Q3.1 was whether a real pHRC singularity avoidance strategy could generate detectable PEN. An experiment (Exp3) was performed by fourteen participants. They interacted with a pHRC system and compared two sets of parameters for a singularity avoidance strategy based on EDLS strategy. The brain activity of the participants was recorded with an EEG device and the PSD was calculated for specific events happening during the interaction. Results show that one set of parameters (mode B) translates into a higher PSD and consequently a lower robot predictability. The reader is reminded that the robot predictability is the ability of the robot behaviour to be predicted by the human operator. Through PEN, and consequently PSD, it is possible to estimate the robot predictability from the human operator's perspective. Mode B corresponds to a strategy with slow symmetric damping rate in proximity to a kinematic singularity.

Question Q3.2 addressed whether human preferences are related to the robot predictability, assessed with PEN. Excluding one participant, the answers obtained through a questionnaire indicate that people preferred the mode causing lower PSD, i.e. the one presenting fast asymmetric damping (mode A). This supports the idea that people prefer a more predictable interaction.

Another experiment (Exp4) was implemented to see whether a robot system that closes the loop on the human cognitive state to reduce PEN was feasible. Five participants performed the experiment. The rewards of the DDPG algorithm depended on a CNN which was classifying PEN. Results show that the PSD at the beginning of the experiment was higher than the PSD at its end, suggesting that the RL algorithm is successfully reducing PEN. Not only do these results demonstrate the feasibility of a closed-loop collaborative system with PEN in the control loop, but also they suggest it could enhance the predictability of the robot behaviour.

Chapter 6

Conclusion and Future Work

This research investigated whether PEN can be detected, classified and used to assess and improve the predictability of robot behaviour (i.e. robot predictability in this research) during pHRC. PEN is an ERN that can be found in the ERP and is the result of a mismatch between the human internal models and the reality. More specifically, in this research, PEN is caused by a mismatch between the expected robot behaviour and the actual robot behaviour, also called prediction error.

In pHRC applications, the cognitive state of the human operator is often neglected. The main control loop often consists of a variant of admittance- or impedance-based controllers. Those are commonly implemented together with other control paradigms, such as assistive strategies, and collision and singularity avoidance strategies. Those strategies together aim at improving the safety of human and robot agents, but they usually result in physical human-robot interactions with complex dynamics. As such, the robot does not operate with a constant admittance or impedance, which can impact on the robot predictability. Moreover, those control strategies are usually tuned to fit generic human operators and do not target a specific user.

Since the detection and application of PEN in a pHRC task was yet to be explored, sub-question Q1 addressed whether an unexpected change in the mechanical admittance of the robot (i.e unexpected robot behaviour) would result in a prediction error, and consequently PEN. Q1 also raises the need for investigating the relationship between PEN and a change of the robot mechanical admittance. The change in admittance was induced by the introduction of resistive forces with first-order dynamics. Two experiments were conducted. The first experiment involved a 1D collaborative task,

then extended to a second experiment with a 2D task. These experiments showed that dynamics of first-order resistive forces have an effect on the robot predictability, as indicated by an induced PEN response. Classifiers for an online detection and classification of PEN were then compared, as a timely and accurate estimation is critical for a real-time pHRC system. Among the compared classifiers a CNN performed best, in the case of two- and three-class classification problems. To investigate whether PEN could be detected in the case of more subtle pHRC strategies, a singularity avoidance strategy was implemented and assessed through PEN. In the same experiment, a questionnaire investigated the relationship between PEN and human preferences. It was found that the dynamics of the singularity avoidance strategy indeed has an effect on PEN. A relationship between PEN and human preferences was also established for the implemented singularity avoidance strategy. It was found that people tend to prefer predictable strategies, with lower PEN amplitudes. Those results led to the application of PEN to a closed-loop control system in a pHRC task. In this application, a CNN is used to set rewards of a reinforcement learning algorithm, with the aim of reducing PEN. It was demonstrated that parameters in the singularity avoidance strategy can be automatically tuned to improve the predictability of the pHRC robot.

In Section 6.1, the contributions to knowledge of each sub-question (i.e. Q1, Q2 and Q3) are summarised. Section 6.2 discusses the main limitations of this research and Section 6.3 suggests possible directions for future works.

6.1 Summary of contributions

This section summarises the contributions to knowledge that resulted from this research and, specifically, from answering sub-questions Q1, Q2 and Q3.

6.1.1 Effect of first-order resistive forces on PEN during pHRC

To investigate the effect of admittance dynamics on the robot predictability in pHRC, two experiments were designed and performed. Collaborative tasks were designed such that unexpected resistive forces with first-order dynamics would change the mechanical admittance of the robot. Experiment 1 (Exp1) involved a 1D task, while Experiment 2 (Exp2) involved a 2D task. The

brain activity was recorded with an EEG device and the data processed to see whether different force profiles would result in different PEN amplitudes in the ERP.

A sudden unexpected resistive force generates PEN, since a clear negativity in the ERP can be seen for most participants, followed by a P300. Out of eleven participants, 81.8% presented a higher PEN amplitude, in the case of an unexpected abrupt resistive force. In the case of a smooth unexpected resistive force, the ERP results show no relevant PEN. As anticipated, in the case of expected resistive forces, either sudden or smooth, participants present no apparent PEN. This suggests that it may not be the introduction of a force that induces PEN, but rather whether the force is expected by the operator. An expected force can be predicted and therefore does not result in a prediction error. These findings indicate that, in the case of an unexpected abrupt force with first-order dynamics, the robot predictability decreases, from the operator's perspective. The profile of this force is proven to have an effect, as a smoother force does not result in a visible PEN in the ERP.

Exp2 was used to test whether results from the 1D experiment are valid also in the case of a task that involves greater movements, as muscle activity adds confounding factors to the data. Two participants performed Exp2. Results from Exp2 confirmed findings from Exp1. Moreover, the direction of motion does not seem to have an influence on PEN.

6.1.2 Methods for estimation of PEN in pHRC

The data processing used in Exp1 and Exp2 to detect PEN was slow and computationally heavy. To use PEN in the robot control system, efficient methods for an online estimation have to be investigated. Six classifiers with different complexity were therefore compared in this research. The data from Exp1 were used to analyse the classifier performances. These classifiers were compared on the basis of performance with a two- and three-class classification problem. In the case of two classes, data collected when sudden unexpected forces are applied represented one class. All the other conditions represented the other class. The two-class problem represents a binary problem in which only sudden unexpected forces induce prediction errors. The three-class classification problem aims at addressing situations in which a more precise estimation of PEN is required. In the case of three classes, data corresponding to unexpected sudden forces represent a high level of prediction error, while data associated to unexpected smooth resistive forces represent

a small prediction error. Expected forces, sudden or smooth, are considered part of the same class, since they cause no prediction error.

In the case of two classes, a CNN performed the best with an average accuracy of 82.1% $\pm$ 5.2%. In the case of three classes, the same classifier performed the best, but with an accuracy of 66.7% $\pm$ 10.2%. It is suspected that the lower accuracy is due to the smaller size of data sets for each class, which consequently results in smaller training sets. If bigger training sets were used and if associated with more data streams coming from the robot, the accuracy of the classifier would probably increase. These results suggest that a difference between smooth unexpected forces and expected forces exists, even if not visible in the ERP.

With both classification problems, the CNN classified data in a timely manner during the testing phase. The average time that the classifier took to classify one feature was 0.34s $\pm$ 0.07s in the case of two classes, and 0.26s $\pm$ 0.05s in the case of three classes. Results suggest the feasibility of using a CNN for an online estimation of prediction errors.

6.1.3 Detection and application of PEN in real pHRC

It was found that dynamics of first-order resistive forces have an effect on the predictability of the robot behaviour. In real pHRC systems, a more subtle change of robot admittance is normally used. Therefore, an EDLS singularity avoidance strategy was chosen to investigate whether different dynamics result in different PEN amplitudes. Two sets of parameters, resulting in two modes (mode A and mode B), were compared in Exp3 with fourteen participants, while freely interacting with the robot in the 3D space. The two sets of parameters define the damping rate and the symmetry of the control strategy.

Parameters corresponding to a fast damping rate and an asymmetric approach, i.e. mode A, mostly resulted in having a higher PSD, when compared to parameters associated with a slow symmetric damping rate (mode B). A lower PSD in the ERP resulted in fact from a fast asymmetric damping rate, which suggests that the predictability of the robot behaviour is higher. Differences between the PSD resulting from the two modes are visible especially in the α-frequency band, but are significant also in the θ band.

Human preferences and their relationship to the robot predictability were also assessed with Exp3. A questionnaire was filled in by participants at the end of the experiment. Most participants preferred a fast asymmetric damping rate (mode A). This aligns with the results from the PSD analysis of ERP, suggesting that participants prefer predicable collaborative tasks.

Another experiment (Exp4) was performed by five participants to see whether a closed-loop system which uses the estimation of the robot predictability is feasible. A RL algorithm is used to tune parameters of the EDLS strategy for singularity avoidance. Results suggest that a robot control system that closes the loop on the human cognitive state is feasible. When comparing the EEG data at the beginning of the experiment with the data at its end, the closed-loop control system reduced the PSD of four participants out of five. These results are for the α-frequency band, for the frontal and central mid-channels (Fz and Cz).

6.2 Discussion and limitations

Collaborative robotics often aims at integrating the mechanical power of robots with the cognitive capabilities of humans. This generally results in human-robot systems that are flexible and with a greater strength capacity, when compared to humans.

In pHRC, the interaction is usually based on the physical exchange of forces. Normally, cognitive effects of how human intentions are transferred to robot actions are hardly considered when designing pHRC systems. Results from recent studies suggest that the way humans interact with mechanical systems with complex dynamics aims at maximising predictability. If the predictability of the robot behaviour could be assessed online, the potential for a human-robot system that aims at increasing the predictability of the robot behaviour becomes a reality.

The current state of EEG technology limits the practicability of EEG-based applications in pHRC. The accuracy of EEG-based methods largely depends on the task and relies on a proper setup which often requires a time-consuming process. This greatly affects the introduction of EEG technology in industrial settings. It is however anticipated that as technology and the field of neuroscience progress the practicability of EEG-based applications will increase. The following sections address some of the assumptions and limitations of this research.

6.2.1 Predictability as a shared responsibility

Normally, humans unconsciously adapt the way they interact with a mechanical system to maximise predictability. The close-loop control system described in this thesis was implemented with the idea that the robot could share the burden of adapting the interaction to maximise such predictability. The way that humans predict the outcome of a task is by creating internal models of the task and updating such models whenever they are proven wrong or when more information becomes available. If the robot keeps adapting its behaviour during the human-robot interaction, the human will need to keep updating their internal models about the robot. This, instead of being beneficial to the predictability of the robot behaviour, might actually reduce that predictability. As a consequence, the human co-worker might take longer to create an accurate internal model of the robot dynamics. Section 6.3.2 suggests possible research directions to address this.

Results in Section 5.3.2 only compare subsets of data collected with the closed-loop system. It would have been interesting to compare the effect of static and adaptive control strategies on the robot predictability. The data collected during Exp3 (Section 5.2.2.2) is however associated with participants constantly switching between two modes, which results in two different admittance profiles, close to singularity.

6.2.2 Classification training data sets from a different task

The closed-loop system involved a CNN to estimate PEN and on that basis assigned a reward for the RL algorithm. This classifier was trained with data collected in Exp1. The task in this experiment is a simple 1D task and the changes in the robot admittance are the result of first-order resistive forces. The CNN trained with these data sets is used to estimate PEN in a much more complex task. The task in Exp4 presents a 3D workspace and the user is free to explore such a space. As a consequence, the operator moves more (e.g. walking, stretching, reaching), which may introduce confounding factors that might affect the accuracy of the CNN. Also the dynamics of the admittance is different in the two tasks. One is the result of the introduction of first-order forces, while the other is obtained by modifying the Jacobian matrix with the EDLS strategy.

A self-collision avoidance strategy is also enabled in the case of the closed-loop system. This might also impact the cognitive state of the user, as a change in admittance is also used to discourage

the user from having parts of the robot colliding. The singularity avoidance strategy and the self-collision avoidance strategy implemented in the closed-loop system are not differentiated at the moment, and the robot is constantly adapting parameters for the EDLS singularity avoidance strategy. The training data sets do not take self-collision avoidance into account as the task in Exp1 was specifically designed to avoid the introduction of such a control strategy. This probably results in the robot adapting the control parameters of the singularity avoidance even in proximity of collision.

6.2.3 Duration of the experiments and number of participants

Most experiments in this research take a long time to be carried out. The need for big enough data sets justifies the duration of the experiments. The quality of the data however deteriorates with respect to the time. To maintain the contact impedance between the scalp and the electrodes at an acceptable level, a conductive gel is applied. The contact impedance however increases when the gel dries.

Moreover, if experiments were too long, other cognitive effects may have added confounding factors. If participants are disengaged from the task their data might become less relevant. The duration of the experiments is the result of a compromise between statistical robustness and data quality.

The number of participants that carried out experiments is also a limitation of this research. The limited number of participants is justified by the time-consuming nature of the experiments. The number of participants that performed Exp4 can be increased to allow a statistical analysis. More participants are currently being recruited.

6.3 Future work

As this thesis represents the seminal work that uses PEN in a pHRC setting, results open new exciting research directions. Future work should try to address the limitations of this research, such as increasing the number of participants, and investigate the accuracy of the CNN used to close the loop on the cognitive state to reduce PEN. This thesis used a singularity avoidance strategy to test

the applicability of PEN detection in pHRC. Whether PEN can be detected and used in other pHRC control strategies (e.g. collision avoidance) has not been explored yet. As the manipulability of the robot arm also affects the perceived robot admittance, it would be interesting to research the effect that this phenomenon has on the robot predictability. The following sections suggest other future works that might follow this research.

6.3.1 Understanding of the learning process with PEN

As PEN is the result of human internal models being proven wrong, experience is likely to be involved in the process. With increasing experience the human operator should be able to create better internal models resulting in more accurate predictions.

It is possible to divide the data sets collected during Exp1, Exp2 and Exp3 in subsets corresponding to different phases of the experiments. The ERP results from the beginning and the end of the experiment might show what effect the learning process has on the predictability of the robot behaviour.

With a closed-loop control strategy that uses PEN in the loop (Exp4), it might be more difficult to isolate the learning process as the robot admittance dynamics keep changing. A comparison between static and adaptive control strategies that use PEN may however result in new insights about how human internal models work.

If the time that a human takes to update their internal models is seen similarly to the time it takes to a person to react, there might be strategies to eventually reduce this time. However, the role that PEN could play in this is still unclear. This might be a possible direction for future research.

6.3.2 Static versus adaptive control

One of the advantages of some adaptive control strategies is that they can target a specific operator, based on preferences that are learnt over time. Static control strategies are instead usually tuned to target generic users.

Humans have the ability to adapt and react quickly to external changes and stimuli. This dynamic behaviour can be conscious or unconscious. In a human-robot system, it is questioned which

party has to adapt to the other, the human or the robot? A human operator will always adapt their behaviour, even if unconsciously. Should the robot then share this responsibility?

The adaptive robot control system implemented in Exp4, when compared to a robot system with a static strategy, could give insights into which strategy enhances more the robot predictability over time.

Even a control strategy that causes high levels of PEN, over time, may see the robot predictability increasing (with PEN decreasing), as the user becomes familiar with the robot dynamics and creates more accurate internal models.

A comparison on the PSD in the α- and θ-frequency bands between a static control strategy and an adaptive control strategy could help answer the question of which approach is better in terms of robot predictability.

6.3.3 Integration of multiple physiological signals

One of the main limitation of EEG signals is their poor signal-to-noise ratio. Especially when movements are involved, artifacts have to be isolated and removed from the EEG data. The activation of muscles can in fact be seen in the EEG signal, especially for specific frequencies. The integration of other physiological signals, like EMG could help isolate and remove those artifacts.

Other physiological signals can also help detect cognitive states. Galvanic Skin Response (GSR) and Heart Rate Variability (HRV) are often used to estimate the human mental state. A robot system that integrates several physiological signals to estimate the human state would most likely obtain a more accurate estimation of the human cognitive state.

The literature presents some works in which the authors tried to combine multiple physiological data, even in pHRC. Future work could try to increase the accuracy of PEN detection by integrating multiple physiological signals.

6.3.4 Engagement and other cognitive features

PEN is not the only feature that can be extrapolated from the EEG data. In this research we have also seen that P300 typically follows a prediction error. P300 is a positive peak that corresponds

to the human memory being processed. After an ERN, P300 is probably due to the human internal models being updated, but it generally also appears when a person experiences surprise.

Human engagement can also be estimated from the EEG data. This information is usually found in the frequency-domain. The estimation of mental fatigue through EEG data is also a common problem, especially in fields related to education. When physiological data are used to estimate the human state in pHRC applications, the robot system is usually trying to estimate engagement or fatigue. As many and large EEG data sets were collected during this thesis, future works could investigate other features, not necessarily related to predictability.

These avenues for future research present exciting opportunities for the research community to make a positive impact in the field of human-robot interaction.

Bibliography

[1] Stefano Aldini, Ashlesha Akella, Avinash K Singh, Yu-Kai Wang, Marc Carmichael, Dikai Liu, and Chin-Teng Lin. Effect of Mechanical Resistance on Cognitive Conflict in Physical Human-Robot Collaboration. In *Proceedings of the 2019 IEEE International Conference on Robotics and Automation (ICRA)*, pages 6137–6143, Montreal, Canada, 2019. ISBN 9781538660263.

[2] Universal Robots UR10 | Cobots.ie. URL `https://cobots.ie/product/ur-team/ur10/`. Accessed on 15/01/2021.

[3] RobotWorx - KUKA LBR IIWA 7 R800. URL `https://www.robots.com/robots/lbr-iiwa-7-r800`. Accessed on 15/01/2021.

[4] CobotsGuide | ABB YuMi. URL `https://cobotsguide.com/2016/06/abb-yumi/`. Accessed on 24/01/2021.

[5] Luka Peternel | Delft Haptics Lab. URL `https://delfthapticslab.nl/cpt_people/luka_peternel/`. Accessed on 24/01/2021.

[6] Mind control: Correcting robot mistakes using EEG brain signals | Robohub. URL `https://robohub.org/mind-control-correcting-robot-mistakes-using-eeg-brain-signals/`. Accessed on 24/01/2021.

[7] Marc G. Carmichael, Stefano Aldini, Richardo Khonasty, Antony Tran, Christian Reeks, Dikai Liu, Kenneth J. Waldron, and Gamini Dissanayake. The ANBOT: An Intelligent Robotic Co-worker for Industrial Abrasive Blasting. In *Proceedings of the 2019 IEEE International Conference on Intelligent Robots and Systems (IROS)*, 2019.

[8] Stefano Aldini, Avinash K Singh, Daniel Leong, Yu-Kai Wang, Marc G Carmichael, Dikai Liu, and Chin-Teng Lin. Detection and Estimation of Cognitive Conflict During Physical Human-Robot Collaboration. *IEEE Transactions on Cognitive and Developmental Systems*, Submitted.

[9] Avinash Kumar Singh, Stefano Aldini, Daniel Leong, Yu-Kai Wang, Marc Gary Carmichael, Dikai Liu, and Chin-Teng Lin. Prediction Error Negativity in Physical Human-Robot Collaboration. In *Proceedings of the IEEE 8th International Winter Conference on Brain-Computer Interface*, Seoul, Korea, 2020.

[10] Stefano Aldini, Avinash K Singh, Marc Carmichael, Yu-Kai Wang, Dikai Liu, and Chin-Teng Lin. Prediction-Error Negativity to Assess Singularity Avoidance Strategies in Physical Human-Robot Collaboration. In *Proceedings of the 2021 IEEE International Conference on Robotics and Automation (ICRA)*, Xi'an, China, 2021.

[11] Rob Campbell. *notBoxPlot*. https://github.com/raacampbell/notBoxPlot, GitHub. Retrieved October 20, 2020. URL `https://github.com/raacampbell/notBoxPlot`.

[12] Marc G. Carmichael, Richardo Khonasty, Stefano Aldini, and Dikai Liu. Human Preferences in Using Damping to Manage Singularities During Physical Human-Robot Collaboration. In *Proceedings of the 2020 IEEE International Conference on Robotics and Automation (ICRA)*, Paris, France, 2020.

[13] J. Edward Colgate, Witaya Wannasuphoprasit, and Michael A. Peshkin. Cobots: Robots for collaboration with human operators. In *Proceedings of the International Mechanical Engineering Congress and Exhibition (GA DSC)*, 1996.

[14] Collaborative Robots Market | Global Trends, Analysis & Forecast - 2027. URL `https://www.inkwoodresearch.com/reports/global-collaborative-robots-market/`. Accessed on 12/01/2021.

[15] Ernesto Gambao, Miguel Hernando, and Dragoljub Surdilovic. A new generation of collaborative robots for material handling. *Gerontechnology*, 2012. ISSN 1569-1101. doi: 10.4017/gt.2012.11.02.362.776.

[16] Andrea Cherubini, Robin Passama, Andre Crosnier, Antoine Lasnier, and Philippe Fraisse. Collaborative manufacturing with physical human-robot interaction. *Robotics and Computer-Integrated Manufacturing*, 2016. ISSN 07365845. doi: 10.1016/j.rcim.2015.12.007.

[17] Takamitsu Aida, Hirokazu Nozaki, and Hiroshi Kobayashi. Development of muscle suit and application to factory laborers. In *2009 IEEE International Conference on Mechatronics and Automation, ICMA 2009*, 2009. ISBN 9781424426935. doi: 10.1109/ICMA.2009.5246279.

[18] L. Masia, H. I. Krebs, P. Cappa, and N. Hogan. Whole-arm rehabilitation following stroke: Hand module. In *Proceedings of the First IEEE/RAS-EMBS International Conference on Biomedical Robotics and Biomechatronics, 2006, BioRob 2006*, 2006. ISBN 1424400406. doi: 10.1109/BIOROB.2006.1639236.

[19] Haoyong Yu, Sunan Huang, Gong Chen, Yongping Pan, and Zhao Guo. Human-Robot Interaction Control of Rehabilitation Robots with Series Elastic Actuators. *IEEE Transactions on Robotics*, 2015. ISSN 15523098. doi: 10.1109/TRO.2015.2457314.

[20] Marc G. Carmichael and Dikai K. Liu. Human biomechanical model based optimal design of assistive shoulder exoskeleton. In *Springer Tracts in Advanced Robotics*, 2015. ISBN 9783319074870. doi: 10.1007/978-3-319-07488-7_17.

[21] Fahimeh Rezazadegan, Jie Geng, Marco Ghirardi, Giuseppe Menga, Salvina Murè, Gianfranco Camuncoli, and Micaela Demichela. Risked-based Design for the Physical Human-Robot Interaction (pHRI): an Overview. *Chemical Engineering Transactions*, 43:1249–1254, 2015. doi: 10.3303/CET1543209.

[22] Marc G. Carmichael and Dikai Liu. Admittance control scheme for implementing model-based assistance-as-needed on a robot. In *Proceedings of the Annual International Conference of the IEEE Engineering in Medicine and Biology Society, EMBS*, 2013. ISBN 9781457702167. doi: 10.1109/EMBC.2013.6609639.

[23] Denny Oetomo and Marcelo H. Ang. Singularity robust algorithm in serial manipulators. *Robotics and Computer-Integrated Manufacturing*, 2009. ISSN 07365845. doi: 10.1016/j.rcim.2007.09.007.

[24] Arati S. Deo and Ian D. Walker. Overview of damped least-squares methods for inverse kinematics of robot manipulators. *Journal of Intelligent & Robotic Systems*, 1995. ISSN 09210296. doi: 10.1007/BF01254007.

[25] Benjamin Navarro, Aicha Fonte, Philippe Fraisse, GÃl'rard Poisson, Benjamin Navarro, Aicha Fonte, Philippe Fraisse, GÃl'rard Poisson, Andrea Cherubini, and Benjamin Navarro. OpenPHRI : an open-source library for safe physical human-robot interaction. *Hal*, 2017.

[26] Alessandro De Luca and Fabrizio Flacco. Integrated control for pHRI: Collision avoidance, detection, reaction and collaboration. In *Proceedings of the IEEE RAS and EMBS International Conference on Biomedical Robotics and Biomechatronics*, 2012. ISBN 9781457711992. doi: 10.1109/BioRob.2012.6290917.

[27] Khalid J. Kazim, Johanna Bethge, Janine Matschek, and Rolf Findeisen. Combined Predictive Path Following and Admittance Control. In *Proceedings of the American Control Conference*, volume 2018-June, pages 3153–3158. Institute of Electrical and Electronics Engineers Inc., 8 2018. ISBN 9781538654286. doi: 10.23919/ACC.2018.8431272.

[28] Pauline Maurice, Neville Hogan, and Dagmar Sternad. Predictability, force, and (anti)resonance in complex object control. *Journal of Neurophysiology*, 2018. ISSN 15221598. doi: 10.1152/jn.00918.2017.

[29] M. S. Ryoo. Human activity prediction: Early recognition of ongoing activities from streaming videos. In *Proceedings of the IEEE International Conference on Computer Vision*, 2011. ISBN 9781457711015. doi: 10.1109/ICCV.2011.6126349.

[30] Steven J Luck. Event-Related Potentials. *APA Handbook of Research Methods in Psychology*, 2005. ISSN 0165-1781. doi: 10.1037/13619-028.

[31] Paul L. Nunez and Ramesh Srinivasan. *Electric Fields of the Brain: The neurophysics of EEG*. 2009. ISBN 9780199865673. doi: 10.1093/acprof:oso/9780195050387.001.0001.

[32] Avinash Kumar Singh, Hsiang Ting Chen, Yu Feng Cheng, Jung Tai King, Li Wei Ko, Klaus Gramann, and Chin Teng Lin. Visual Appearance Modulates Prediction Error in Virtual Reality. *IEEE Access*, 2018. ISSN 21693536. doi: 10.1109/ACCESS.2018.2832089.

[33] Inaki Iturrate, Luis Montesano, and Javier Minguez. Single trial recognition of error-related potentials during observation of robot operation. In *2010 Annual International Conference of the IEEE Engineering in Medicine and Biology Society, EMBC'10*, 2010. ISBN 9781424441235. doi: 10.1109/IEMBS.2010.5627380.

[34] Inaki Iturrate, Luis Montesano, and Javier Mínguez. Robot reinforcement learning using EEG-based reward signals. In *Proceedings - IEEE International Conference on Robotics and Automation*, 2010. ISBN 9781424450381. doi: 10.1109/ROBOT.2010.5509734.

[35] Christian I. Penaloza, Yasushi Mae, Masaru Kojima, and Tatsuo Arai. Brain signal-based safety measure activation for robotic systems. *Advanced Robotics*, 2015. ISSN 15685535. doi: 10.1080/01691864.2015.1057615.

[36] Stefan K. Ehrlich and Gordon Cheng. Human-agent co-adaptation using error-related potentials. *Journal of neural engineering*, 2018. ISSN 17412552. doi: 10.1088/1741-2552/aae069.

[37] Andres F. Salazar-Gomez, Joseph Delpreto, Stephanie Gil, Frank H. Guenther, and Daniela Rus. Correcting robot mistakes in real time using EEG signals. In *Proceedings - IEEE International Conference on Robotics and Automation*, 2017. ISBN 9781509046331. doi: 10.1109/ICRA.2017.7989777.

[38] Richardo Khonasty, Marc G Carmichael, Dikai Liu, and Stefano Aldini. Effect of External Force and Bimanual Operation on Upper Limb Pose during Human-Robot Collaboration. *The proceedings of the Australasian Conference on Robotics and Automation (ACRA)*, 2017.

[39] Marc Garry Carmichael, Stefano Aldini, and Dikai Liu. Human user impressions of damping methods for singularity handling in human-robot collaboration. In *Australasian Conference on Robotics and Automation, ACRA*, 2017. ISBN 9781510860117.

[40] Stefano Aldini, Marc G Carmichael, and Dikai Liu. A Risk Reduction Framework for Design of Physical Human-Robot Collaboration. In *Australasian Conference on Robotics and Automation, ACRA*, Adelaide, Australia, 2019.

[41] Stefano Aldini, Yujun Lai, Marc G Carmichael, Gavin Paul, and Dikai Liu. Real-time Estimation of the Strength Capacity of the Upper Limb for Physical Human-Robot Collaboration. In *Proceedings of the 43rd Annual International Conference of the IEEE Engineering in Medicine and Biology Society (EMBC)*, Guadalajara, Mexico, 2021. Submitted.

[42] A De Santis. *Modelling and control for Human–Robot Interaction: physical and cognitive aspects*. PhD thesis, Università degli Studi di Napoli Federico II, Italy, 2007.

[43] Bilge Mutlu, Nicholas Roy, and Selma Šabanović. Cognitive human-robot interaction. In *Springer Handbook of Robotics*, pages 1907–1933. Springer International Publishing, 1 2016. ISBN 9783319325521. doi: 10.1007/978-3-319-32552-1_71.

[44] Hami Kazerooni. Human-Robot Interaction via the Transfer of Power and Information Signals. *IEEE Transactions on Systems, Man and Cybernetics*, 1990. ISSN 21682909. doi: 10.1109/21.52555.

[45] Antonio Bicchi, Michele Bavaro, Gianluca Boccadamo, Davide De Carli, Roberto Filippini, Giorgio Grioli, Marco Piccigallo, Alessandro Rosi, Riccardo Schiavi, Soumen Sen, and Giovanni Tonietti. Physical human-robot interaction: Dependability, safety, and performance. In *International Workshop on Advanced Motion Control, AMC*, 2008. ISBN 9781424417032. doi: 10.1109/AMC.2008.4516033.

[46] Mathieu Bélanger-Barrette. Collaborative Robot Ebook Sixth Edition. *Robotiq*, 2015.

[47] Valeria Villani, Fabio Pini, Francesco Leali, and Cristian Secchi. Survey on human-robot collaboration in industrial settings: Safety, intuitive interfaces and applications. *Mechatronics*, 2018. ISSN 09574158. doi: 10.1016/j.mechatronics.2018.02.009.

[48] Bram Vanderborght, Alin Albu-Schaeffer, Antonio Bicchi, Erienne Burdet, Darwin G. Caldwell, Raffaella Carloni, Manuel Catalano, Oliver Eiberger, Werner Friedl, Gowrishankar Ganesh, Manolo Garabini, Markus Grebenstein, Giorgio Grioli, Sami Haddadin, Hannes Hoppner, Amir Jafari, Matteo Laffranchi, Dirk Lefeber, Florian Petit, Stefano Stramigioli, Nikos Tsagarakis, Michael Van Damme, Ronald Van Ham, Ludo C. Visser, and Sebastian Wolf. Variable impedance actuators: A review. *Robotics and Autonomous Systems*, 2013. ISSN 09218890. doi: 10.1016/j.robot.2013.06.009.

[49] Van Ronald Ham, Thomas G. Sugar, Bram Vanderborght, Kevin W. Hollander, and Dirk Lefeber. Compliant actuator designs: Review of actuators with passive adjustable compliance/controllable stiffness for robotic applications. *IEEE Robotics and Automation Magazine*, 2009. ISSN 10709932. doi: 10.1109/MRA.2009.933629.

[50] Takayuki Hoshi and Hiroyuki Shinoda. Robot skin based on touch-area-sensitive tactile element. In *Proceedings - IEEE International Conference on Robotics and Automation*, 2006. ISBN 0780395069. doi: 10.1109/ROBOT.2006.1642231.

[51] Markus Kühne, Sebastian Wolf, Thomas Bahls, Maxime Chalon, Werner Friedl, Markus Grebenstein, Hannes Höppner, Dominic Lakatos, Nico Mansfeld, Mehmet Can Özparpucu, Florian Petit, Jens Reinecke, Roman Weitschat, and Alin Albu-Schäffer. Soft robotics with variable stiffness actuators: Tough robots for soft human robot interaction. In *Soft Robotics: Transferring Theory to Application*. 2015. ISBN 9783662445068. doi: 10.1007/978-3-662-44506-8_18.

[52] Universal Robots. Collaborative robots from Universal Robots. URL `https://www.universal-robots.com/products/`. Accessed on 25/07/2018.

[53] Rethink Robotics. Smart Collaborative Robots for Factory Automation. URL `http://www.rethinkrobotics.com/smart-collaborative-difference/`. Accessed on 25/07/2018.

[54] ABB. IRB 14000 YuMi - Industrial Robots From ABB Robotics. URL `http://new.abb.com/products/robotics/industrial-robots/yumi`. Accessed on 25/07/2018.

[55] KUKA AG. LBR iiwa. URL `https://www.kuka.com/en-au/products/robotics-systems/industrial-robots/lbr-iiwa`. Accessed on 25/07/2018.

[56] International Organization for Standardization. ISO/TS 15066:2016 - Robots and robotic devices - Collaborative robots, 2016. URL `https://www.iso.org/standard/62996.html`.

[57] Bruno Siciliano and Luigi Villani. *Robot force control*. New York, 1999. ISBN 9788578110796. doi: 10.1017/CBO9781107415324.004.

[58] International Organization for Standardization. ISO 10218-1:2011 - Robots and robotic devices - Safety requirements for industrial robots - Part 1: Robots, 2011. URL `https://www.iso.org/standard/51330.html`.

[59] International Organization for Standardization. ISO 10218-2:2011 - Robots and robotic devices - Safety requirements for industrial robots - Part 2: Robot systems and integration, 2011. URL `https://www.iso.org/standard/41571.html`.

[60] Przemyslaw A. Lasota, Terrence Fong, and Julie A. Shah. A Survey of Methods for Safe Human-Robot Interaction. *Foundations and Trends in Robotics*, 2017. ISSN 1935-8253. doi: 10.1561/2300000052.

[61] Michiel P. de Looze, Tim Bosch, Frank Krause, Konrad S. Stadler, and Leonard W. O'Sullivan. Exoskeletons for industrial application and their potential effects on physical work load. *Ergonomics*, 59(5):671–681, 5 2016. ISSN 0014-0139. doi: 10.1080/00140139.2015.1081988.

[62] Hami Kazerooni, Ryan Steger, and Lihua Huang. Hybrid control of the Berkeley Lower Extremity Exoskeleton (BLEEX). In *International Journal of Robotics Research*, 2006. ISBN 078038914X. doi: 10.1177/0278364906065505.

[63] Nahema Sylla, Vincent Bonnet, FrÃl'dÃl'ric Colledani, and Philippe Fraisse. Ergonomic contribution of ABLE exoskeleton in automotive industry. *International Journal of Industrial Ergonomics*, 44(4), 2014. ISSN 18728219. doi: 10.1016/j.ergon.2014.03.008.

[64] International Organization for Standardization. ISO 8372:2012 - Robots and robotic devices - Vocabulary, 2012. ISSN 5925731107. URL `https://www.iso.org/standard/55890.html`. Accessed on ISO 8373.

[65] H. I. Krebs and B. T. Volpe. Rehabilitation Robotics. *Handbook of Clinical Neurology*, 2013. ISSN 00729752. doi: 10.1016/B978-0-444-52901-5.00023-X.

[66] Emily Mower, David J. Feil-Seifer, Maja J. Matarić, and Shrikanth Narayanan. Investigating implicit cues for user state estimation in human-robot interaction using physiological measurements. In *Proceedings - IEEE International Workshop on Robot and Human Interactive Communication*, 2007. ISBN 1424416345. doi: 10.1109/ROMAN.2007.4415249.

[67] Tomohito Takubo, Hirohiko Arai, Yasuo Hayashibara, and Kazuo Tanie. Human-robot cooperative manipulation using a virtual nonholonomic constraint. *International Journal of Robotics Research*, 2002. ISSN 02783649. doi: 10.1177/027836402321261904.

[68] V. Fernandez, C. Balaguer, D. Blanco, and M. A. Salichs. Active human-mobile manipulator cooperation through intention recognition. *Proceedings - IEEE International Conference on Robotics and Automation*, 2001. ISSN 10504729. doi: 10.1109/ROBOT.2001.933025.

[69] Eugenio Guglielmelli, Paolo Dario, Cecilia Laschi, Riccardo Fontanelli, Marco Susani, Peter Verbeeck, and Jean-Claude Gabus. Humans and technologies at home: from friendly appliances to robotic interfaces. *Proceedings. 5th IEEE International Workshop on Robot and Human Communication RO-MAN'96 Tsukuba (Cat. No.96TH8179)*, 1996.

[70] Roger Gassert and Volker Dietz. Rehabilitation robots for the treatment of sensorimotor deficits: A neurophysiological perspective, 6 2018. ISSN 17430003. Accessed on Journal of NeuroEngineering and Rehabilitation.

[71] Hermano Igo Krebs, Bruce T. Volpe, Dustin Williams, James Celestino, Steven K. Charles, Daniel Lynch, and Neville Hogan. Robot-aided neurorehabilitation: A robot for wrist rehabilitation. *IEEE Transactions on Neural Systems and Rehabilitation Engineering*, 15(3): 327–335, 9 2007. ISSN 15344320. doi: 10.1109/TNSRE.2007.903899.

[72] Francisco J. Badesa, Ricardo Morales, Nicolas Garcia-Aracil, J. M. Sabater, Alicia Casals, and Loredana Zollo. Auto-adaptive robot-aided therapy using machine learning techniques. *Computer Methods and Programs in Biomedicine*, 116(2):123–130, 2014. ISSN 18727565. doi: 10.1016/j.cmpb.2013.09.011.

[73] Matthias Schindelholz and Kenneth J. Hunt. Feedback control of heart rate during robotics-assisted treadmill exercise. *Technology and Health Care*, 20(3):179–194, 2012. ISSN 09287329. doi: 10.3233/THC-2012-0668.

[74] Sami Haddadin and Elizabeth Croft. Physical Human-Robot Interaction. In B Siciliano and O Khatib, editors, *Springer Handbook of Robotics*, chapter 69, pages 1835–1874. Springer, Cham, 2016. ISBN 978-3-319-32552-1. doi: https://doi.org/10.1007/978-3-319-32552-1_69.

[75] Claire C. Gordon, Cynthia L. Blackwell, Bruce Bradtmiller, Joseph L. Parham, Patricia Barrientos, Stephen P. Paquette, Brian D. Corner, Jeremy M. Carson, Joseph C. Venezia, Belva M. Rockwell, Michael Mucher, and Shirley Kristensen. 2012 Anthropometric Survey of U.S. Army Personnel: Methods and Summary Statistics. Technical report, U.S. Army Natick Soldier Research, Development and Engineering Center, Natick, MA, 2015.

[76] Katherine R Saul, Meghan E Vidt, Garry E Gold, and Wendy M Murray. Upper Limb Strength and Muscle Volume in Healthy Middle-Aged Adults. *Journal of Applied Biomechanics*, 31(6):484–491, 8 2015. doi: 10.1123/jab.2014-0177.

[77] Eric Meisner, Volkan Isler, and Jeff Trinkle. Controller design for human-robot interaction. *Autonomous Robots*, 2008. ISSN 09295593. doi: 10.1007/s10514-007-9054-7.

[78] Tamio Arai, Ryu Kato, and Marina Fujita. Assessment of operator stress induced by robot collaboration in assembly. *CIRP Annals - Manufacturing Technology*, 2010. ISSN 00078506. doi: 10.1016/j.cirp.2010.03.043.

[79] Pramila Rani, Jared Sims, Robert Brackin, and Nilanjan Sarkar. Online stress detection using psychophysiological signals for implicit human-robot cooperation. *Robotica*, 2002. ISSN 02635747. doi: 10.1017/S0263574702004484.

[80] Valeria Villani, Lorenzo Sabattini, Cristian Secchi, and Cesare Fantuzzi. Natural interaction based on affective robotics for multi-robot systems. In *2017 International Symposium on Multi-Robot and Multi-Agent Systems, MRS 2017*, 2018. ISBN 9781509063093. doi: 10.1109/MRS.2017.8250931.

[81] Dana Kulíc and Elizabeth Croft. Affective state estimation for human-robot interaction. In *IEEE Transactions on Robotics*, 2007. ISBN 0929-5593. doi: 10.1109/TRO.2007.904899.

[82] Alexander Koenig, Ximena Omlin, Lukas Zimmerli, Mark Sapa, Carmen Krewer, Marc Bolliger, Friedemann Mller, and Robert Riener. Psychological state estimation from physiological recordings during robot-assisted gait rehabilitation. *The Journal of Rehabilitation Research and Development*, 2011. ISSN 0748-7711. doi: 10.1682/JRRD.2010.03.0044.

[83] Herbert F. Jelinek, Katherine G. August, Md Hasan Imam, Ahsan H. Khandoker, Alexander Koenig, and Robert Riener. Cortical response to psycho-physiological changes in

auto-adaptive robot assisted gait training. In *Proceedings of the Annual International Conference of the IEEE Engineering in Medicine and Biology Society, EMBS*, 2011. ISBN 9781424441211. doi: 10.1109/IEMBS.2011.6091725.

[84] Carlo J De Luca. The Use of Surface Electromyography in Biomechanics. *Journal of Applied Biomechanics*, 13(2):135–163, 8 1997. doi: 10.1123/jab.13.2.135.

[85] Ahmet Erdemir, Scott McLean, Walter Herzog, and Antonie J van den Bogert. Model-based estimation of muscle forces exerted during movements. *Clinical Biomechanics*, 22 (2):131–154, 8 2007. doi: 10.1016/J.CLINBIOMECH.2006.09.005.

[86] Luka Peternel, Tomoyuki Noda, Tadej Petrič, Ales Ude, Jun Morimoto, and Jan Babič. Adaptive control of exoskeleton robots for periodic assistive behaviours based on EMG feedback minimisation. *PLoS ONE*, 11(2), 2 2016. ISSN 19326203. doi: 10.1371/journal.pone.0148942.

[87] Luka Peternel, Cheng Fang, Nikos Tsagarakis, and Arash Ajoudani. A selective muscle fatigue management approach to ergonomic human-robot co-manipulation. *Robotics and Computer-Integrated Manufacturing*, 58:69–79, 8 2019. ISSN 0736-5845. doi: 10.1016/J.RCIM.2019.01.013.

[88] Tien Tuan Dao. From deep learning to transfer learning for the prediction of skeletal muscle forces. *Medical & Biological Engineering & Computing*, 57(5):1049–1058, 8 2019. doi: 10.1007/s11517-018-1940-y.

[89] Kexiang Li, Jianhua Zhang, Lingfeng Wang, Minglu Zhang, Jiayi Li, and Shancheng Bao. A review of the key technologies for sEMG-based human-robot interaction systems, 9 2020. ISSN 17468108. Accessed on Biomedical Signal Processing and Control.

[90] Jay Friedenberg and Gordon Silverman. *Cognitive Science: An Introduction to the Study of Mind*. 2005. ISBN 1412925681. doi: 10.1017/CBO9781107415324.004.

[91] Xiaoqian Mao, Mengfan Li, Wei Li, Linwei Niu, Bin Xian, Ming Zeng, and Genshe Chen. Progress in EEG-based brain robot interaction systems. *Computational Intelligence and Neuroscience*, 2017. doi: 10.1155/2017/1742862.

[92] F. Galán, M. Nuttin, E. Lew, P. W. Ferrez, G. Vanacker, J. Philips, and J. del R Millán. A brain-actuated wheelchair: Asynchronous and non-invasive Brain-computer interfaces for continuous control of robots. *Clinical Neurophysiology*, 2008. ISSN 13882457. doi: 10.1016/j.clinph.2008.06.001.

[93] Inaki Iturrate, Jevier M. Antelis, Andrea Kübler, and Javier Minguez. A noninvasive brain-actuated wheelchair based on a P300 neurophysiological protocol and automated navigation. *IEEE Transactions on Robotics*, 2009. ISSN 15523098. doi: 10.1109/TRO.2009.2020347.

[94] Brice Rebsamen, Cuntai Guan, Haihong Zhang, Chuanchu Wang, Cheeleong Teo, Marcelo H. Ang, and Etienne Burdet. A brain controlled wheelchair to navigate in familiar environments. *IEEE Transactions on Neural Systems and Rehabilitation Engineering*, 2010. ISSN 15344320. doi: 10.1109/TNSRE.2010.2049862.

[95] Yuanqing Li, Jiahui Pan, Fei Wang, and Zhuliang Yu. A hybrid BCI system combining P300 and SSVEP and its application to wheelchair control. *IEEE Transactions on Biomedical Engineering*, 2013. ISSN 00189294. doi: 10.1109/TBME.2013.2270283.

[96] Ting Li, Jun Hong, Jinhua Zhang, and Feng Guo. Brain-machine interface control of a manipulator using small-world neural network and shared control strategy. *Journal of Neuroscience Methods*, 2014. ISSN 1872678X. doi: 10.1016/j.jneumeth.2013.11.015.

[97] E. Hortal, D. Planelles, A. Costa, E. Iáñez, A. Úbeda, J. M. Azorín, and E. Fernández. SVM-based Brain-Machine Interface for controlling a robot arm through four mental tasks. *Neurocomputing*, 2015. ISSN 18728286. doi: 10.1016/j.neucom.2014.09.078.

[98] Eric A. Pohlmeyer, Babak Mahmoudi, Shijia Geng, Noeline Prins, and Justin C. Sanchez. Brain-machine interface control of a robot arm using actor-critic rainforcement learning. In *Proceedings of the Annual International Conference of the IEEE Engineering in Medicine and Biology Society, EMBS*, 2012. ISBN 9781424441198. doi: 10.1109/EMBC.2012.6346870.

[99] Cong Wang, Bin Xia, Jie Li, Wenlu Yang, Dianyun Xiao, Alejandro Cardona Velez, and Hong Yang. Motor imagery BCI-based robot arm system. In *Proceedings - 2011 7th International Conference on Natural Computation, ICNC 2011*, 2011. ISBN 9781424499533. doi: 10.1109/ICNC.2011.6021923.

[100] E. Hortal, D. Planelles, A. Costa, E. Iáñez, A. Úbeda, J. M. Azorín, and E. Fernández. SVM-based Brain-Machine Interface for controlling a robot arm through four mental tasks. *Neurocomputing*, 2015. ISSN 18728286. doi: 10.1016/j.neucom.2014.09.078.

[101] Luca Tonin, Gloria Beraldo, Stefano Tortora, Luca Tagliapietra, Jose del R. Millan, and Emanuele Menegatti. ROS-Neuro: A common middleware for BMI and robotics. The acquisition and recorder packages. In *2019 IEEE International Conference on Systems, Man and Cybernetics (SMC)*, pages 2767–2772. IEEE, 10 2019. ISBN 978-1-7281-4569-3. doi: 10.1109/SMC.2019.8914364.

[102] B. A. Francis and W. M. Wonham. The internal model principle of control theory. *Automatica*, 1976. ISSN 00051098. doi: 10.1016/0005-1098(76)90006-6.

[103] Joel Cooper. *Cognitive dissonance: Fifty years of a classic theory*. 2007. ISBN 9781446214282. doi: 10.4135/9781446214282.

[104] M. Falkenstein, J. Hohnsbein, J. Hoormann, and L. Blanke. Effects of crossmodal divided attention on late ERP components. II. Error processing in choice reaction tasks. *Electroencephalography and Clinical Neurophysiology*, 1991. ISSN 00134694. doi: 10.1016/0013-4694(91)90062-9.

[105] Charlotte Stagg, Peter Hindley, Andrea Tales, and Stuart Butler. Visual mismatch negativity: The detection of stimulus change. *NeuroReport*, 2004. ISSN 09594965. doi: 10.1097/00001756-200403220-00017.

[106] Bruno Kopp, Fred Rist, and Uwe Mattler. N200 in the flanker task as a neurobehavioral tool for investigating executive control. *Psychophysiology*, 1996. ISSN 00485772. doi: 10.1111/j.1469-8986.1996.tb00425.x.

[107] Greg Hajcak, Jason S. Moser, Clay B. Holroyd, and Robert F. Simons. The feedback-related negativity reflects the binary evaluation of good versus bad outcomes. *Biological Psychology*, 2006. ISSN 03010511. doi: 10.1016/j.biopsycho.2005.04.001.

[108] Klaus Gramann, Joseph T. Gwin, Daniel P. Ferris, Kelvin Oie, Tzyy Ping Jung, Chin Teng Lin, Lun De Liao, and Scott Makeig. Cognition in action: Imaging brain/body dynamics in mobile humans. *Reviews in the Neurosciences*, 22(6), 2011. ISSN 03341763. doi: 10.1515/RNS.2011.047.

[109] Aina Puce and Matti S. Hämäläinen. A review of issues related to data acquisition and analysis in EEG/MEG studies, 2017. ISSN 20763425. Accessed on Brain Sciences.

[110] Gi Yeul Bae and Steven J. Luck. Decoding motion direction using the topography of sustained ERPs and alpha oscillations. *NeuroImage*, 184, 2019. ISSN 10959572. doi: 10.1016/j.neuroimage.2018.09.029.

[111] G E Chatrian, E Lettich, and P L Nelson. Ten percent electrode system for topographic studies of spontaneous and evoked EEG activity. *American Journal Of EEG Technology*, 1985. ISSN 00029238. doi: 10.1080/00029238.1985.11080163.

[112] Arnaud Delorme and Scott Makeig. EEGLAB: An open source toolbox for analysis of single-trial EEG dynamics including independent component analysis. *Journal of Neuroscience Methods*, 2004. ISSN 01650270. doi: 10.1016/j.jneumeth.2003.10.009.

[113] Scott Makeig, Anthony J. Bell., Tzyy-Ping Jung, and Terrence J. Sejnowski. Independent Component Analysis of Electroencephalographic Data. *Advances in Neural Information Processing Systems*, 1996. ISSN 10495258. doi: 10.1109/ICOSP.2002.1180091.

[114] Chi Yuan Chang, Sheng Hsiou Hsu, Luca Pion-Tonachini, and Tzyy Ping Jung. Evaluation of Artifact Subspace Reconstruction for Automatic EEG Artifact Removal. *Conference proceedings of the Annual International Conference of the IEEE Engineering in Medicine and Biology Society*, 2018. doi: 10.1109/EMBC.2018.8512547.

[115] Andrea Mognon, Jorge Jovicich, Lorenzo Bruzzone, and Marco Buiatti. ADJUST: An automatic EEG artifact detector based on the joint use of spatial and temporal features. *Psychophysiology*, 2011. ISSN 00485772. doi: 10.1111/j.1469-8986.2010.01061.x.

[116] John Polich. Updating P300: An integrative theory of P3a and P3b. *Clinical Neurophysiology*, 2007. doi: 10.1016/j.clinph.2007.04.019.

[117] Gert Pfurtscheller. The hybrid BCI. *Frontiers in Neuroscience*, 2010. doi: 10.3389/fnpro.2010.00003.

[118] Jan E. Trost. Statistically nonrepresentative stratified sampling: A sampling technique for qualitative studies. *Qualitative Sociology*, 1986. ISSN 01620436. doi: 10.1007/BF00988249.

[119] International Federation of Clinical Neurophysiology. *Recommendations for the Practice of Clinical Neurophysiology: Guidelines of the International Federation of Clinical Physiology (EEG Suppl. 52)*. Elsevier Science B.V., 1999.

[120] Erol Başar, Canan Başar-Eroglu, Sirel Karakaş, and Martin Schürmann. Gamma, alpha, delta, and theta oscillations govern cognitive processes. *International Journal of Psychophysiology*, 2001. ISSN 01678760. doi: 10.1016/S0167-8760(00)00145-8.

[121] Honghui Zhang, Andrew J. Watrous, Ansh Patel, and Joshua Jacobs. Theta and Alpha Oscillations Are Traveling Waves in the Human Neocortex. *Neuron*, 2018. ISSN 10974199. doi: 10.1016/j.neuron.2018.05.019.

[122] F. Lotte, L. Bougrain, A. Cichocki, M. Clerc, M. Congedo, A. Rakotomamonjy, and F. Yger. A review of classification algorithms for EEG-based brain-computer interfaces: A 10 year update. *Journal of Neural Engineering*, 2018. ISSN 17412552. doi: 10.1088/1741-2552/aab2f2.

[123] Jian Bo Yang, Minh Nhut Nguyen, Phyo Phyo San, Xiao Li Li, and Shonali Krishnaswamy. Deep convolutional neural networks on multichannel time series for human activity recognition. In *IJCAI International Joint Conference on Artificial Intelligence*, 2015. ISBN 9781577357384.

[124] Diederik P Kingma and Jimmy Lei Ba. Adam: A method for stochastic gradient descent. *ICLR: International Conference on Learning Representations*, 2015.

[125] SciKit MLP. URL `https://scikit-learn.org/stable/modules/generated/sklearn.neural_network.MLPClassifier.html`. Accessed on 13/01/2021.

[126] Robin Tibor Schirrmeister, Jost Tobias Springenberg, Lukas Dominique Josef Fiederer, Martin Glasstetter, Katharina Eggensperger, Michael Tangermann, Frank Hutter, Wolfram Burgard, and Tonio Ball. Deep learning with convolutional neural networks for EEG decoding and visualization. *Human Brain Mapping*, 38(11), 2017. ISSN 10970193. doi: 10.1002/hbm.23730.

[127] Christopher M. Bishop. *Pattern Recoginiton and Machine Learning*. 2006. ISBN 978-0-387-31073-2.

[128] Vernon J. Lawhern, Amelia J. Solon, Nicholas R. Waytowich, Stephen M. Gordon, Chou P. Hung, and Brent J. Lance. EEGNet: A compact convolutional neural network for EEG-based brain-computer interfaces. *Journal of Neural Engineering*, 2018. ISSN 17412552. doi: 10.1088/1741-2552/aace8c.

[129] William A. Wolovich and Howard Elliott. Computational Technique for Inverse Kinematics. In *Proceedings of the IEEE Conference on Decision and Control*, 1984.

[130] Yoshihiko Nakamura and Hideo Hanafusa. Inverse kinematic solutions with singularity robustness for robot manipulator control. *Journal of Dynamic Systems, Measurement and Control, Transactions of the ASME*, 108(3), 1986. ISSN 15289028. doi: 10.1115/1.3143764.

[131] Marc G Carmichael, Dikai Liu, and Kenneth J Waldron. A framework for singularity-robust manipulator control during physical human-robot interaction. *The International Journal of Robotics Research*, 2017. ISSN 0278-3649. doi: 10.1177/0278364917698748.

[132] Avinash K Singh and Chin-Teng Lin. EnK: Encoding time-information in convolution. ArXivID 2006.04198v1. URL `https://arxiv.org/abs/2006.04198`. Accessed on 05/01/2021.